UC Berkeley
Research Reports

Title

Model of Human Vehicle Driving- A Predictive Nonlinear Optimization Approach

Permalink

https://escholarship.org/uc/item/7c93b0fx

Author

Prokop, Gunther

Publication Date

2000-10-01

This paper has been mechanically scanned. Some errors may have been inadvertently introduced.

Model of Human Vehicle Driving –
A Predictive Nonlinear Optimization
Approach

Gunther Prokop

Report for MOU 250

CALIFORNIA PARTNERS FOR ADVANCED TRANSIT AND HIGHWAYS

Model of human vehicle driving – a predictive nonlinear optimization approach

Gunther Prokop

13th June 2000

Acknowledgments

Abstract

Title : Model of human vehicle driving – a predictive nonlinear optimization approach

Author : Günther Prokop

Date : 13th June 2000

When driving a vehicle the human acts as a controller in a highly dynamic environment. Thus human behavior in that control loop has to a large extent been described using control theoretical methodology. We develop a driver model, in which driving is seen as a model predictive control task in such a way that the driver accumulates knowledge about his/her vehicle's handling properties. He/she builds a model out of that knowledge and uses it to predict the vehicle's future reactions on his/her control inputs. The human's behavioral optimization is reflected in the driver model by using that prediction model in order to optimize control inputs such, that a set of criteria, which reflect human well-being, are minimized. Prediction models and criteria depend on the current driving situation and on personal driver preferences. The principal properties of the driver model are discussed using very simple standard maneuvers like driving straight and cornering under different preferences. The method is then applied to a more complex track. The findings from that are backed up by experiments done in real world and in a driving simulator.

Keywords

Automobile Driving, Driving Simulations, Human Factors, Control Algorithms

Executive Summary

When driving a vehicle the human acts as a controller in a highly dynamic environment. The human operator must process different sensory perceptions suitably to continuously generate control input to the plant. He/she works as a dynamic controller, which uses his/her model information about the plant, together with his/her sensory perception to achieve his/her control aim. Thus human behavior in that control loop can to a large extent be described using control theoretical methodology.

Realistic driver models are particularly useful in three respects: first, it enables us to evaluate vehicle handling properties by computer simulation in a very realistic manner. Thus the test setup in a computer simulation can be exactly the same as in a real world experiment, so that - provided the model is realistic - the same conclusions can be drawn. Second, when developing driver support systems such as ABS, ESP, brake assistant etc. the driver is a non-negligible part of the system, introducing his/her own dynamics. If the human in the control loop is not properly considered, he/she can destroy much of the benefit gained by these systems. Third, when developing vehicle guidance controllers, they should be designed such that the human finds them acceptable. The chance to achieve that is large, if such a controller acts in a similar way than the human him-/herself would do. Thus, in this application driver models are needed for prediction and adaptation.

Starting from basic assumptions coming from every day's experience we try to deduct a quantitative answer to the question of human behavior as a dynamic controller. These assumptions are:

- **Man can use and coordinate his sensory perception.** If the human is to control a dynamic plant, he/she must have the possibility of perceiving important output quantities with sufficient accuracy. Provided this, the human is able to relate different perceptive inputs to each other, in order to get a clear image of the current system state. Therefore, we can assume that the human is capable of deducing the current state of motion from his/her sensory perception.

- **Man has the ability to learn dynamic system's behavior.** Thus, to accumulate information about the plant dynamics by operating it. He/she does so by continuously comparing the plant behavior in response to his/her input signals versus the behavior he/she would have expected from his/her imagination gathered so far. Consequently, the human can constantly improve his/her imagination of the dynamic plant, and he/she is able to predict its behavior ever more precisely.

- **Man is able to optimize his/her behavior.** Experience shows that the human, as soon as he/she has understood to a certain extent the system to be controlled, is able to optimize his/her behavior by exercising. In the context of driver modeling mainly the vehicle's trajectory on the road and its velocity, but also the gear sequence are adjusted optimally by the human driver.

We develop a driver model, in which driving is seen as a model predictive control task in such a way that the driver accumulates knowledge about his/her vehicle's handling properties. He/she builds a model out of that knowledge and uses it to predict the vehicle's future reactions on his/her control inputs. The human's behavioral optimization is reflected in the driver model by using that prediction model in order to optimize control inputs such, that a set of criteria, which reflect human well-being, are minimized. Prediction models and criteria depend on the current driving situation and on personal driver preferences.

The optimization is performed using a Sequential Quadratic Programming algorithm. The objectives $f(p)$ of that optimization are connected to the optimization parameters p by dynamic constraints. A procedure is shown to calculate analytical partial derivatives $\frac{\partial f(p)}{\partial p}$ of the cost functions $f(p)$ with respect to the optimization parameters p, in order to improve numerical convergence of the optimization.

The principal properties of the driver model are discussed using a one track vehicle model as the plant including aerodynamic drag, an HSRI tire model and the engine characteristics being modeled by a look-up table in combination with a first order filter (PT1).

Simple standard maneuvers like driving straight and cornering under different preferences are used to study the principal behavior of the resulting driver model. The method is then applied to a more complex track, the Hockenheim Motodrom, Germany. The findings from that are backed up by experiments done in real world and in a driving simulator.

The results show several things:

- The behavior predicted by the driver model corresponds well with real human behavior under the conditions tested in the experiment. Comparison of simulation and experiment shows that the human driver is involuntarily able to optimize his/her behavior for given preferences. This backs up the hypothesis that driving can in principle be characterized as a continuous optimization task. However, it is necessary to extend the real world experiments to higher speeds and more complex tracks.

- The vehicle's trajectory during curve negotiation differs considerably from the curvature minimizing trajectory. It depends strongly on the active preference, and has to be considered in combination with the velocity profile along it. This corresponds well with experiences from racing driving.

- Experimental investigations in a static driving simulator have only limited meaningfulness in the context of modeling driver control behavior. The sensory perception is simply too different from that on a real road, since any acceleration input to the human is missing. Either a dynamic driving simulator or extended real world testing is necessary for further validation of the model.

Contents

Chapter 1

Introduction

Technology serves man. Man operates machines. Interaction between man and machine is as old as technology itself. In applications, which contain fast movements and non-negligible dynamics, the human operator must process different sensory perceptions suitably to continuously generate control input to the plant. He works as a dynamic controller, which uses his model information about the plant, together with his sensory perception to achieve his control aim.

Every day's experience shows that the human is able to control and stabilize dynamic plants of surprisingly high complexity, involving high order dynamics and nonlinearities of all possible kinds.

Consider for example a child, balancing a bar, which rests vertically on the palm of his/her hand. In the first place, the child will recognize the instability of that vertical bar. Secondly, he would realize that he can know the current state of motion of the bar by watching it and sensing the forces imposed on his hand. He will then see that he can influence the bar's motion by moving his hand, and soon – after a bit of training – the child will be able to balance the vertical bar on his hand, thus to control and essentially stabilize a formerly unstable dynamic plant.

Playing soccer seems to be a really natural thing for most of us – at least in our culture. Fact is that the human gate, which is crucial in this task, is one of the most highly developed skills of man as far as the control of dynamic plants is concerned. But walking and running is only part of the game. Soccer is interesting because the players are interacting with a ball, precisely controlling its movements and taking into account its dynamic motion under the influence of impacts, friction, and tricky aerodynamic forces.

One could think of a lot of other examples, where humans control complex dynamic plants without any apparent difficulty, and virtually involuntarily. Seemingly, man has developed skills, which allow him to perform such tasks. One of the important questions arising from this observation is, if and how human behavior in this context can be described systematically, and if his reaction to certain "inputs" can be predicted to some extent.

Research in this area is certainly mainly biological, behavioral, and to some extent psychological.

Engineers, however, are concerned with these issues as they try to design appliances to be operated by humans. In some cases these appliances exhibit non-negligible dynamics. Undoubtedly, such devices should be built in such a way, that they support the operator's actions and — dynamically — make his intuitive reactions to a certain perception stabilize the plant, so that it can be easily controlled.

To accomplish this aim, we chose a descriptive approach to human behavior, rather than to try to explain those particular human skills by biological means. The term "descriptive" means that we try only to describe human behavior in the control loop without explaining it physiologically or psychologically. Starting from basic assumptions coming from every day's experience, such as the examples mentioned above, we try to deduct a quantitative answer to the question of human behavior as a dynamic controller.

These assumptions are:

- o **Man can use and coordinate his sensory perception.** If the human is to control a dynamic plant, he must have the possibility of perceiving important output quantities with sufficient accuracy. Provided this, the human is able to relate different perceptive inputs to each other, in order to get an even clearer image of the current system state. Therefore, we can assume that the human is capable of deducing the current state of motion from his sensory perception.

- o **Man** has **the ability** to **learn dynamic system's behavior.** Thus, to accumulate information about the plant dynamics by just operating it. He does so by continuously comparing the plant behavior in response to his input signals versus the behavior he would have expected from his imagination gathered so far. Consequently, the human can constantly improve his imagination of the dynamic plant, and he is able to predict its behavior more and more precisely.

- o **Man is able** to **optimize his behavior.** Experience shows that the human, as soon as he has understood to a certain extent the system to be controlled, is able to optimize his behavior. Seemingly, this optimization skill is somehow part of human nature. In most cases, this happens almost involuntarily, as it is the case when learning to walk or to ride a bicycle. But there are other cases, where really conscious decisions are involved in this optimization, for example when playing chess[1] or in the soccer game mentioned above.

Driving a vehicle is a task, which is nowadays performed by almost every adult person in industrialized countries. Under normal conditions, most people are able to drive safely Statistics show however, that road accidents keep happening, which means that under certain

---

[1]Chess can be considered as a highly complex discrete-time dynamic system.

circumstances human beings are not able to keep their vehicle safely under control. Thus, humans fail to stabilize their cars in particular situations.

The need for enhanced driver assistance systems to support the driver in his task in today's vehicles is therefore obvious. On the other hand, to determine, if a particular system really fulfills the requirements it is designed for, and if it still does so in interaction with the human, is not trivial. Driver assistance systems usually influence the dynamic properties of the vehicle, causing the operator to change his behavior and possibly destroy the desired effect.

It is therefore necessary to study the human operator's actions and reactions as part of the dynamic plant, in order to evaluate the impact of driver assistance systems on road safety.

Vehicle driving is thus a good and useful example for the study of human behavior in the loop. It has become even more important during the last couple of years, since substantial improvements in computer technology and ever more elaborate simulation techniques allow a great deal of design and development work to be done by simulation. Accurate simulation models of the driver support this.

1.1 Research concept
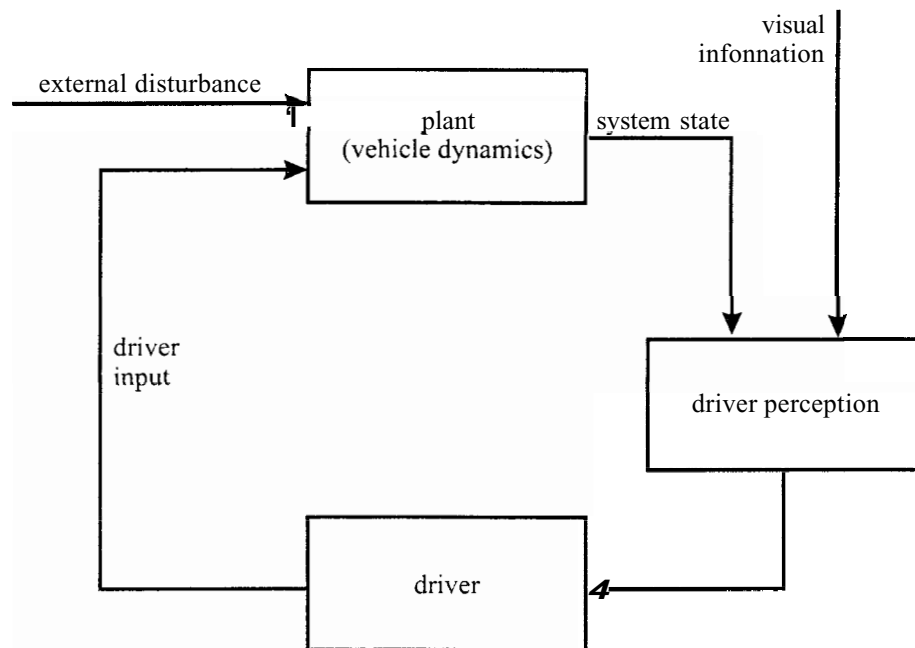
Figure 1.1:Control loop consisting of vehicle, plant, and
external disturbances

The driver of a vehicle is part of a closed control loop consisting of a plant, which is the vehicle itself, and the driver, who is to control the plant, see Fig. 1.1. The vehicle's dynamics

is excited by external disturbances, which partly can be perceived by the driver a certain time in advance. The input passed from vehicle and environment to the driver consists of visual information, accelerations, velocity information, position and velocity of potential obstacles etc.. It provides the information needed by the human to judge a certain situation and react appropriately.

In doing so, the driver can essentially act on the steering wheel, the accelerator and brake pedals, as well as on the gear shift and the clutch pedal. These devices are the control inputs the driver uses for his action.

Research on driver behavior must start with a proper description of the plant to be controlled, namely the vehicle's dynamics. We will introduce two dynamic vehicle models in chapter 2. The vehicle model must contain all effects, which can possibly affect the driver's behavior. However, the modeling techniques to be used for this part are quite straightforward, and since, in addition, they are not part of the research, their description is very compressed in chapter 2.

The proposed approach to driver modeling is essentially a model predictive control method based on the above mentioned assumptions on the nature of human behavior in the control loop. With increasing driving experience the human accumulates model information about the vehicle's dynamic behavior. He uses this model continuously, together with his sensory perception to generate steering, throttle, brake, gear, and clutch inputs as needed to stabilize the car.

There are three tasks to be carried out by the driver. They constitute an hierarchical controller, which reflects the human's thinking during the ride:

- *o* Cognitive decision: This is the highest hierarchical level in the controller. Based upon his expert knowledge about driving, the human decides on his preferences during the ride in a particular situation, e. g. if he wants to go as fast as possible or, on the other hand, he considers a situation dangerous and tries to decelerate as quickly as possible. Another possible goal is to minimize accelerations on the passengers to enhance riding comfort. The cognitive decision task must therefore provide a set of weighting factors to give a trade-off between the cost functions of the subsequent trajectory optimization.

  It is also necessary in the cognitive decision task to decide on the model to be used for optimizing a trajectory. Some possible models are described in chapter 3. This is important to describe the human ability to adapt to changing dynamic behavior of the plant.

  The cognitive decision task is mainly a decision making process, based on the driver's expert knowledge. It is also a process, where possible decisions are not markedly separated from each other. Therefore, a fuzzy-rule based decision making approach seems suitable to implement this task effectively.

- *o* Trajectory optimization: Once the driver has decided on his preferences during the ride, he must convert this into proper action by generating a trajectory, which he wants
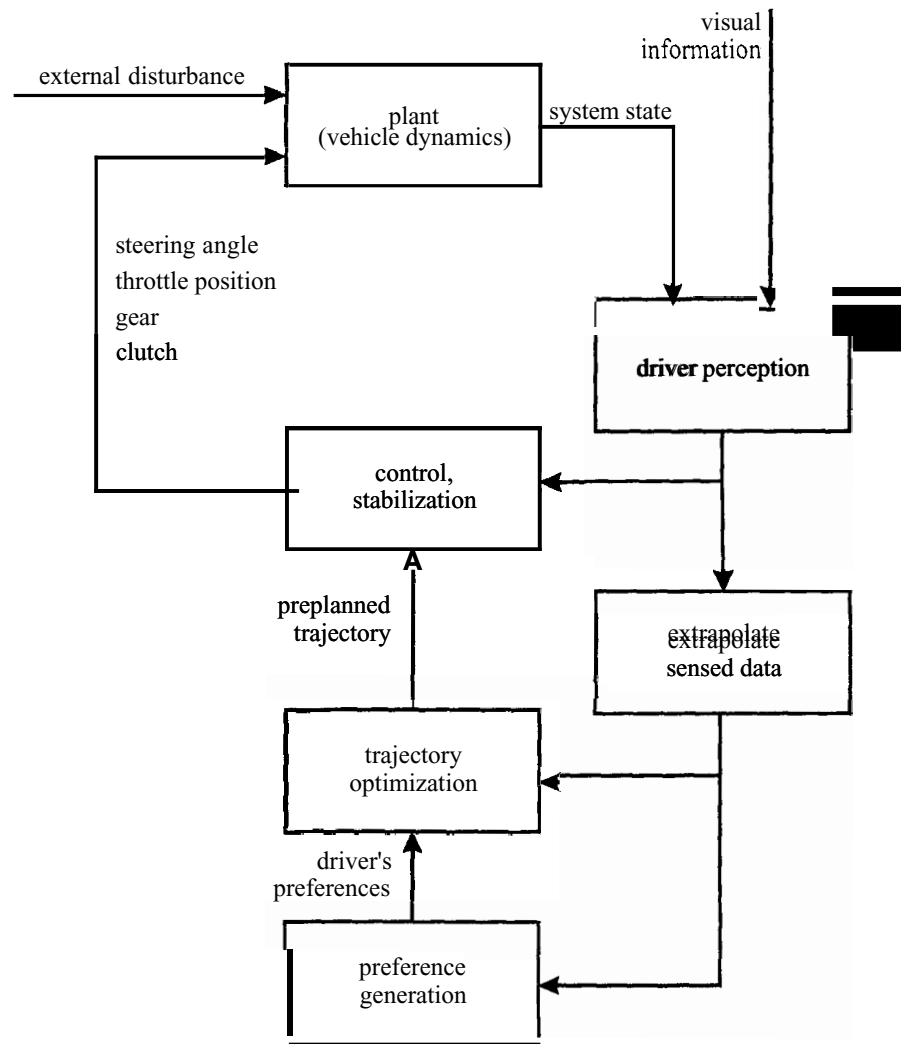
Figure 1.2: Basic 3-stage control concept for the description of driver behavior

the vehicle to follow, and a velocity profile along it. He utilizes his sensory perception to estimate the current state of motion. Together with his information from looking ahead and the model information about his vehicle he is able to predict the reactions of his vehicle to certain driving inputs.

According to the above assumptions on human behavior, man is able to optimize his action, provided that he has sufficient knowledge (=experience) about the plant dynamics. He is thus able to work in a model-predictive controller fashion, i. e. to optimize his future action at one time, apply the optimized action for one time instance, and optimize again. Depending on the complexity of the situation, the sampling time of this action varies from about 0.2 s to *3* s, according to [15].

In mathematical terms the trajectory optimization task constitutes a nonlinear vector

optimization problem under dynamic equality and inequality constraints. In chapter 5 the corresponding optimization problems are formulated, such that they can be solved using standard numerical optimization algorithms.

- **Control and stabilization:** The lowest control level reflects the continuous stabilization of the plant by the driver. The task is to continuously adjust throttle, brake, and steering angle to minimize deviations from the trajectory, which has been preplanned in the trajectory optimization level.

  During simulation, this is done at a sampling rate, which makes it virtually act as a continuous controller when considering the high time constants involved in human action.

  This stabilization task generally constitutes a nonlinear vector Optimization problem, which is to be solved considerably more often than the trajectory planning problem. Its formulation and solution are given in chapter 6. However, the high sampling frequency required makes the simulation of this task very costly in terms of CPU-time. Several possibilities are being discussed therefore in chapter 6 to reduce computational effort.

Chapter 2

Vehicle sirnulation models

The mechanical model of the plant, which is to be controlled, is the basis of all further investigations. All effects necessary for the human control task must be included. Since our focus is on the human controlling the dynamics of a vehicle, we have to set up a model describing a road vehicle's lateral and longitudinal dynamics in the frequency range, in which human control takes place.

This model must be distinguished from the simplified models described in chapter **3.** The latter are used by the driver to generate his input signals. Unlike that, we try here to describe the physics of the plant, regardless of the driver's knowledge about it. The models developed in this chapter are used as plant models as depicted in Fig. 1.1.

The methods used therefore are standard multibody modeling techniques. They are not described in detail here. We rather refer to a variety of textbooks on this topic, e. g. [1, 5, 8, 12].

Starting from the kinematic properties of the vehicle, the dynamic equations of motion of second order

$$M(q)\ddot{q} + h(q, \dot{q}) = B(q)f(t, q, \dot{q}) \tag{2.1}$$

are derived to describe its mechanical dynamic behavior. $q \in \mathbb{R}^n$ denotes thereby a vector of suitably chosen minimal coordinates with n being the number of degrees of freedom. $M(q) \in \mathbb{R}^{n \times n}$ is the positive definite mass matrix, depending on q. $h(q, \dot{q}) \in \mathbb{R}^n$ contains possible centrifugal and Coriolis-forces.

$f(t, q, \dot{q})$ is a vector consisting of all forces acting on the system due to both external excitations and force elements. B is the input matrix for those forces.

2.1 Vehicle dynamics

2.1.1 One-track vehicle model

The kinematics of the one-track vehicle model is depicted in Fig. 2.1. The basic assumption

Figure 2.1: One-track vehicle model

underlying this model is that the respective left and right wheels can be considered as one wheel in the middle of the vehicle. Consequently, no roll motion along the car's longitudinal axis (x-axis in Fig. 2.1) is considered. There is also no suspension kinematics included; front and rear suspension consist of linear spring/damper units, which connect the unsprung masses (=wheels) with the sprung mass (=body).

c_F denotes thereby the front suspension spring stiffness, d_F is the front suspension damping coefficient, and c_{tF} is the front tire vertical stiffness. c_R, d_R, and c_{tR} are the respective quantities for the rear axle. m and $\Theta \in \mathbb{R}^{3\times3}$ denote mass and rotational inertia of the body with respect to its center of gravity CG. The pairs m, Θ_F and m, Θ_R are the respective

inertial parameters for the front and the rear wheel. l_F and l_R are the horizontal distances of front and rear axles from CG. s is the height of CG above the wheel axes under static load.

The body's position is given by the position vector of CG $r_B := \begin{bmatrix} x & y & x \end{bmatrix}^T$. Its orientation is described by the yaw angle ψ and the pitch angle ϑ. z_F and z_R give the front and rear suspension deflections. φ is the steering angle at the front wheel, relative to the body. α_F and α_R are the absolute angle of rotation of the front and rear wheels, respectively.

From this model a set q of minimal coordinates can be determined:

$$q = \begin{bmatrix} x & y & z & \psi & \vartheta & \phi & z_F & z_R & \alpha_F & \alpha_R \end{bmatrix}^T \in \mathbb{R}^{10}. \tag{2.2}$$

Kinematics

The translational and rotational velocity vectors of the three bodies, in terms of the minimal coordinates q according to Eq. 2.2, can be calculated from the kinematic properties of the system, which are given in Fig. 2.1.

Let us define:

$$
\begin{aligned}
\omega_B &:= && \text{angular velocity of car body} \\
v_B &:= && \text{translational velocity of car body} \\
\omega_F &:= && \text{angular velocity of front wheel} \\
v_F &:= && \text{translational velocity of front wheel} \\
\omega_R &:= && \text{angular velocity of rear wheel} \\
v_R &:= && \text{translational velocity of rear wheel}
\end{aligned}
$$

and the Jacobians of the three bodies with respect to translation and rotation:

$$
\begin{aligned}
J_{Br} &:= \frac{\partial \omega_B}{\partial \dot{q}} &&: \text{body Jacobian (rotational)} \\
J_{Bt} &:= \frac{\partial v_B}{\partial \dot{q}} &&: \text{body Jacobian (translational)} \\
J_{Fr} &:= \frac{\partial \omega_F}{\partial \dot{q}} &&: \text{front wheel Jacobian (rotational)} \\
J_{Ft} &:= \frac{\partial v_F}{\partial \dot{q}} &&: \text{front wheel Jacobian (translational)} \\
J_{Rr} &:= \frac{\partial \omega_R}{\partial \dot{q}} &&: \text{rear wheel Jacobian (rotational)} \\
J_{Rt} &:= \frac{\partial v_R}{\partial \dot{q}} &&: \text{rear wheel Jacobian (translational)}
\end{aligned}
$$

The translational acceleration $\dot{v}_i; i = B, F, R$ and rotational acceleration $\dot{\omega}_i; i = B, F, R$ for each body can now be given assuming that none of the minimal coordinates is an explicit

function of time, see [5]:

$$\dot{v}_i = J_{it}\ddot{q} + \underbrace{\left(\sum_k \frac{\partial J_{it}}{\partial q_k}\dot{q}_k\right)\dot{q} + \sum_k \frac{\partial v_i - J_{it}\dot{q}}{\partial q_k}\dot{q}_k}_{=:\,\dot{v}_i^*} \quad ; \quad i = B, F, R$$

$$\dot{\omega}_i = J_{ir}\ddot{q} + \underbrace{\left(\sum_k \frac{\partial J_{ir}}{\partial q_k}\dot{q}_k\right)\dot{q} + \sum_k \frac{\partial v_i - J_{ir}\dot{q}}{\partial q_k}\dot{q}_k}_{=:\,\dot{\omega}_i^*} \quad ; \quad i = B, F, R$$

(2.3)

Kinetics

The mass matrix $M(q)$ in Eq. 2.1 is calculated using the Jacobians, see [1, 5]:

$$M(q) = J^T(q)\hat{M}J(q) \,, \tag{2.4}$$

where

$$\hat{M} = \begin{bmatrix} mI_3 & 0 & \cdots & & & 0 \\ 0 & m_F I_3 & & & & \\ & & m_R I_3 & & & \vdots \\ \vdots & & & \Theta & & \\ & & & & \Theta_F & 0 \\ 0 & & \cdots & & 0 & \Theta_R \end{bmatrix},$$

$$J(q) = \begin{bmatrix} J_{Bt} & J_{Ft} & J_{Rt} & J_{Br} & J_{Fr} & J_{Rr} \end{bmatrix}^T.$$

The vector $h(q, \dot{q})$ is

$$h(q, \dot{q}) = J^T(q) \begin{bmatrix} m\dot{v}_B^* \\ m_F\dot{v}_F^* \\ m_R\dot{v}_R^* \\ \Theta\dot{\omega}_B^* + \tilde{\omega}_B\Theta\omega_B \\ \Theta_F\dot{\omega}_F^* + \tilde{\omega}_F\Theta_F\omega_F \\ \Theta_R\dot{\omega}_R^* + \tilde{\omega}_R\Theta_R\omega_R \end{bmatrix} \tag{2.5}$$

Spring and damper forces in suspension and steering

Suspension forces act vertically between sprung and unsprung mass, see Fig. 2.2
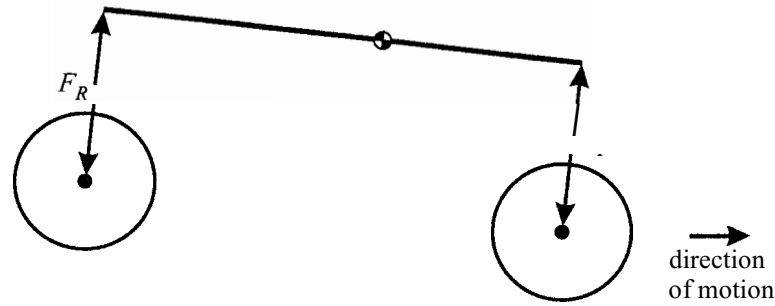
Figure **2.2:** Suspension forces

Assuming that front and rear suspension consist of linear spring/damper elements, the forces acting between body and wheel are linear functions of the suspension deflections z_F, z_R, and their velocities $\dot{z}_F$, $\dot{z}_R$:

$$
\begin{aligned}
F_F &= c_F z_F + d_F \dot{z}_F &&, && \text{frontsuspension} \\
F_R &= c_R z_R + d_R \dot{z}_R &&, && \text{rearsuspension}
\end{aligned}
\tag{2.6}
$$

2.2   External forces

The system Eq. 2.1 is excited by external forces, which are due to the contact between tire and road, aerodynamic forces, engine torque, and braking.

2.2.1   Tire model

The tires are the primary element to both carry the vehicle load and guide it along its track. The correct calculation of the contact forces between road and tire are therefore crucial in any simulation of vehicle behavior.

The aim is to find a mapping – preferably a force law – which relates the kinematic quantities describing the relative motion between tire and road to resulting tire forces and torques.

The tire model used in our context was first developed by Dugoff et al., [3]and is commonly called HSRI-model (Highway Safety Research Institute). Wiegner, [17], added the aligning torque, and Cffelmann included the influence of varying wheel load. A comprehensive overview over the so enhanced HSRI tire model can be found e. g. in [5, 6, 7].

Relative kinematics between tire and road

The motion of the tire is described by several kinematic quantities, which are depicted in Fig. 2.3:
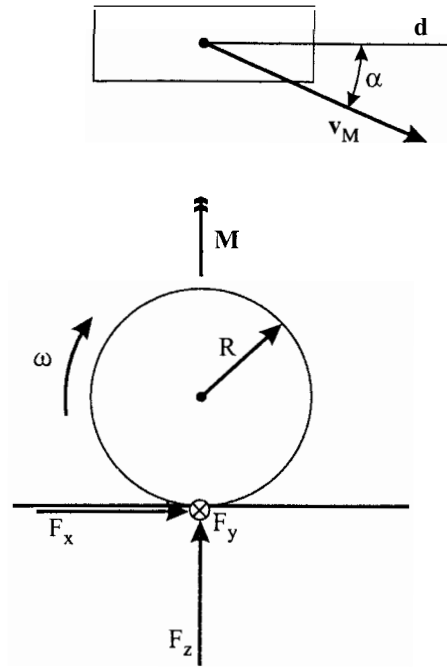
Figure 2.3: Relative kinematics and resulting contact forces between tire and road

Table 2.1: Kinematic quantities

$\boldsymbol{v}_M$: planar absolute velocity vector of the wheel center,

ω_M : angular velocity of the wheel around its axle,

γ : camber angle,

α : slip angle.

The longitudinal slip s between tire and road is defined as

$$
s = \begin{cases}
-\dfrac{||\boldsymbol{v}_M||\cos\alpha - R\omega}{||\boldsymbol{v}_M||\cos\alpha} & ; & ||\boldsymbol{v}_M||\cos\alpha \geq R\omega \ \text{brake} \\[3mm]
\dfrac{R\omega - ||\boldsymbol{v}_M||\cos\alpha}{R\omega} & ; & ||\boldsymbol{v}_M||\cos\alpha < R\omega \ \text{accelerate}
\end{cases}
\tag{2.7}
$$

The **modified** HSRI **tire model**

The following description of the modified HSRI tire model is an excerpt of all the literature mentioned above. It can be comprehended in detail e. g. in [5].

Given several parameters describing the mechanical properties of the tire:

With the kinematic quantities defined in Table 2.1 and in Eq. 2.7, the following intermediate quantities are calculated with F_z being the current vertical tire force, and F_{z0} being its static value:

Table 2.2: Tire properties

f_R	:	traction potential
k_R	:	traction coefficient
C_s	:	longitudinal slip stiffness
C_α	:	cornering stiffness
$2l_R$	:	length of tire contact patch
c_R	:	carcass lateral stiffness

The slip velocity v_s becomes

$$v_s = ||\boldsymbol{v}_M|| \cos\alpha \sqrt{s^2 + \tan^2\alpha}\,. \tag{2.8}$$

With this we can give an estimate for the coefficient of friction μ:

$$\mu = f_R \left(1 - k_R v_s\right)\,. \tag{2.9}$$

Using an intermediate quantity $\bar{s}$, where

$$\bar{s} = \frac{\sqrt{(C_s s)^2 + (C_\alpha \tan\alpha)^2}}{\mu\,(1-s)}\,. \tag{2.10}$$

the longitudinal tire force F_x, the lateral tire force F_y, and the resulting aligning torque M, see Fig. 2.3, can be calculated depending on the value of $\bar{s}$.

If $\bar{s} \le 0.5$, pure stiction is assumed between tire and road. The resulting forces and torques are:

$$
\begin{aligned}
F_x &= -C_s F_z \frac{s}{1-s} \\[2mm]
F_y &= C_\alpha F_z \frac{\tan\alpha}{1-s} \\[2mm]
M &= F_y \frac{l_R}{3} + F_x \left(\frac{4}{3} l_R \tan\alpha + \frac{F_y}{c_R}\right)\,.
\end{aligned}
\tag{2.11}
$$

If $\bar{s} > 0.5$, mixed sticking/sliding friction is assumed, and the resulting forces and torques are computed as:

$$
\begin{aligned}
F_x &= -C_s F_z \frac{s}{1-s} \frac{\bar{s} - 0.25}{\bar{s}^2} \\[2mm]
F_y &= C_\alpha F_z \frac{\tan\alpha}{1-s} \frac{\bar{s} - 0.25}{\bar{s}^2} \\[2mm]
M &= F_y l_R \left(\frac{12 - \frac{1}{\bar{s}^2}}{12 - \frac{3}{\bar{s}}} - 1\right) + F_x \left(\frac{l_R\left(\bar{s} - \frac{1}{3}\right)}{\bar{s}\left(\bar{s} - \frac{1}{4}\right)} \tan\alpha + \frac{F_y}{c_R}\right)\,.
\end{aligned}
\tag{2.12}
$$
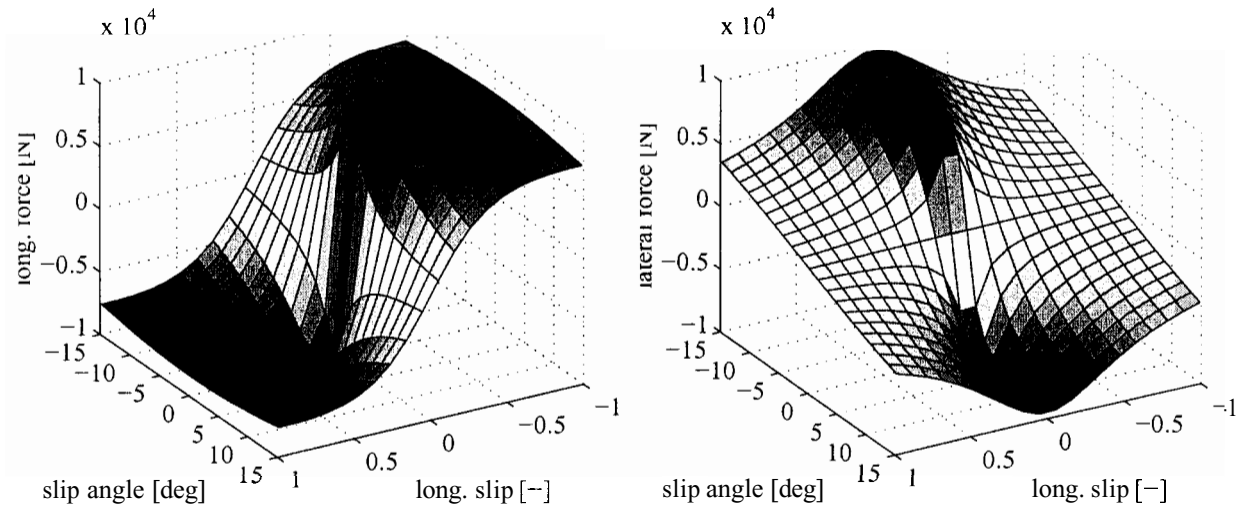
Figure 2.4: Characteristics of modified HSRI tire model

Eqs. 2.8 through 2.12 provide a mapping from kinematic quantities, which depend only on the system state, to forces acting on the system. Therefore, mechanically the modified HSRI tire model is a force law, which contains no inherent dynamics. For most cases, especially for small slip angles α, the resulting forces match well with measured data. There is, however, dynamics involved, particularly at fast transient movements. For further information on how such effects can be taken into account see [5, 6].

The characteristics resulting from the modified HSRI tire model are depicted in Fig. 2.4 for a typical tire/road combination.

2.2.2   Aerodynamic drag

Aerodynamic forces onto the vehicle result from both the vehicle movement and the wind speed. Assuming the vehicle's velocity vector at the center of gravity (CG) is $\boldsymbol{v}_B$, and the wind speed vector is $\boldsymbol{v}_W$, the relative motion between CG and air is expressed by the relative velocity vector

$$\boldsymbol{\Delta v} = \boldsymbol{v}_W - \boldsymbol{v}_B \,.\tag{2.13}$$

The horizontal aerodynamic force $\boldsymbol{F}_W$ onto the vehicle can then be approximated by

$$\boldsymbol{F}_W = c_W A \frac{\varrho}{2} ||\boldsymbol{\Delta v}||^2 \frac{\boldsymbol{\Delta v}}{||\boldsymbol{\Delta v}||} \,,$$

where c_W is the vehicle's coefficient of drag, A is its projected area, and ϱ denotes the density of air. The resulting aerodynamic force is assumed to act on the center of pressure, as depicted in Fig. 2.5.
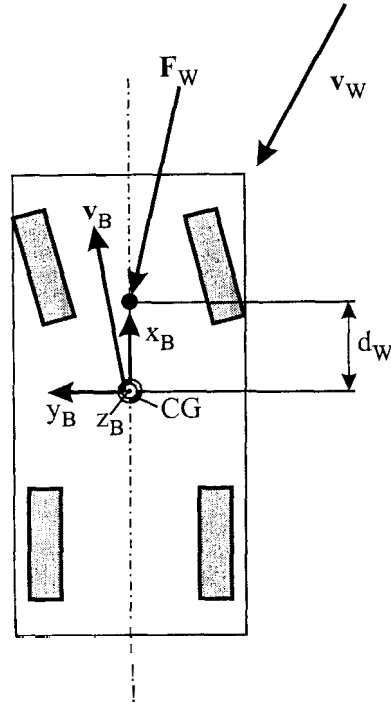
Figure 2.5: Wind velocities and resulting aerodynamic forces

2.2.3 Drive train dynamics

A simplified model of the vehicle's drive train has been built, see Fig. 2.6. The engine produces a torque M_e, depending on throttle position and engine speed. M_e is transmitted via clutch, gearbox, and differential gear to the wheels, which finally drive the vehicle.

A lookup table as shown in Fig. 2.7 is used to determine the stationary engine torque $\overline{M}_e$ as a function of engine speed n_e and throttle position ϱ. The transient behavior of the engine is then approximated by a first order dynamic filter of the form

$$\tau \dot{M}_e + M_e = \overline{M}_e, \tag{2.15}$$

where τ is a time constant.

The clutch operates as a discrete switch, which is manually operated by the driver:

$$i_{clutch} \quad \begin{cases} 0 & ; \quad \text{clutch open} \\ 1 & ; \quad \text{clutch engaged} \end{cases} \tag{2.16}$$

We assume further on a conventional manual gear shift with discrete, fixed gear ratios

$$i_{gear}(\eta) \quad ; \quad \eta = 1, \ldots, n_{gear}, \tag{2.17}$$
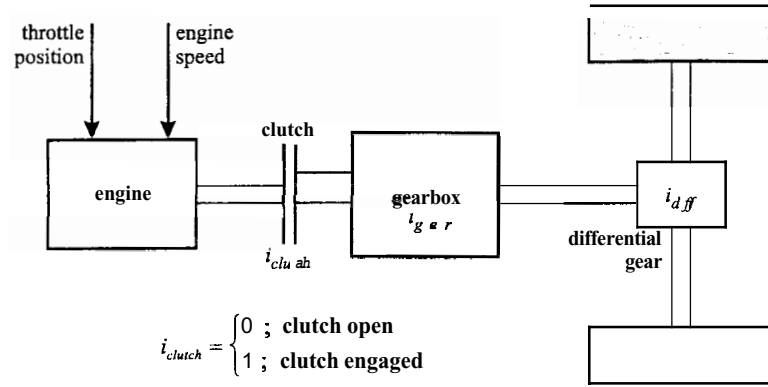
Figure 2.6: Vehicle drive train

which can be manually chosen by the driver.

The drive torque M_w transmitted to the wheel is then

$$M_w = i_{clutch} i_{gear} i_{diff} M_e \, .$$
(2.18)

2.3   Road parameterization

To keep the description of the road properties simple, a simple two-lane road with no inter-sections is assumed for all further investigations. However, the development of a driver model does not depend on that property. Thus, more complex traffic situations involving traffic at intersections can be implemented by adjusting the road parameterization appropriately.

According to Fig. 2.8 the middle line of the road is a space curve $r_R(s_R)$, defined in the inertial coordinate frame by its components $_I x_R(s_R)$, $_I y_R(s_R)$, and $_I z_R(s_R)$:

$$_I r_R(s_R) = \begin{pmatrix} _I x_R(s_R) \\ _I y_R(s_R) \\ _I z_R(s_R) \end{pmatrix} .$$
(2.19)

The distance s_R traveled from a zero position $r_{R0} = r_R(s_R = 0)$ acts as a curve parameter to describe the middle line.

Attached to the middle line are lane width $w_l(s_R)$ and sight distance $d_R(s_R)$.

In the numerical implementation $r_R(s_R)$ is given by discretely sampled position vectors, see Fig. 2.9

$$r_{Ri} = r_R(i \Delta s_R) \qquad ; \qquad i = 0, \ldots, n_R \, ,$$
(2.20)
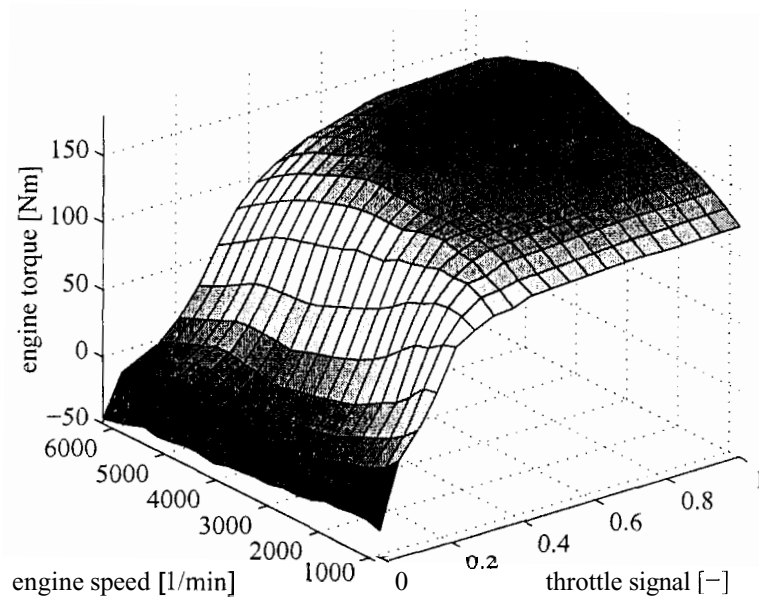
Figure **2.7:** Lookup table for stationary engine torque

with Δs_R being a (constant) small road length increment. Discretized values for lane width and sight distance are defined accordingly:

$$
\begin{aligned}
w_{li} &= w_l(i\Delta s_R) &&; & i &= 0,\ldots,n_R,\\
d_{Ri} &= d_R(i\Delta s_R) &&; & i &= 0,\ldots,n_R.
\end{aligned}
\tag{2.21}
$$

Vehicle's position relative to road

Starting from the road discretization (2.20), (2.21), a first order approximate for the vehicle's position and orientation with respect to the road's middle line can be stated.

We introduce the unity vectors $\boldsymbol{u_R}$ along the road middle line and $\boldsymbol{u_B}$ along the vehicle's middle axis

$$
\begin{aligned}
\boldsymbol{u}_R &= \frac{\boldsymbol{r}_{R(i+1)} - \boldsymbol{r}_{Ri}}{\left|\boldsymbol{r}_{R(i+1)} - \boldsymbol{r}_{Ri}\right|}\\[2mm]
{}_I\boldsymbol{u}_B &= \begin{pmatrix} \cos\psi \\ \sin\psi \end{pmatrix}.
\end{aligned}
\tag{2.22}
$$

The distance $s_R(t)$ traveled by the vehicle with respect to the road's middle line at the time t is

$$
s_R(t) = i\Delta s_R + \Delta s
\tag{2.23}
$$
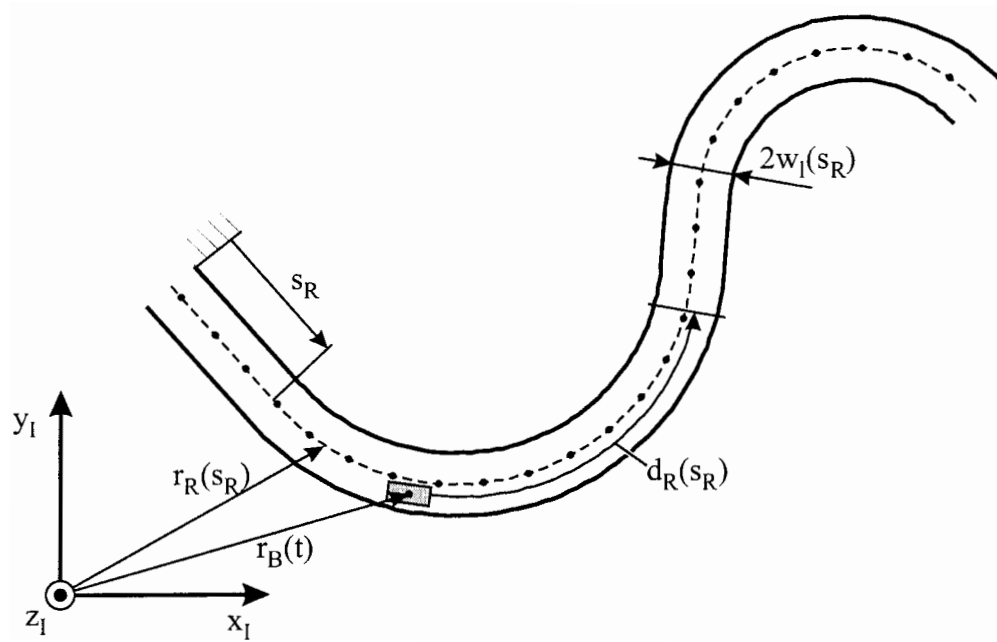
Figure *2.8:* Road parameterization

$$\Delta s = \boldsymbol{u}_R^T \left(\boldsymbol{r}_B(t) - \boldsymbol{r}_{Ri} \right) \ .$$

The lateral deviation $\Delta w(t)$ from the middle line is

$$\Delta w(t) = \boldsymbol{n}_R^T \left(\boldsymbol{r}_B(t) - \boldsymbol{r}_{Ri} \right) \qquad \boldsymbol{n} = \begin{pmatrix} 0 & -1 \\ 1 & 0 \end{pmatrix} \boldsymbol{u}_R \qquad (2.24)$$

The vehicle's orientation $\Delta\psi(t)$ relative to the road is

$$\Delta\psi(t) = \psi(t) - \arctan \frac{u_{R,2}}{u_{R,1}} . \qquad (2.25)$$
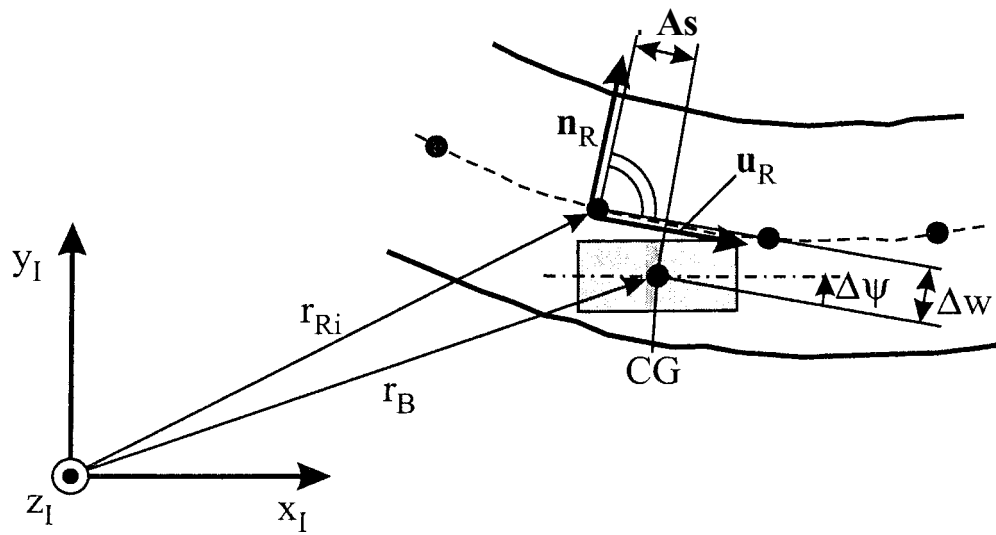
Figure **2.9:** Discretization of road description; vehicle's relative position and orientation

Chapter **3**

The driver's prediction models

Apparently human drivers have the ability to predict the vehicle future trajectory to a certain extend. The accuracy of this forecast depends strongly on the driver's experience. In order to accomplish this task, the driver needs a picture of the plant. In this project several different prediction models are assumed accordingly to the different levels of driving skills. All models have in common that they have simplified lateral and longitudinal dynamics. The simplest model consists of a mass point model without any drive train dynamics. The most complex model used in this simulation is a one track model which takes into account drive train dynamics as well as tire saturation.

Single point mass model with static drive train and linear engine characteristics

This simplified model can be related to a beginner, but also skilled drivers are supposed to employ this kind of model in uncritical situations, in which the very simplified vehicle dynamics is sufficient to plan a sensible trajectory. This model applies by moderate velocities and small lateral acceleration.

The driver assumes a stationary engine characteristic. The engine torque M_e is piecemeal proportional to the throttle position ϱ and does not depend on the engine speed. Beginners are not supposed to have a very accurate image of the vehicle's longitudinal dynamics. Therefore, a very simple engine model is sufficient. This engine model can also be used by skilled drivers in relaxed driving situations, such as undisturbed highway cruising or driving in low-density traffic with a moderate speed. In these cases it is not important to describe precisely the longitudinal behavior of the vehicle.

Single point mass model with dynamic drive train and linear engine characteristics

This engine model represents a more accurate model of the vehicle engine and, therefore, a better image of the vehicle's longitudinal behavior. This model becomes important, when the driver has to estimate the vehicle's longitudinal acceleration, e.g. if he wants to overtake within a certain distance or tries to merge into the traffic from a lane with lower speed.

The model can be related to a beginner with little driving experience, so that he is able to foresee better the vehicle's future longitudinal behavior.

In this case the static engine torque $\overline{M}_e$ is passed through a PT1 filter in order to describe the engine's dynamics of 1st order.

Single point mass model with static drive train and field-interpolated engine characteristics

Drivers with more driving experience are supposed to be able to describe the engine's behavior better than just with a piecemeal linear engine torque solely dependent on the throttle position. They also take into account the dependency of the engine torque on the engine speed. Therefore: the engine is modeled not only as a function of the throttle position ϱ but also as a function of the engine speed n_e.

This model is applicable in the same situations as the static engine torque only as a function of ϱ, like e.g. highway cruising and undisturbed driving in general. The field interpolation have exclusively experienced drivers though, who have a better picture of the vehicle in general. Therefore, they also have a better image of the engine torque characteristics.

Single point mass model with dynamic drive train and field-interpolated engine characteristics

If precise longitudinal forecasts become important for the driver' drive train dynamics must be included. Experienced drivers who need to accelerate very quickly in order e.g. to overtake or merge into traffic are supposed to use this model. It takes drive train dynamics into account as well as a better torque representation. The engine torque is a function of the throttle position ϱ and of the engine speed n_e. In order to describe the engine's dynamic behavior, the static engine torque is passed through a PT1 filter.

One track model with linear tire model and dynamic drive train with field-interpolated engine characteristics

With increasing speed, or during fast maneuvers a precise imagination of the vehicle dynamics becomes more important. In this respect the one track model gives a better description of the vehicle than just a mass point model. So does the one track model take into account dynamics around the yaw axis, which is neglected in the single mass point models. In order to precisely describe the vehicle's longitudinal behavior, a dynamic engine model (1st order dynamics) is used. In addition, the used engine model is a function of the throttle position ϱ and the engine speed n_e. With higher velocities it is also easily possible to exceed the tire saturation forces which leads to skidding and following from that to a possible loss of the vehicle's control. Therefore, the driver must take tire saturation into consideration. In this prediction model a linear tire model is used. Following from that it is only possible for the driver to estimate roughly the tire saturation. Driver who are not very familiar with extreme driving maneuvers may have such a picture of the tire saturation forces. However they have enough experience in order to have a good representation of the vehicle's dynamics.

One track model with force saturation tire model and dynamic drive train with field-interpolated engine characteristics

In this research project it is assumed that very experienced drivers have such a imagination of their vehicle. It represents a better dynamic picture of the vehicle due to a one track model instead of mass point model. These drivers also have a refined picture of the vehicle's longitudinal behavior which is described by a 1st order dynamic drive train. The engine characteristic is dependent on the throttle position and the engine speed. In order to drive safely even in demanding situations they have a precise imagination of the tire saturation. Therefore, they can make use of the entire saturation spectrum without running the risk of unintentionally exceeding the possible tire forces.

Though it must be mentioned that this vehicle still does not include roll motion along the longitudinal axis which is important for the transient behavior of the vehicle by drastic changes of direction. Vertical aerodynamic forces which become crucial at very high speed are also not considered in this model. In this cases, the used prediction model is not valid.

3.1   General model description

All the models mentioned above have the following underlying main assumptions.

- *o* Contact forces between tire and road on both, left and right vehicle sides are equal (one track assumption).

- ● Aerodynamic forces are proportional to the square of the vehicle's velocity, and act solely in the opposite direction of the vehicle's longitudinal axis.

- ● The driving torque at the wheel is dependent on the used engine model. The engine torque is then multiplied by the present gear ratio, see chapter 3.1.2.

- *o* No roll motion along the longitudinal axis of the vehicle.

These assumptions apply for the single mass point models as well as for the one track models, Details in respect of the different models are described in chapter 3.2.1 and 3.3.1. Further common features of the used vehicle models are described in the chapters 3.1.1 to 3.1.4.

3.1.1   Longitudinal input ϱ

The vehicle is accelerated by a driving force, generated by the engine and the brake discs, respectively. One can assume that a driver does not hit accelerator and brake pedal at the same time.

Thus, a system input $\varrho \in [-1{:}1]$ is introduced. The throttle signal ϱ is zero, if the driver neither accelerates nor brakes. $\varrho = -1$, if the driver is braking with full force and $\varrho = +1$
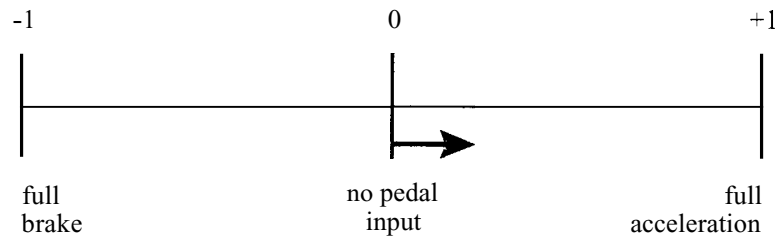
Figure 3.1: Definition of the longitudinal input signal ϱ.

indicates a fully opened throttle. The accelerator and brake pedal signals ϱ^+ and ϱ^- can be uniquely extracted from ϱ

$$
\begin{aligned}
\varrho^+ &= \tfrac{1}{2}\varrho(1 + \operatorname{sgn}\varrho) \quad \text{accelerator signal} \\
\varrho^- &= \tfrac{1}{2}\varrho(1 - \operatorname{sgn}\varrho) \quad \text{brake signal} \ .
\end{aligned}
\tag{3.1}
$$

See also Fig. 3.2.
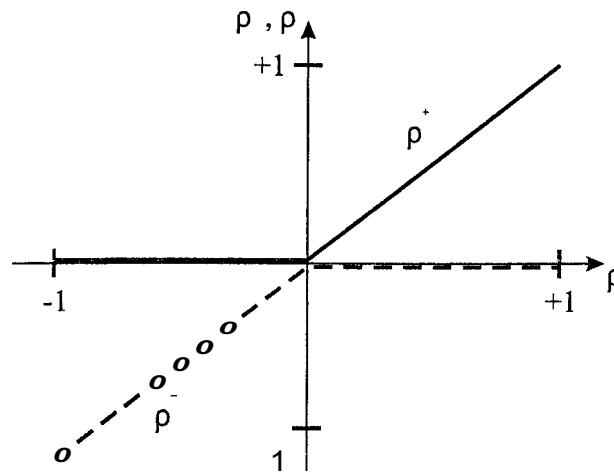
Figure **3.2:** Extraction of ϱ^+ and ϱ^- from ϱ.

3.1.2 Driving torque M_a

In order to accelerate the vehicle, the input signal ϱ^+ has to be converted into a driving torque M_a, which acts directly on the wheels. Therefore, the acceleration is depended on the used engine and the transmission. The resulting driving torque $M_a(\varrho^+)$, propelling the vehicle is

$$
M_a(\varrho^+) = i_{clutch} i_{gear}(\eta) i_{diff} M_e(\varrho^+).
\tag{3.2}
$$

i_{diff} is the ratio of the differential gear, and $i_{gear}(\eta)$ denotes the gear ratio depending on the current gear η. i_{clutch} gives the current clutch position and indicates therefore, if the engine torque is transmitted or not.

$$i_{clutch} = \begin{cases} 0 & ; \quad \text{clutch open} \\ 1 & ; \quad \text{clutch engaged} \end{cases} \tag{3.3}$$

The engine torque $M_e(\varrho^+)$ is dependent on the used engine type and can also be influenced by the current engine speed.
In case of the one track model the driving torque has to be distributed on the front wheel and rear wheel. Therefore, a distribution factor ε has to be introduced

$$\begin{aligned} M_{af} &= (1-\epsilon)M_a \\ M_{ar} &= \epsilon M_a \, . \end{aligned} \tag{3.4}$$

M_{af} is the driving torque transmitted to the front wheel and M_{ar} is the driving torque transmitted to the rear wheel.

$$\epsilon = \begin{cases} 0 & ; \quad \text{front wheel drive} \\ 0 < \epsilon < 1 & ; \quad 4 - \text{wheel drive} \\ 1 & ; \quad \text{rear wheel drive} \end{cases} \tag{3.5}$$

Static engine torque $\overline{M}_e(\varrho^+)$ as linear function of ϱ^+
A static engine torque is used in driving situations where the longitudinal behavior is not crucial to fulfill the driving task, e.g. highway cruising with an almost constant speed. Beginners who do not have any experience may also use this kind of engine model to describe the longitudinal behavior of their vehicle. The engine torque is calculated as a piecemeal proportional function of the throttle position ϱ^+. The engine characteristics is depicted in Fig. **3.3**

$$\overline{M}_e(\varrho^+) = \begin{cases} a_{M1}\varrho^+ + b_{M1} & ; \quad \varrho^+ \leq \varrho_0 \\ a_{M2}\varrho^+ + b_{M2} & ; \quad \varrho^+ > \varrho_0 \end{cases} \tag{3.6}$$

Dynamic engine torque $M_e(\overline{M}_e(\varrho'))$
A dynamic engine model becomes important where a precise prediction of the vehicle's longitudinal behavior is crucial to fulfill successfully the current driving task, e.g. overtaking. Only experienced drivers are supposed to have such a precise picture of the vehicle's longitudinal dynamics. The static engine torque $\overline{M}_e(\varrho^+)$ is passed through a PT1 filter in order to represent the dynamic behavior of the engine (1st order dynamics). T_m is the time constant of the transient engine behavior.

$$T_m\dot{M}_e(\varrho^+) + M_e(\varrho^+) = \overline{M}_e(\varrho^+) \, . \tag{3.7}$$
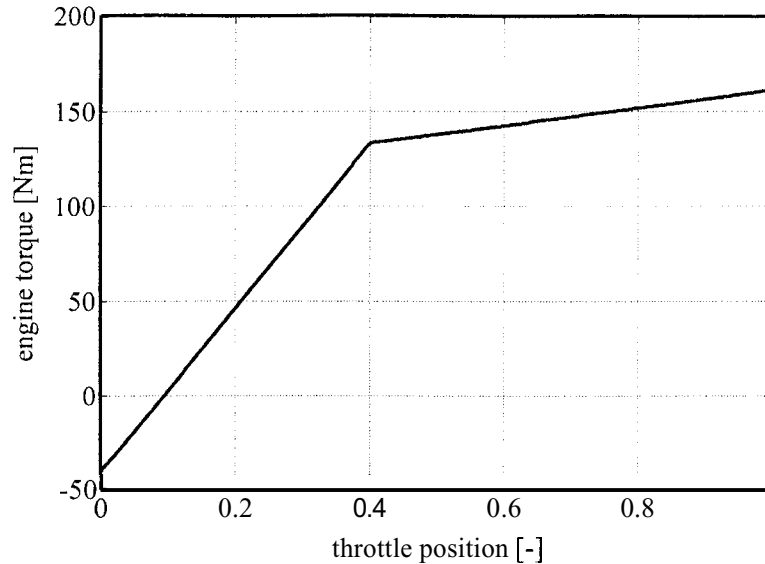
Figure **3.3:** Static engine torque $\overline{M}_e$ as function of throttle position ϱ^+.

Static engine torque $\overline{M}_e(\varrho^+, n_e)$ as function of ϱ^+ and engine speed n_e
This engine model is supposed to be used by the driver in the same situations as the static engine model which is solely dependent on the throttle input ϱ^+. Therefore, in driving situations where a precise knowledge about the vehicle's longitudinal behavior is not important to fulfill the driving task. The static engine torque is determined by a lookup table, see Fig. 3.4. Thus, the engine torque depends on the throttle position ϱ^+ and the engine speed n_e. The used algorithm to extract the static engine torque $\overline{M}_e(\varrho^+, n_e)$ is based upon geometrical calculations. The area E which is defined through data points from the given engine characteristics $M_{0,kj}(\varrho_{0,k}, n_{e0,j})$, $k, j = 1,..., 3$ is intersected with the line $g(\varrho^+, n_e)$, which is defined through the current throttle position and engine speed. ϱ and n_e lie within the area of the orthogonal projection of E. Therefore, we can determine the static engine torque as

$$\overline{M}_e = E(M_{0,kj}) \cap g(\varrho^+, n_e) \,, \tag{3.8}$$

see also Fig. 3.4.

Dynamic engine torque $M_e(\overline{M}_e(\varrho^+, n_e))$
This engine model is supposed to be used by the driver, if the driving situation requires a precise picture of the vehicle's longitudinal dynamics, e.g. in order to overtake or merge into a lane with faster traffic. The static engine torque $\overline{M}_e(\varrho^+, n_e)$ is passed through a PT1 filter in order to represent a dynamic behavior of the engine (1st order dynamics). T_m is the time constant' of the transient engine behavior.

$$T_m \dot{M}_e(\varrho^+, n_e) + M_e(\varrho^+, n_e) = \overline{M}_e(\varrho^+, n_e) \,. \tag{3.9}$$
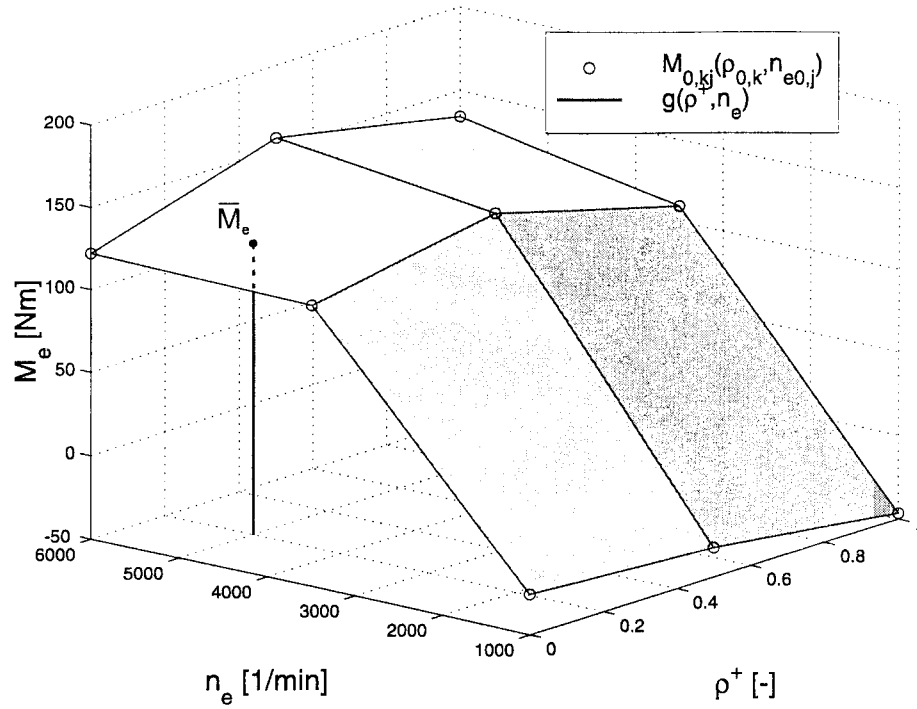
Figure 3.4: Static engine torque $\overline{M}_e$ as function of throttle position ϱ^+ and engine speed n_e.

3.1.3   Brake torque M_b

For braking the input signal ϱ^- is translated into the torque M_b, which is directly applied to the wheels. K_{brake} is a proportional factor relating the driver's input signal ϱ^- to a brake torque. The equation for the resulting force is

$$M_b(\varrho^-) = K_{brake}\varrho^- \text{sgn} v \,. \tag{3.10}$$

v denotes the vehicle's velocity in the longitudinal direction. It is either 9 (single mass point model) or x (one track model). In case of a one track model, the brake torque has to be transmitted to the front wheel and rear wheel. Therefore, a distribution factor ζ is introduced.

$$\zeta = \begin{cases} 0 & ; \quad \text{rear brake} \\ 0 < \zeta < 1 & ; \quad \text{distributed brake torque} \\ 1 & ; \quad \text{front brake} \end{cases} \tag{3.11}$$

The equations for the front brake torque M_{bf} and the rear brake torque M_{br} are

$$\begin{aligned} M_{bf} &= \zeta M_b \\ M_{br} &= (1 - \zeta)M_b \,. \end{aligned} \tag{3.12}$$

3.1.4 Aerodynamic force F_W

The employed force law for the aerodynamic force is

$$F_W(v) = -c_W A_W \frac{\rho_W}{2} v^2 . \tag{3.13}$$

c_W is thereby the aerodynamic drag coefficient, A_W denotes the projected area of the vehicle, and ρ_W is the density of air. v is the vehicle speed in longitudinal driving direction. Therefore, it is in case of the single mass point model $v = \dot{s}$ and in case of the one track model $v = \dot{x}$. It is assumed, that all aerodynamic forces act solely in opposite direction of the vehicle's longitudinal axis.

3.2 Single mass point model

This class of prediction models represents only a very simplified vehicle dynamics. The driver is supposed to use this class of vehicle models in situations where a exact determination of the vehicle's dynamics and tire forces is not crucial to fulfill successfully the current driving task, e.g. highway cruising with almost constant speed and driving on roads with big curve radii. But also beginners who do not have the experience yet in order to have a very precise image of the vehicle's dynamics are also supposed to use this kind of prediction model.

3.2.1 Model description

Some of the basic assumptions underlying this prediction model were already mentioned in chapter 3.1. The specific assumptions, which only apply for the single mass point prediction models. are:

- Only slow yaw motions are allowed, dynamics around yaw axis is neglected:

- direction of motion coincides with vehicle's longitudinal axis;

- kinematic rolling constraints at wheels are fulfilled.

In this vehicle representation, the vehicle mass is concentrated at a certain point. which is called the *center of gravity (CG)*.The vehicle's path is described by the CG's trajectory. The vehicle's orientation ψ is assumed to be tangential to the CG trajectory. With $\dot{s}(t)$ being the momentary travel speed along the trajectory at time t, the traveled distance $s(t)$ acts as a path parameter.
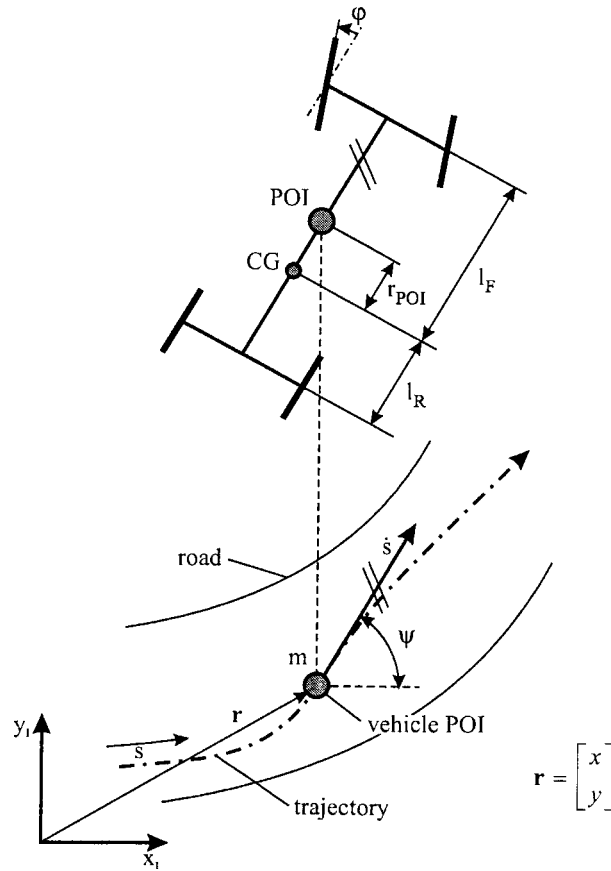
Figure **3.5:** Vehicle as a mass point – CG: center of gravity

3.2.2   **Yaw** angle

The trajectory curvature $K(t)$ at time t can be calculated from the steering angle $\varphi(t)$ and the vehicle's wheelbase $l_R + l_F$, see Fig. 3.5

$$K(\varphi) = \frac{d\psi}{ds} = \frac{\tan\varphi}{\sqrt{(l_R + l_F)^2 + (l_R)^2 \tan^2\varphi}} \,. \tag{3.14}$$

Following from that we can solve Eq. 3.14 in respect to the vehicle's yaw angle ψ and write

$$\psi = \int K(\varphi(t))\frac{ds(t)}{dt}dt = \int K(\varphi(t))\dot{s}(t)dt \,, \tag{3.15}$$

with $\dot{s}(t)$ being the momentary travel speed along the vehicle's trajectory.

3.2.3 Equations of motion

By introducing a state vector z and by considering the assumptions mentioned above, we obtain the following sets of differential equations of motion .

Without drive train dynamics

In this case is the has the introduced state-space vector z the form

$$z = \begin{bmatrix} \dot{s} & \psi & x & y \end{bmatrix}^T .$$
(3.16)

Therefore, is the set of differential equations as follows

$$z = \begin{vmatrix} \frac{1}{m}\left(\frac{1}{R}\left(M_a(\varrho^+) + M_b(\varrho^-)\right) - F_W\right) \\[2ex] K(\varphi)\dot{s} \\[2ex] \dot{s}\cos\psi \\[2ex] \dot{s}\sin\psi \end{vmatrix} = g_1\left(z(t,p),p\right),$$
(3.17)

with M_a from Eq. 3.2 and M_b from Eq. 3.10. The term F_W is according to Eq. 3.13 and $K(\varphi)$ is from Eq. 3.14.

With drive train dynamics

If drive train dynamics are included the state vector z has the following form! because the engine torque has to be integrated as well.

$$z = \begin{bmatrix} M_e & \dot{s} & \psi & x & y \end{bmatrix} .$$
(3.18)

The equations of motion written in state-space form are

$$z = \begin{vmatrix} -\frac{1}{T_m}M_e + \frac{1}{T_m}\overline{M}_e \\[2ex] \frac{1}{m}\left(\frac{1}{R}\left(M_a(M_e) + M_b(\varrho^-)\right) - F_W\right) \\[2ex] K(\varphi)\dot{s} \\[2ex] \dot{s}\cos\psi \\[2ex] \dot{s}\sin\psi \end{vmatrix} = g_1\left(z(t,p),p\right),$$
(3.19)

with $\overline{M}_e$ either from Eq. 3.6 or determined by a lookup table, see Fig. 3.4 and M_a from Eq. 3.2. M_b is from Eq. 3.10, F_W from Eq. 3.13 and $K(\varphi)$ is from Eq. 3.14.

3.3   One **track** model

With increasing speed, or driving difficult maneuvers a precise imagination of the vehicle dynamics becomes more important. In this respect the one track model gives a better description of the vehicle than just a mass point model. In addition, with higher velocities it is easily possible to exceed the tire saturation forces which leads to skidding and following from that to a possible loss of the vehicle control. Therefore, the driver must take tire saturation into consideration. Experienced drivers are supposed to use this kind of vehicle model e.g. while cornering with high speed.

3.3.1   Model description

One specific assumption in addition to the general assumptions described in chapter 3.1 apply for the one track models.

- In spite of rolling constraints at the wheels, a force law is employed to calculate the tire saturation. Either a linear tire model or a tire model with force saturation.

See Fig. 3.6 for the model's kinematics

m and Θ denote mass and rotational inertia of the body with respect to its center of gravity CG. Θ_F and Θ_R are the the rotational inertia of the front and the rear wheel. l_F and l_R are the horizontal distances of the front and rear axles from the CG.

The body's position is given by the position vector of CG, $r_B := \begin{bmatrix} x & y \end{bmatrix}^*$. The orientation of the vehicle body is described by the yaw angle ψ. φ is the steering angle at the front wheel, relative to the body and g is the gravitational acceleration.

3.3.2   Tire models

The underlying quantities in order to determine the tire forces are the longitudinal tire slip s and the slip angle α. The are calculated similarly for the linear tire model and the HSRI tire model. The index $_f$ denotes the front. tire and $_r$ the rear tire. The definition of the
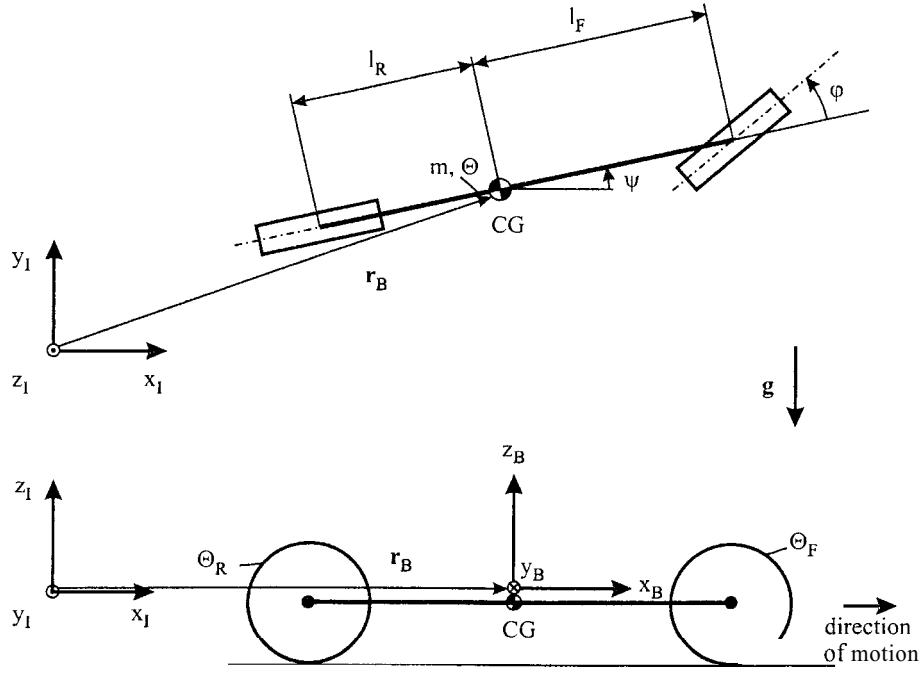
Figure 3.6: Vehicle as a one track model – CG: center of gravity

longitudinal slip is

$$
s_f = \left|
\begin{array}{ll}
-\dfrac{R\omega_f - \dot{x}\cos\varphi + \left(\dot{y} + l_f\,\dot{\psi}\right)\sin\varphi}{R\omega_f} & \text{driving slip} \\[2mm]
\quad \text{if } \left(\dot{x}\cos\varphi + \left(\dot{y} + l_f\,\dot{\psi}\right)\sin\varphi < R\omega_f\right) & \\[6mm]
\dfrac{\dot{x}\cos\varphi + \left(\dot{y} + l_f\,\dot{\psi}\right)\sin\varphi - R\omega_f}{\dot{x}\cos\varphi + \left(\dot{y} + l_f\,\dot{\psi}\right)\sin\varphi} & \text{brake slip.} \\[2mm]
\quad \text{if } \left(\dot{x}\cos\varphi + \left(\dot{y} + l_f\,\dot{\psi}\right)\sin\varphi \geq R\omega_f\right) &
\end{array}
\right.
\tag{3.20}
$$

$$
s_r = \left|
\begin{array}{ll}
-\dfrac{R\omega_r - x}{R\omega_r} \quad, & \dot{x} < R\omega_f \ \text{drivingslip} \\[4mm]
\dfrac{X - R\omega_r}{\dot{x}} & x \geq R\omega_f \ \text{brakeslip.}
\end{array}
\right.
\tag{3.21}
$$

R is the tire radius which is equal for the front wheel and rear wheel. ω is the rotational speed of the tires.

α_f and α_r are the slip angles for the front or rear tire, respectively. The slip angles have the following definition

$$\alpha_f = \varphi - \arctan \frac{-\dot{y} + l_f \dot{\psi}}{\dot{x}}$$

$$\alpha_r = -\arctan \frac{\dot{y} - l_r \dot{\psi}}{\dot{x}},$$

$$(3.22)$$

where φ is the steering angle and $\dot{x}$ and $\dot{y}$ are the longitudinal and lateral velocity of the vehicle's CG, respectively. $\dot{\psi}$ is the vehicle's yaw rate. See Fig. 3.6 for the vehicle's kinematics.

Linearized tire model

Driving situations where' only small tire slip and small slip angles occur, a linear tire model is sufficient for calculating the tire forces.

The linear tire model is based upon the HSRI-tire model in chapter 2.2.1. The kinematics are depicted in Fig. 2.3. The longitudinal tire stiffness coefficient C_{lo} and the lateral tire stiffness coefficient C_{la} are the local gradients of the HSRI tire model characteristics, see Fig. 2.4. The gradients refer to the characteristics where the slip s is zero.

It is also possible to use the linear tire coefficients in order to take further effects e.g. the suspension system into account [5]. The resulting linear longitudinal tire forces are

$$\overline{F}_{xf} = -\kappa_f C_{lo} s_f$$
$$\overline{F}_{xr} = -\kappa_r C_{lo} s_r$$

$$(3.23)$$

s_f and s_r, respectively, is the longitudinal slip for the front and rear tire, see Ey. 2.7. κ indicates whether the slip is driving slip ($\kappa = -1$) or brake slip ($\kappa = 1$). C_{lo} is the longitudinal tire stiffness.

$$\begin{aligned} \kappa &= -1 & &\text{factor for driving slip} \\ \text{n} &= 1 & &\text{factor for brake slip} \end{aligned}$$

$$(3.24)$$

The lateral tire forces can be described with the following equations

$$\overline{F}_{yf} = C_{la} \tan \alpha_f$$
$$\overline{F}_{yr} = C_{la} \tan \alpha_r,$$

$$(3.25)$$

where C_{la} denotes the lateral tire stiffness and α_f, a, are the slip angles at the front and rear wheel, respectively.

Tire model with force saturation

If the tire slip and the tire slip angle become bigger, a linear tire model is not precise enough anymore to describe the actual tire forces, e.g. while cornering with high speed were the tire forces can be pushed to the limit of tire saturation. Therefore, a more complex model is used to determine the tire saturation.

The tire model used for this prediction model is similar to the tire model used for the plant model explained in chapter 2.2.1. However the tire model used for the prediction model is simplified in respect, that no aligning torque is calculated and that the vertical force F_z is static. The kinematics of the general HSRI tire model is depicted in 2.4. In the following are quantities for the front wheel are denoted with the index f and for the rear wheel with index r. The reduced set of equations is as follows.

The static vertical forces F_{zf} and F_{zr} are calculated as

$$\begin{aligned} F_{zf} &= mg\frac{l_r}{l_f+l_r} \\ F_{zr} &= mg\frac{l_f}{l_f+l_r}, \end{aligned}$$

(3.26)

with m is the vehicle mass g the gravitational acceleration and l_f and l_r the distance of the front and rear axle to the CG. The slip velocities v_{sf} and v_{sr} are defined as

$$\begin{aligned} v_{sf} &= (\dot{x}\cos\varphi + (\dot{y}+l_f\dot{\psi})\sin\varphi)\sqrt{s^2+\tan^2\alpha} \\ v_{sr} &= \dot{x}\sqrt{s^2+\tan^2\alpha}, \end{aligned}$$

(3.27)

The term $(\dot{x}\cos\varphi + (\dot{y}+l_f\dot{\psi})\sin\varphi)$ represents the planar absolute velocity of the axle of the front wheel in rolling direction. Similar *to* that, $\dot{x}$ denotes the planar absolute velocity of the axle of the rear wheel in rolling direction. In addition with the coefficients of friction μ_f and μ_r

$$\begin{aligned} \mu_f &= f_R(1-k_R v_{sf}) \\ \mu_r &= f_R(1-k_R v_{sr}), \end{aligned}$$

(3.28)

and the intermediate quantities $\bar{s}_f$ and $\bar{s}_r$

$$\begin{aligned} \bar{s}_f &= \frac{\sqrt{(C_s s_f)^2+(C_\alpha\tan\alpha_f)^2}}{\mu_f(1-s_f)} \\ \bar{s}_r &= \frac{\sqrt{(C_s s_r)^2+(C_\alpha\tan\alpha_r)^2}}{\mu_r(1-s_r)}, \end{aligned}$$

(3.29)

is it possible to calculate the tire forces for the front and rear wheel.

If pure static friction is assumed ($\overline{s_f} \leq 0.5$; $\overline{s_r} \leq 0.5$) the lateral and longitudinal forces for the front and rear tire are

$$
\begin{aligned}
F_{xf} &= -\kappa_f C_s F_{zf} \frac{s_f}{1 - s_f} \\
F_{yf} &= C_\alpha F_{zf} \frac{\tan \alpha_f}{1 - s_f}
\end{aligned}
\tag{3.30}
$$

$$
\begin{aligned}
F_{xr} &= -\kappa_r C_s F_{zr} \frac{s_r}{1 - s_r} \\
F_{yr} &= C_\alpha F_{zr} \frac{\tan \alpha_r}{1 - s_r} \, .
\end{aligned}
\tag{3.31}
$$

If mixed static/sliding friction is assumed ($\overline{s_f} > 0.5$; $\overline{s_r} > 0.5$), the resulting forces for the front tire and rear tire can be calculated as

$$
\begin{aligned}
F_{xf} &= -\kappa_f C_s F_{zf} \frac{s_f}{1 - s_f} \frac{\overline{s_f} - 0.25}{\overline{s_f}^2} \\
F_{yf} &= C_\alpha F_{zf} \frac{\tan \alpha_f}{1 - s_f} \frac{\overline{s_f} - 0.25}{\overline{s_f}^2}
\end{aligned}
\tag{3.32}
$$

$$
\begin{aligned}
F_{xr} &= -\kappa_r C_s F_{zr} \frac{s_r}{1 - s_r} \frac{\overline{s_r} - 0.25}{\overline{s_r}^2} \\
F_{yr} &= C_\alpha F_{zr} \frac{\tan \alpha_r}{1 - s_r} \frac{\overline{s_r} - 0.25}{\overline{s_r}^2} \, .
\end{aligned}
\tag{3.33}
$$

The intermediate tire quantities $\mathbf{sf}$ and $\mathbf{sf}$ are from Eq. 3.29. The factor κ is according to Eq. 3.24. C_s denotes the longitudinal slip stiffness and C_α the cornering stiffness. The slip angle α_f and α_r is from Eq. 3.22 and the tire slip s_f and s_r from Eq. 3.20 and Eq. 3.21, respectively. The vertical tire forces F_{zf} and F_{zr} are calculated according to Eq. 3.26.

3.3.3 Equations of motion

The state-space vector describing the one track model is

$$
z = \begin{bmatrix} \dot{x} & \dot{y} & \dot{\psi} & \omega_f & \omega_r & \dot{M_e} \end{bmatrix}^T
\tag{3.34}
$$

Following from that, the differential equations describing the motion of the one track model are in state-space form

$$
\dot{z} = \begin{bmatrix}
\frac{1}{m}\left(F_{xf}\cos\varphi + F_{xr} - F_{yf}\sin\varphi - F_W\right) + \dot{y}\dot{\psi} \\[2mm]
\frac{1}{m}\left(F_{xf}\sin\varphi + F_{yf}\cos\varphi + F_{yr}\right) - \dot{x}\dot{\psi} \\[2mm]
\frac{1}{\Theta}\left(F_{xf}l_f\sin\varphi + F_{yf}l_f\cos\phi - F_{yr}l_r\right) \\[2mm]
\frac{1}{\Theta_f}\left(M_{af}(M_e) + M_{bf} - RF_{xf}\right) \\[2mm]
\frac{1}{\Theta_r}\left(M_{ar}(M_e) + M_{br} - RF_{xr}\right) \\[2mm]
-\frac{1}{T_m}M_e + \frac{1}{T_m}\overline{M}_e\left(\varrho^+, n_e\right)
\end{bmatrix} = g_1\left(z(t,p), p\right) . \tag{3.35}
$$

The forces F_x and F_y are dependent on the used tire model. If a linear tire model is used the equations Eq. 3.23 to Eq. 3.25 describe the tire forces. In the case of a tire model with force saturation F_x and F_y are calculated according to Eq. 3.30 to Eq. 3.32.

The driving torques M_{af} and M_{ar} are defined by Eq. 3.2 to Eq. 3.5. The static engine torqe $\overline{M}_e$ is from Eq. 3.8. The dynamic engine behavior is according to Eq. 3.9.

The braking torques M_{bf} and M_{br} are related linearly to the driver's input signal ρ^-. They arc calculated according to the equations from Eq. 3.10 to Eq. 3.12.

The aerodynamic force F_W is proportional to the square of the velocity and is from Eq. 3.13.

Chapter 4

Analytical gradients of prediction models

In order to solve the optimizing problem in chapter 5 it is important not just to compute the solution of the respective state vector but the sensitivity of the state vector $z(\boldsymbol{p}, t)$ with respect to the optimization parameters throttle position ϱ, steering angle φ and gear ratio η. Principally, it is possible to determine the sensitivity with differential quotients. But in order to get sensible optimization results differential quotients tend to be too imprecise for dynamic problems. Therefore, the analytical derivative of the state vector $\boldsymbol{z}$ needs to be calculated. The analytical derivatives represented in this chapter are according to optimization step one, see chapter 5.2. Optimization step three is basically the same as step one, but with a fixed gear sequence η. Therefore, no derivatives of the state vector with respect to the gear sequence are computed in this step.

4.1   General scheme

4.1.1   Problem formulation

The state equations describing the driver's prediction models with initial conditions are

$$\dot{\boldsymbol{z}}(t, \boldsymbol{p}) = \boldsymbol{g}\left(\boldsymbol{z}(t, \boldsymbol{p}), \boldsymbol{p}\right) \tag{4.1}$$

$$\boldsymbol{z}(t = 0) = \boldsymbol{z}_0 \,, \tag{4.2}$$

with $\boldsymbol{g}\left(\boldsymbol{z}(t, \boldsymbol{p}), \boldsymbol{p}\right)$ from Eq. 3.17, Eq. 3.19 or Eq. 3.35 and with $\boldsymbol{p}$ being a vector of parameters, e.g. from Eq. 5.2.

In order to calculate the analytic derivatives $\dfrac{d\boldsymbol{f}}{d\boldsymbol{p}}$ of optimization objectives such as $\mathbf{f} = \boldsymbol{f}\left(\boldsymbol{z}(t, \boldsymbol{p}), \boldsymbol{p}\right)$, we need to know

$$\frac{d\boldsymbol{f}}{d\boldsymbol{p}}(\boldsymbol{p}) = \frac{\partial \boldsymbol{f}}{\partial \boldsymbol{z}} \frac{d\boldsymbol{z}}{d\boldsymbol{p}}(t, \boldsymbol{p}) + \frac{\partial \boldsymbol{f}}{\partial \boldsymbol{p}}(\boldsymbol{p}) \,. \tag{4.3}$$

Consequently, we ask for the solution $z(t, p)$ of the initial value problem Eq. 4.1, and for its derivative $\frac{dz}{dp}(t\,p)$ with respect to time.

4.1.2 Derivative **of** the state equation solution

The derivative of Eq. 4.1 with respect to the parameter vector p is

$$\frac{d\dot{z}}{dp}(t, p) = \frac{\partial g}{\partial z}(t, p)\frac{dz}{dp}(t, p) + \frac{\partial g}{\partial p}(t, p) \tag{4.4}$$

$$\frac{dz}{dp}(t = 0) = \frac{dz_0}{dp} = 0 \tag{4.5}$$

According to the rules of differential calculus, see [2] we know that

$$\frac{dz}{dxdy} = \frac{dz}{dydx}. \tag{4.6}$$

Therefore, we can write Eq. 4.4

$$\frac{d\dot{z}}{dp}(t, p) = \left(\frac{dz}{dp}\right)^{\bullet}(t, p) \tag{4.7}$$

Following from that the augmented state equations for the calculation of system states and their analytic derivatives $\frac{dz}{dp}(t,p)$ are

$$\begin{bmatrix} z(t, p) \\ \\ \frac{dz}{dp} \end{bmatrix}^{\bullet} = \begin{bmatrix} g(z(t, p), p) \\ \\ \frac{\partial g}{\partial z}(t, p)\frac{dz}{dp}(t, p) + \frac{\partial g}{\partial p}(t, p) \end{bmatrix} \tag{4.8}$$

$$\begin{bmatrix} z(t = 0) \\ \\ \frac{dz}{dp}(t = 0) \end{bmatrix} = \begin{bmatrix} z_0 \\ \\ 0 \end{bmatrix}. \tag{4.9}$$

To formulate Eq. 4.8 for each prediction model we need to extract $\frac{\partial g}{\partial z}(t, p)$ and $\frac{\partial g}{\partial p}(t, p)$ from its respective state equation.

4.2   Derivative of the input vector

In order to finally calculate Eq. 4.8 we need to calculate the analytical derivatives of $\boldsymbol{q}$ with respect to the parameterized input vector $\overline{\boldsymbol{p}}$ at the time t. The derivative of $\boldsymbol{p}$ is later needed to calculate the derivatives of the different components of the prediction models.

$$
\frac{\partial \boldsymbol{p}}{\partial \overline{\boldsymbol{p}}}(\overline{\boldsymbol{p}}, t)|_t = \begin{pmatrix} \frac{\partial}{\partial \overline{\boldsymbol{p}}}\left(\varrho\left(t_i\right) + \frac{\varrho\left(t_{i+1}\right) - \varrho\left(t_i\right)}{t_{i+1} - t_i}\left(t - t_i\right)\right) \\ \frac{\partial}{\partial \overline{\boldsymbol{p}}}\left(\varphi\left(t_i\right) + \frac{\varphi\left(t_{i+1}\right) - \varphi\left(t_i\right)}{t_{i+1} - t_i}\left(t - t_i\right)\right) \\ \frac{\partial}{\partial \overline{\boldsymbol{p}}}\left(\eta\left(t_i\right) + \frac{\eta\left(t_{i+1}\right) - \eta\left(t_i\right)}{t_{i+1} - t_i}\left(t - t_i\right)\right) \end{pmatrix} \; ; \; t_i \le t \le t_{i+1} \, . \tag{4.10}
$$

In order to simplify further descriptions of derivatives with respect to the parameterized input vector $\overline{\boldsymbol{p}}$ the abbreviation $()' := \frac{\partial ()}{\partial \overline{p}}$ is used from now on.

4.3   Derivatives of model components

The different prediction models described in chapter 3 are built up of several components. Starting with the description of the derivatives of the components which have all prediction models in common. The remaining components which make up the entire prediction models are explained one after another, so that we can eventually put all components together to formulate equation Eq. 4.8.

4.3.1   Driving torque

The driving torque propels the vehicle and acts on the vehicle wheels as defined in Eq. 3.2

$$
M_a(\varrho^+) = i_{clutch} i_{gear}(\eta) i_{diff} M_e(\varrho^+) \, . \tag{4.11}
$$

The derivatives of the torque M_a with respect to the three input parameters are

$$
\begin{aligned}
\frac{\partial M_a}{\partial \varrho} &= i_{clutch} i_{gear}(\eta) i_{diff} \frac{\partial M_e}{\partial \varrho} \\[2mm]
\frac{\partial M_a}{\partial \varphi} &= i_{clutch} i_{gear}(\eta) i_{diff} \frac{\partial M_e}{\partial \varphi} \\[2mm]
\frac{\partial M_a}{\partial \eta} &= i_{clutch} i_{gear}(\eta) i_{diff} \frac{\partial M_e}{\partial \eta} + i_{clutch} \frac{\partial i_{gear}(\eta)}{\partial \eta} i_{diff} M_e \, .
\end{aligned} \tag{4.12}
$$

The terms $\frac{\partial M_e}{\partial \varrho}$, $\frac{\partial M_e}{\partial \varphi}$ and $\frac{\partial M_e}{\partial \overline{\eta}}$ describe the sensitivity of the engine torque M_e with respect to changes of the input parameters. Therefore, the derivatives M_a' are dependent on the respective derivatives of the engine torque M_e, hence from the used engine type.

In case of the one track model, the driving torque is distributed among the front and rear wheel, respectively, see Eq. 3.4. The resulting derivatives of the driving torque of the front wheel M_{af} and the rear wheel M_{ar} are then

$$
\begin{aligned}
M_{af}' &= (1 - \epsilon) M_a' \\
M_{ar}' &= \epsilon M_a',
\end{aligned}
\tag{4.13}
$$

with the distribution factor ϵ according to Eq. 3.5.

Static engine torque $\overline{M}_e(\varrho^+)$ as linear function of ϱ^+
The definition of this engine type is

$$
\overline{M}_e(\varrho^+) = \begin{cases} a_{M1}\varrho^+ + b_{M1} & ; \quad \varrho^+ \le \varrho_0 \\ a_{M2}\varrho^+ + b_{M2} & ; \quad \varrho^+ > \varrho_0 \end{cases},
\tag{4.14}
$$

see Eq. 3.6. If this engine model is directly used for a prediction model without being passed through a PT1 filter, then is $\overline{M}_e(\varrho^+) = M_e(\varrho^+)$. Thus, the derivatives with respect to the input parameters are

$$
\frac{\partial M_e(\varrho^+)}{\partial \overline{\varrho}} = \frac{\partial \overline{M}_e(\varrho^+)}{\partial \overline{\varrho}} = \begin{cases} a_{M1}\frac{\partial \varrho^+}{\partial \overline{\varrho}} & ; \quad \varrho^+ \le \varrho_0 \\ a_{M2}\frac{\partial \varrho^+}{\partial \overline{\varrho}} & ; \quad \varrho^+ > \varrho_0 \end{cases}
$$

$$
\frac{\partial M_e(\varrho^+)}{\partial \overline{\varphi}} = \frac{\partial \overline{M}_e(\varrho^+)}{\partial \overline{\varphi}} = 0
\tag{4.15}
$$

$$
\frac{\partial M_e(\varrho^+)}{\partial \overline{\eta}} = \frac{\partial \overline{M}_e(\varrho^+)}{\partial \overline{\eta}} = 0.
$$

In this specific case any changes of the steering angle φ and the gear ratio η do not influence the engine torque and therefore, do not influence the driving torque M_a. The engine torque or driving torque, respectively is solely dependent on changes of the throttle signal ϱ. The term $\frac{\partial \varrho^+}{\partial \overline{\varrho}}$ is form Eq. 4.10.

Dynamic engine torque $M_e(\overline{M}_e(\varrho^+))$
The equation describing the dynamic engine torque $M_e(\overline{M}_e(\varrho^+))$ is according to Eq. 3.7

$$
\dot{M}_e = \frac{1}{T_m}\left(\overline{M}_e(\varrho^+) - M_e\right).
\tag{4.16}
$$

Regarding the case where the static engine torque $\overline{M}_e(\varrho^+)$ is solely dependent on the throttle position, the derivative of the dynamic engine torque with respect to the input parameter $\overline{\varrho}$ is as follows

$$\frac{\partial \dot{M}_e}{\partial \overline{\varrho}} = \frac{1}{T_m} \left(\frac{\partial \overline{M}_e(\varrho^+)}{\partial \overline{\varrho}} - \frac{\partial M_e}{\partial \overline{\varrho}} \right) \tag{4.17}$$

With $\frac{\partial M_e(\varrho^+)}{\partial \overline{\varrho}}$ from Eq. 4.15 and $\frac{\partial M_e}{\partial \overline{\varrho}}$ from the solution of the initial value problem Eq. 4.8.

Static engine torque $\overline{M}_e(\varrho^+, n_e)$ as function of ρ^+ and engine speed n_e
The static engine torque is determined by a lookup table, see Fig. 3.4. It depends on the throttle position ϱ^+ and the engine speed n_e. Therefore, the derivative of $\overline{M}_e(\varrho^+, n_e)$ with respect to the input parameter vector $\overline{p}$ is a function of the partial derivatives $\frac{d\rho^+}{d\varrho}$ and n'_e. It can be written as

$$M'_e(\varrho^+, n_e) = \frac{\partial \overline{M}_e}{\partial \varrho}(\varrho^+, n_e)\frac{\partial \varrho}{\partial \overline{\varrho}} + \frac{\partial \overline{M}_e}{\partial n_e}(\varrho^+, n_e)n'_e \tag{4.18}$$

The partial derivatives $\frac{\partial \overline{M}_e}{\partial \varrho}$ and $\frac{\partial \overline{M}_e}{\partial n_e}$ depend on the used algorithm for determining the engine torque from a lookup table. In this case, simple geometrical calculations are used to determine the engine torque, see Eq. 3.8. The derivatives of the static engine torque with respect to the input parameter vector can then be calculated as

$$\overline{M}'_e = \frac{\partial}{\partial \overline{p}} \left(E(M_{0,kj}) \cap g(\varrho^+, n_e) \right) . \tag{4.19}$$

$\partial \varrho$ is according to Eq. 4.10. The derivative of the engine speed n'_e with respect to the input parameter vector $\overline{p}$ can be calculated based on Eq. 5.10 as

$$n'_e = \frac{60}{2\pi} i_{diff} i_{gear} \frac{\partial \eta}{\partial \overline{\eta}} \frac{v}{R} + \frac{60}{2\pi} i_{diff} i_{gear} \eta \frac{v'}{R} . \tag{4.20}$$

Where $\frac{\partial \eta}{\partial \overline{\eta}}$ is from Eq. 4.10 and v' is the derivative of the vehicle's velocity in longitudinal direction with respect to the input parameter vector $\overline{p}$ from the solution of the initial value problem Eq. 4.8.

Dynamic engine torque $M_e(\overline{M}_e(\varrho^+, n_e))$
Eq. 3.9 defines the dynamic engine torque $M_e(\overline{M}_e(\varrho^+, n_e))$ as

$$\dot{M}_e = \frac{1}{T_m} \left(\overline{M}_e(\varrho^+, n_e) - M_e \right) \tag{4.21}$$

The derivative of the dynamic engine torque with respect to the input parameters is

$$M'_e = \frac{1}{T_m} \left(\overline{M}'_e(\varrho^+, n_e) - M'_e \right) , \tag{4.22}$$

with the derivative of the static engine torque, $\overline{M}'_e$ from Eq. 4.18 and M'_e from the solution of the initial value problem Eq. 4.8.

4.3.2 **Brake** torque

The definition of the brake torque is according to Eq. 3.10

$$M_b(\varrho^-) = K_{brake}\varrho^- \mathrm{sgn}v . \tag{4.23}$$

The brake input signal ϱ^- is translated into a brake torque, which is directly applied to the vehicle wheels. In order to get the sensitivity of M_b in respect to the input parameters, we need to derive M_b with respect to the input parameter vector $\overline{p}$. The resulting analytical derivative of Eq. 4.23 with respect to $\overline{p}$ is

$$\frac{\partial M_b}{\partial \overline{\varrho}}(\varrho^-) = K_{brake}\frac{\partial \varrho^-}{\partial \overline{\varrho}}\mathrm{sgn}v + K_{brake}\varrho^- \frac{\partial \mathrm{sgn}v}{\partial \overline{\varrho}}$$

$$\frac{\partial M_b}{\partial \overline{\varphi}}(\varrho^-) = K_{brake}\varrho^- \frac{\partial \mathrm{sgn}v}{\partial \overline{\varphi}} \tag{4.24}$$

$$\frac{\partial M_b}{\partial \overline{\eta}}(\varrho^-) = K_{brake}\varrho^- \frac{\partial \mathrm{sgn}v}{\partial \overline{\eta}} ,$$

with

$$\frac{\partial \mathrm{sgn}v}{\partial \overline{p}} \tag{4.25}$$

The term $\frac{\partial \varrho^-}{\partial \overline{\varrho}}$ is from Eq. 4.10. Since no velocity $v = 0$ is allowed for all of the used prediction models equation 4.25 is always zero.

In case of the one track prediction model, the brake torque is distributed among the front wheel and rear wheel. Therefore, the derivatives of the brake torque of the front wheel M'_{bf} and of the rear wheel M'_{br} with respect to the input parameters are

$$\begin{aligned} M'_{bf} &= \zeta M'_b \\ M'_{br} &= (1 - \zeta)M'_b , \end{aligned} \tag{4.26}$$

with the distribution factor ζ according to Eq. 3.11.

4.3.3   Aerodynamic force

The aerodynamic force; acting on the vehicle is defined in Eq. 3.13 as

$$F_W(v) = -c_W A_W \frac{\rho_W}{2} v(\boldsymbol{p})^2 \tag{4.27}$$

It is acting in the opposite direction of the vehicles longitudinal driving direction. Due to the dependency of F_W of the vehicle velocity v, which is dependent on the parameter input vector $\boldsymbol{p}$, we need also to calculate the derivatives of F_W with respect to $\overline{\boldsymbol{p}}$. The resulting analytical derivative of $F_W(v)$ is according to that

$$F_W'(v) = -c_W A_W \rho_W v(\boldsymbol{p})' , \tag{4.28}$$

with u' from the solution of the initial value problem Eq. 4.8.

4.3.4   Yaw angle (mass point model)

In the single mass point model is the steering angle φ directly correlated with trajectory curvature $K(\varphi)$. We can use this correlation in order to calculate the vehicle's yaw angle ψ. The definition, which was given in Eq. 3.14 was

$$K(\varphi) = \frac{d\psi}{ds} = \frac{\tan\varphi}{\sqrt{(l_R + l_F)^2 + (l_R)^2 \tan^2\varphi}} . \tag{4.29}$$

$K(\varphi)$ is solely dependent of φ, therefore, derivatives with respect to the input parameter ϱ and η become zero. The derivative of Eq. 4.29 with respect to steering angle is

$$\frac{dK(\varphi)}{d\overline{\varphi}} = \frac{d\varphi}{d\overline{\varphi}} \frac{(1 + \tan^2\varphi)(l_r + l_f)^2}{\left((l_r + l_f)^2 + l_r^2 \tan^2\varphi\right)^{3/2}} , \tag{4.30}$$

with $\frac{d\varphi}{d\overline{\varphi}}$ from Eq. 4.10.

4.3.5   Tire forces (one track model)

The wheels of the single point mass models fulfill a perfect rolling constraint where as the tire forces of the one track models are represented by a force law, which allows slipping. In order to determine the sensitivity of the dynamics of the one track models with respect to the input parameter vector $\boldsymbol{p}$ we also need to compute the sensitivity of the tire forces with respect of the input vector. The starting point to calculate the tire forces is the longitudinal

tire slip s and the slip angle α. The longitudinal slip of the front tire was previously defined as

$$
\text{sf} = \begin{cases}
-\dfrac{R\omega_f - \dot{x}\cos\varphi + \left(\dot{y} + l_f\,\dot{\psi}\right)\sin\varphi}{R\omega_f} \\
\text{if } \left(2\cos\varphi + \left(\dot{y} + l_f\,\dot{\psi}\right)\sin\varphi < R\omega_f\right) \\[2mm]
\dfrac{\dot{x}\cos\varphi + \left(\dot{y} + l_f\,\dot{\psi}\right)\sin\varphi - R\omega_f}{\dot{x}\cos\varphi + \left(\dot{y} + l_f\,\dot{\psi}\right)\sin\varphi} \\
\text{if } \left(\dot{x}\cos\varphi + \left(\dot{y} + l_f\,\dot{\psi}\right)\sin\varphi \geq R\omega_f\right)
\end{cases}
\tag{4.31}
$$

see also Eq. 3.20. Therefore, the derivatives of the longitudinal tire slip of the front tire can be calculated in the case of driving slip $\dot{x}\cos\varphi + \left(\dot{y} + l_f\,\dot{\psi}\right)\sin\varphi < R\omega_f$ as

$$
s_f' = \frac{\left(\dot{x}'\cos\varphi + \dot{x}\sin\varphi\varphi' + (\dot{y}' + l_f\dot{\psi}')\sin\varphi + (y + l_f\dot{\psi})\cos\varphi\varphi'\right)R\omega_f}{(R\omega_f)^2}
$$
$$
- \frac{\left(\dot{x}\cos\varphi + (\dot{y} + l_f\dot{\psi})\sin\varphi\right)R\omega_f'}{(R\omega_f)^2}
\tag{4.32}
$$

In case of brake slip, if $\dot{x}\cos\varphi + \left(\dot{y} + l_f\,\dot{\psi}\right)\sin\varphi \geq R\omega_f$, the derivative s_f' of tire slip s_f with respect to the input vector is calculated as

$$
s_f' = \frac{-R\omega_f'\left(\dot{x}\cos\varphi + (\dot{y} + l_f\dot{\psi})\sin\varphi\right)}{\left(\dot{x}\cos\varphi + (\dot{y} + l_f\dot{\psi})\sin\varphi\right)^2}
$$
$$
+ \frac{R\omega_f\left(\dot{x}'\cos\varphi + \dot{x}\sin\varphi\varphi' + (\dot{y}' + l_f\dot{\psi}')\sin\varphi + (\dot{y} + l_f\dot{\psi})\cos\varphi\varphi'\right)}{\left(\dot{x}\cos\varphi + (\dot{y} + l_f\dot{\psi})\sin\varphi\right)^2}
\tag{4.33}
$$

φ' is from Eq. 4.10. The quantities $\dot{x}'$, $\dot{y}'$, $\dot{\psi}'$ and ω_f' are from the solution of the initial value problem Eq. 4.8. They denote the sensitivity of the respective quantity of the state-space vector $z(t, p)$ with respect to the input vector p.

We can calculate similar to that derivatives of the tire slip at the rear wheel. The equations describing the slip are according to Eq. 3.21

$$
s_r = \begin{cases}
-\dfrac{R\omega_r - \dot{x}}{R\omega_r} & ; & \dot{x} < R\omega_f \text{ accelerate} \\[3mm]
\dfrac{\dot{x} - R\omega_r}{\dot{x}} & ; & \dot{x} \geq R\omega_f \text{ brake}
\end{cases}
\tag{4.34}
$$

The derivatives of the slip s, with respect to the input vector $\boldsymbol{p}$ describe the sensitivity of the tire slip with respect to the input vector. They can be calculated as

$$
s_r' = \begin{cases} \dfrac{\omega_r \dot{x}' - \dot{x}\omega_r'}{R\omega_r^2} & x < R\omega_f \text{ accelerate} \\[4mm] \dfrac{R\omega_r \dot{x}' - R\dot{x}\omega_r'}{\dot{x}^2} & ; \quad \dot{x} \geq R\omega_f \text{ brake} \end{cases} , \tag{4.35}
$$

where the quantities $\dot{x}'$ and $\dot{\omega}_f'$ are from the solution of the initial value problem Eq. 4.8. They denote the sensitivity of the respective quantity of the state-space vector $\boldsymbol{z}(t,\boldsymbol{p})$ with respect to the input vector $\boldsymbol{p}$.

In addition to the tire slip, the slip angle α is needed in order to determine the tire forces. The respective slip angles for the front wheel and for the rear wheel were defined in Eq. 3.22 as

$$
\alpha_f = \varphi - \arctan \frac{\dot{y} + l_f \dot{\psi}}{\dot{x}} \tag{4.36}
$$

$$
\alpha_r = -\arctan \frac{\dot{y} - l_r \dot{\psi}}{x}
$$

In order to calculate the sensitivity of the lateral tire forces F_y at the front and rear wheel we also need to derive the slip angles with respect to the input vector $\boldsymbol{p}$. Following from that, we can calculate the derivatives as

$$
\alpha_f' = \varphi' + \frac{\dot{x}'\left(\dot{y} + l_f\dot{\psi}\right) - \dot{x}\left(\dot{y}' + l_f\dot{\psi}'\right)}{\dot{x}^2 + (\dot{y} + l_f\dot{\psi})^2}
$$

$$
\alpha_r' = \frac{\dot{x}'\left(\dot{y} - l_r\dot{\psi}\right) - \dot{x}\left(\dot{y}' - l_r\dot{\psi}'\right)}{\dot{x}^2 + (\dot{y} - l_r\dot{\psi})^2} \tag{4.37}
$$

The quantities $\dot{x}'$, $\dot{y}'$ and ψ' are from the solution of the initial value problem Eq. 4.8. They denote the sensitivity of the respective quantity of the state-space vector $\boldsymbol{z}(t,\boldsymbol{p})$ with respect to the input vector $\boldsymbol{p}$.

Linear tire model
The linear tire model represents a linear correlation between the slip quantities s and α and the tire forces which can be transmitted to the road. Eq. 3.23 to Eq. 3.25 define the tire forces as

$$
\begin{aligned} \overline{F_{xf}} &= -\kappa_f C_{lo} s_f \\ \overline{F_{xr}} &= -\kappa_r C_{lo} s_r \end{aligned} \tag{4.38}
$$

$$\overline{F_{yf}} = C_{la} \tan \alpha_f$$
$$\overline{F_{yr}} = C_{la} \tan \alpha_r \tag{4.39}$$

Following from that we can calculate the sensitivity of the tire forces with respect to the input vector $\boldsymbol{p}$. The resulting derivatives of the tire forces with respect to the input vector, which represent the sensitivity are

$$\overline{F_{xf}}' = -\kappa_f C_{lo} s_f'$$
$$\overline{F_{xr}}' = -\kappa_r C_{lo} s_r' \tag{4.40}$$

$$\overline{F_{yf}}' = C_{la}(1 + \tan^2 \alpha_f)\alpha_f'$$
$$\overline{F_{yr}}' = C_{la}(1 + \tan^2 \alpha_r)\alpha_r', \tag{4.41}$$

with the derivatives of the tire slip s_f' from Eq. 4.32 and Eq. 4.33. s_r' is from Eq. 4.35. The quantities α_f' and α_r' are from Eq. 4.37.

Tire model **with force saturation**
A better representation of the tire forces gives the tire model with force saturation. Especially if the tire slip and the slip angles become bigger, the linear tire model is not sufficient anymore. In order to determine the tire saturation of the tire model with force saturation, several quantities have to be calculated. Each of them is dependent on the input vector $\boldsymbol{p}$. Therefore, in order to calculate the sensitivity of the tire forces with respect to the input vector, we need to calculate the respective derivative of the quantities on which this tire model is based upon. In the following description of the tire model and its derivatives with respect to the input vector $\boldsymbol{p}$, all necessary quantities are summarized for the front and rear tire. Therefore, in order to calculate the forces and their analytical derivatives, the specific quantities for the front, tire and rear tire must be substituted. The equations for the slip velocity v_s, the friction coefficient μ and the auxiliary quantity $\overline{s}$ are defined from Eq. 3.27 to Eq. 3.29 as

$$v_s = v_M \sqrt{s^2 + \tan^2 \alpha}$$

$$\mu = f_R \left(1 - k_R v_s\right) \tag{4.42}$$

$$\overline{s}_r = \frac{\sqrt{(C_s s)^2 + (C_\alpha \tan \alpha)^2}}{\mu (1 - s)}$$

v_M is the absolute velocity of the center of the tire in rolling direction. It is $(\dot{x} \cos \varphi + \left(\dot{y} + l_f \dot{\psi}\right) \sin \varphi)$ for the front tire and $\dot{x}$ for the rear tire. Following from that, is the sensitivity of v_M or the derivative of v_M with respect to the input vector $\boldsymbol{p}$, respectively

$$v_M' = \dot{x}' \cos \varphi - \dot{x} \sin \varphi \varphi' + (\dot{y}' + l_f \dot{\psi}') + (\dot{y} + l_f \dot{\psi}) \cos \varphi \varphi' \quad \text{front tire}$$
$$\tag{4.43}$$
$$v_M' = \dot{x}' \quad \text{rear tire}.$$

Therefore, the derivatives of Eq. 4.42 with respect to the input vector p can be calculated as

$$
\begin{aligned}
v'_s &= v'_M\sqrt{s^2 + \tan^2 a} + \frac{1}{2}\frac{\dot{x}\left(2ss' + 2\tan\alpha(1 + \tan^2\alpha)\alpha'\right)}{\sqrt{s^2 + \tan^2 a}} \\[2mm]
\mu' &= f_R\left(1 - k_R v'_s\right) \\[2mm]
\bar{s}' &= \frac{1}{2}\frac{2C_s^2 ss' + 2C_\alpha^2\tan\alpha\left(1 + \tan^2\alpha\right)\alpha'}{\sqrt{(C_s s)^2 + (C_\alpha\tan\alpha)^2}\,\mu\left(1 - s\right)} - \frac{\sqrt{(C_s s)^2 + (C_\alpha\tan\alpha)^2}\,\mu'}{\mu^2\left(1 - s\right)} \\[2mm]
&\quad + \frac{\sqrt{(C_s s)^2 + (C_\alpha\tan\alpha)^2}\,s'}{\mu\left(1 - s\right)}\,,
\end{aligned}
\tag{4.44}
$$

with the derivatives of the tire slip s' from Eq. 4.32 and Eq. 4.33 in case of the front tire, or s' from Eq. 4.35 in case of the rear tire. The derivative of the slip angle α' is according to Eq. 4.37. v'_M is form Eq. 4.43.

The previously described quantities and their derivatives are now used to calculate the tire forces and their sensitivity with respect to the input vector q. The tire forces are computed differently in case of pure static friction or mixed static and sliding friction.

Pure static friction is assumed if the auxiliary quantity $\bar{s}$ is $\bar{s} \leq 0.5$. The lateral an longitudinal tire forces, as defined in Eq. 3.30, are

$$
\begin{aligned}
F_x &= -\kappa C_s F_z \frac{s}{1 - s} \\
F_y &= C_\alpha F_z \frac{\tan\alpha}{1 - s}\,.
\end{aligned}
\tag{4.45}
$$

Therefore, the analytical derivatives of Eq. 4.45, which represent the susceptibility of the tire forces with respect to the input vector p are

$$
\begin{aligned}
F'_x &= -\kappa C_s F_z \frac{s'}{(-1 + s)^2} \\
F'_y &= C_\alpha F_z \frac{(1 + \tan^2 a)\alpha'}{1 - s} + C_\alpha F_z \frac{\tan\alpha\, s'}{(1 - s)^2}\,,
\end{aligned}
\tag{4.46}
$$

If mixed staticjsliding friction is assumed, in case of $\bar{s} > 0.5$, the tire forces are according to Eq. 3.32 defined as

$$
\begin{aligned}
F_x &= -\kappa C_s F_z \frac{s}{1 - s}\frac{\bar{s} - 0.25}{\bar{s}^2} \\
F_y &= C_\alpha F_z \frac{\tan\alpha}{1 - s}\frac{\bar{s} - 0.25}{\bar{s}^2}\,.
\end{aligned}
\tag{4.47}
$$

In this case, the susceptibility of the tire forces with respect to the input vector p is represented by

$$
\begin{aligned}
F'_x &= -\kappa C_s F_z \frac{s'(\bar{s} - 0.25) + s\bar{s}'}{(1-s)\bar{s}^2} - C_s F_z \frac{ss'(\bar{s} - 0.25)}{(1-s)^2\bar{s}^2} \\
&\quad +2C_s F_z \frac{s(\bar{s} - 0.25)\bar{s}'}{(1-s)\bar{s}^3} \\
F'_y &= C_\alpha F_z \frac{(1+\tan^2 a)a'(\bar{s} - 0.25) + \tan\alpha\bar{s}'}{(1-s)\bar{s}^2} \\
&\quad +C_\alpha F_z \frac{\tan\alpha(\bar{s} - 0.25)s'}{(1-s)^2\bar{s}^2} - 2C_\alpha F_z \frac{\tan\alpha(\bar{s} - 0.25)\bar{s}'}{(1-s)\bar{s}^3}
\end{aligned}
\tag{4.48}
$$

In both cases, pure static friction and mixed static/sliding friction, are the derivatives of the tire slip s' from Eq. 4.32 and Eq. 4.33 in case of the front tire, or s' from Eq. 4.35 in case of the rear tire. The derivative of the slip angle a' is according to Eq. 4.37. The derivative $\bar{s}'$ of the auxiliary quantity $\bar{s}$ is from Eq. 4.44.

4.4 Augmented equations of motion

In order to calculate not only the dynamics of the prediction models, but also the sensitivity of the prediction models with respect to the input vector p, the state-space vector $z(p,t)$ has to be augmented to $\bar{z}(p,t)$. The resulting state-space vector $\bar{z}(p,t)$ for each of the prediction models as well as the augmented equations of motion are described in the following chapters.

4.4.1   Single mass point model with static drive train

In the case of a single mass point model with no drive train dynamics, the state-space vector $z(p,t)$, Ey. 3.16 is expanded into $\bar{z}(p,t)$ and has the form

$$
\bar{z}(p,t) = \begin{bmatrix} z(t,p \end{bmatrix} \qquad \psi \quad x \quad y \quad | \quad \dot{s}' \quad \psi' \quad x' \quad y' \end{bmatrix}^t .
\tag{4.49}
$$

Following from that, the augmented equations in state-space form are, see Ey. 4.8

$$
\dot{\bar{z}}(p,t) = \begin{bmatrix} z(t,p) \\ z' \end{bmatrix}^\bullet = \begin{bmatrix} g\left(z(t,p),p\right) \\ \frac{\partial g}{\partial z}(t,p)z'(t,p) + g'(t,p) \end{bmatrix},
\tag{4.50}
$$

with $g\left(z(t,p),p\right)$ from Eq. 3.17. The terms $\frac{\partial g}{\partial z}(t,p)$ and $g'(t,p)$ can then be calculated as

$$\frac{\partial g}{\partial x}(t,p) = \begin{vmatrix} 0 & 0 & 0 & 0 \\ K(\varphi) & 0 & 0 & 0 \\ \cos\psi & -\dot{s}\sin\psi & 0 & 0 \\ \sin\$ & \dot{s}\cos\psi & 0 & 0 \end{vmatrix} \tag{4.51}$$

$$g'(t,p) = \begin{bmatrix} \frac{1}{m}\left(\frac{1}{R}\left(M_a' + M_b'\right) - F_W'\right) \\ K(\varphi)'\dot{s} \\ 0 \\ 0 \end{bmatrix} \tag{4.52}$$

Substituted in Eq. 4.50 the augmented state-space equations of motion are

$$\overline{x} = \begin{vmatrix} \frac{1}{m}\left(\frac{1}{R}\left(M_a + M_b\right) - F_W\right) \\ K(\varphi)\dot{s} \\ \dot{s}\cos\psi \\ \dot{s}\sin\psi \\ \frac{1}{m}\left(\frac{1}{R}\left(M_a' + M_b'\right) - F_W'\right) \\ K(\varphi)'\dot{s} + K(\varphi)\dot{s}' \\ \dot{s}'\cos\psi - \dot{s}\sin\psi\psi' \\ \dot{s}'\sin\psi - \dot{s}\cos\psi\psi' \end{vmatrix}, \tag{4.53}$$

with M_a' from Eq. 4.12 and M_b' from equation Eq. 4.24. The term F_W' is according to Eq. 4.28 and $K(\varphi)'$ is from Eq. 4.30.

4.4.2 Single mass point model with dynamic drive train

If the prediction model includes drive train dynamics the differential equations of the engine torque have to be solved, too. Therefore, the state-space vector $\boldsymbol{z}$ from equation Eq. 3.18 has to be expanded to $\overline{z}(\boldsymbol{p}, t)$ and becomes

$$\overline{z}(t, \boldsymbol{p}) = \begin{bmatrix} \boldsymbol{z}(t, \boldsymbol{p}) \\ \\ \boldsymbol{z}' \end{bmatrix} = \begin{bmatrix} M_e & \dot{s} & \psi & x & y & | & M_e' & \dot{s}' & \psi' & x' & y' \end{bmatrix}^T . \tag{4.54}$$

The expanded equations of motion in state-space form are following from Eq. 4.8

$$\dot{\overline{z}}(\boldsymbol{p}, t) = \begin{bmatrix} \boldsymbol{z}(t, \boldsymbol{p}) \\ \\ \boldsymbol{z}' \end{bmatrix}^{\bullet} = \begin{bmatrix} \boldsymbol{g}\left(\boldsymbol{z}(t, \boldsymbol{p}), \boldsymbol{p}\right) \\ \\ \frac{\partial \boldsymbol{g}}{\partial \boldsymbol{z}}(t, \boldsymbol{p})\boldsymbol{z}'(t, \boldsymbol{p}) + \boldsymbol{g}'(t, \boldsymbol{p}) \end{bmatrix} , \tag{4.55}$$

with $\boldsymbol{g}\left(\boldsymbol{z}(t, \boldsymbol{p}), \boldsymbol{p}\right)$ from Eq. 3.19. Therefore, we can calculate the terms $\frac{\partial \boldsymbol{g}}{\partial \boldsymbol{z}}(t, \boldsymbol{p})$ and $\boldsymbol{g}'(t, \boldsymbol{p})$ as follows

$$\frac{\partial \boldsymbol{g}}{\partial \boldsymbol{z}}(t, \boldsymbol{p}) = \begin{bmatrix} -\frac{1}{T_m} & 0 & 0 & 0 & 0 \\ 0 & K(\varphi) & 0 & 0 & 0 \\ 0 & \cos\psi & -\dot{s}\sin\psi & 0 & 0 \\ 0 & \sin\psi & \dot{s}\cos\psi & 0 & 0 \end{bmatrix} \tag{4.56}$$

$$\boldsymbol{g}'(t, \boldsymbol{p}) = \begin{bmatrix} \frac{1}{T_m}\overline{M}_e' \\ \frac{1}{m}\left(\frac{1}{R}\left(M_a' + M_b'\right) - F_W'\right) \\ K(\varphi)'\dot{s} \\ 0 \\ 0 \end{bmatrix} . \tag{4.57}$$

Inserted in Eq. 4.55 we can write the equations of motion of the single mass point model with drive train dynamics as

$$
\dot{\overline{z}} = \begin{vmatrix}
-\frac{1}{T_m} M_e + \frac{1}{T_m} \overline{M}_e \\[2mm]
\frac{1}{m}\left(\frac{1}{R}\left(M_a + M_b\right) - F_W\right) \\[2mm]
K(\varphi)\dot{s} \\[2mm]
\dot{s}\cos\psi \\[2mm]
\dot{s}\sin\psi \\[2mm]
-\frac{1}{T_m} M_e' + \frac{1}{T_m} \overline{M}_e' \\[2mm]
\frac{1}{m}\left(\frac{1}{R}\left(M_a' + M_b'\right) - F_W'\right) \\[2mm]
K(\varphi)'\dot{s} + K(\varphi)\dot{s}' \\[2mm]
\dot{s}'\cos\psi - \dot{s}\sin\psi\psi' \\[2mm]
\dot{s}'\sin\psi - \dot{s}\cos\psi\psi'
\end{vmatrix} ,
\tag{4.58}
$$

with $\overline{M}_e'$ from Eq. 4.14 if a engine with linear torque characteristics, just depending on the throttle position is used. If a engine with a field-interpolated torque characteristics is used, $\overline{M}_e'$ is calculated according to Eq. 4.19. M_a' is from Eq. 4.12 and M_b' is from equation Eq. 4.24. The term F_W' is according to Eq. 4.28 and $K(\varphi)'$ is from Eq. 4.30.

4.4.3   One **track** model

In the case of a one track model with the state-space vector $z(\boldsymbol{p}, t)$ from Eq. 3.34 the resulting augmented state-space vector $\overline{z}(\boldsymbol{p}, t)$ becomes

$$
\overline{z}(\boldsymbol{p}, t) = \begin{vmatrix} \boldsymbol{z}(t, \boldsymbol{p} \end{vmatrix} \quad \begin{aligned} [M_e & & \dot{x} & & \dot{y} & & \psi & & \omega_f & & \omega_r| \\ & M_e' & & \dot{y}' & & \dot{x}' & & \dot{\psi}' & & \omega_f' & & \omega_r']^T . \end{aligned}
\tag{4.59}
$$

Following from that, the augmented equations of motion in state-space form are as defined in Eq. 4.8

$$
\dot{\bar{z}}(p, t) =
\begin{bmatrix}
z(t, p) \\[4pt]
z'
\end{bmatrix}^{\bullet}
=
\begin{bmatrix}
g\left(z(t, p), p\right) \\[6pt]
\dfrac{\partial g}{\partial z}(t, p) z'(t, p) + g'(t, p)
\end{bmatrix},
\tag{4.60}
$$

with $g\left(z(t, p), p\right)$ from Eq. 3.35. The terms $\dfrac{\partial g}{\partial z}(t, p)$ and $g'(t, p)$ can then be calculated as

$$
\frac{\partial g}{\partial z}(t, p) =
\begin{bmatrix}
-\frac{1}{T_m} & 0 & 0 & 0 & 0 & 0 \\[8pt]
0 & 0 & \dot{\psi} & 0 & 0 & 0 \\[8pt]
0 & -\dot{\psi} & 0 & 0 & 0 & 0 \\[8pt]
0 & 0 & 0 & 0 & 0 & 0 \\[8pt]
0 & 0 & 0 & 0 & 0 & 0 \\[8pt]
0 & 0 & 0 & 0 & 0 & 0
\end{bmatrix}
\tag{4.61}
$$

$$
g'(t, p) =
\begin{bmatrix}
\frac{1}{T_m}\overline{M}'_e \\[12pt]
\frac{1}{m}\left(F'_{xf}\cos\varphi - F_{xf}\sin\varphi\varphi' + F'_{xr} - F'_{yf}\sin\varphi - F_{yf}\cos\varphi\varphi' - F'_w\right) \\[12pt]
\frac{1}{m}\left(F'_{xf}\sin\varphi + F_{xf}\cos\varphi\varphi' + F'_{yf}\cos\varphi - F_{yf}\sin\varphi\varphi' + F'_{yr}\right) \\[12pt]
\frac{1}{\Theta}\left(F'_{xf}l_f\sin\varphi + F_{xf}l_f\cos\varphi\varphi' + F'_{yf}l_f\cos\phi - F_{yf}l_f\sin\varphi\varphi' - F'_{yr}l_r\right) \\[12pt]
\frac{1}{\Theta_f}\left(M'_{af} + M'_{bf} - RF'_{xf}\right) \\[12pt]
\frac{1}{\Theta_r}\left(M'_{ar} + M'_{br} - RF'_{xr}\right)
\end{bmatrix}
$$

The quantity φ' is from Eq. 4.10. The derivatives of the tire forces F'_x and F'_y are dependent on the used tire model. In case of a linear tire model they can be calculated according to Eq. 4.38 and Eq. 4.39. Whereas in case of a tire model with force saturation, Eq. 4.46 and Eq. 4.48 describe the derivatives of the tire forces. The derivative of the static engine torque $\overline{M}'_e$ is from Eq. 4.19. M'_{af} and M'_{ar}, which represent the derivatives of the driving torque

with respect to the input vector $\boldsymbol{p}$ are from Eq. 4.13. The derivatives of the brake torques M'_{bf} and M'_{br} are from Eq. 4.26. F'_W which is the susceptibility of the aerodynamic force with respect to the input vector $\boldsymbol{p}$ is according to Eq. 4.28.

With the equation Eq. 4.61 substituted in Eq. 4.60 we can formulate the complete augmented equations of motion for the one track prediction model, which are necessary to solve the initial value problem of Eq. 4.8. The augmented equations of motion in state-space form are

$$\dot{\bar{z}} = \begin{vmatrix} -\frac{1}{T_m}M_e + \frac{1}{T_m}\overline{M}_e \\[2mm] \frac{1}{m}(F_{xf}\cos\varphi + F_{xr} - F_{yf}\sin\varphi - F_W) + \dot{y}\dot{\psi} \\[2mm] \frac{1}{m}(F_{xf}\sin\varphi + F_{yf}\cos\varphi + F_{yr}) - \dot{x}\dot{\psi} \\[2mm] \frac{1}{\Theta}(F_{xf}l_f\sin\varphi + F_{yf}l_f\cos\phi - F_{yr}l_r) \\[2mm] \frac{1}{\Theta_f}(M_{af} + M_{bf} - RF_{xf}) \\[2mm] \frac{1}{\Theta_r}(M_{ar} + M_{br} - RF_{xr}) \\[2mm] -\frac{1}{T_m}M'_e + \frac{1}{T_m}\overline{M}'_e \\[2mm] \frac{1}{m}(F'_{xf}\cos\varphi - F_{xf}\sin\varphi\varphi' + F'_{xr} - F'_{yf}\sin\varphi - F_{yf}\cos\varphi\varphi' - F'_w) + \dot{y}'\dot{\psi} + \dot{y}\dot{\psi}' \\[2mm] \frac{1}{m}(F'_{xf}\sin\varphi + F_{xf}\cos\varphi\varphi' + F'_{yf}\cos\varphi - F_{yf}\sin\varphi\varphi' + F'_{yr}) - \dot{x}'\dot{\psi} - \dot{x}\dot{\psi}' \\[2mm] \frac{1}{\Theta}(F'_{xf}l_f\sin\varphi + F_{xf}l_f\cos\varphi\varphi' + F'_{yf}l_f\cos\phi - F_{yf}l_f\sin\varphi\varphi' - F'_{yr}l_r) \\[2mm] \frac{1}{\Theta_f}(M'_{af} + M'_{bf} - RF'_{xf}) \\[2mm] \frac{1}{\Theta_r}(M'_{ar} + M'_{br} - RF'_{xr}) \end{vmatrix}$$

Chapter 5

The trajectory planning task

The driver's plant imaginations described in chapter 3 are involuntarily utilized by the driver to predict and finally optimize his future behavior. In doing so, he works as a nonlinear predictive controller. The basic process thereby is that, starting from the current time t_0, the driver predicts the vehicle's future reaction to his driver inputs for several seconds in advance from his plant imagination.

His ability to optimize behavior is mathematically described as the solution of an optimization problem. The driver "solves" this optimization problem at every time that he is replanning his future action.

5.1 Problem formulation

The trajectory planning task to be done by the driver constitutes a mixed continuous/discrete vector optimization problem under dynamic equality and inequality constraints:

$$\boldsymbol{p}^*(t) = \min_{\boldsymbol{p}(t)} \left\{ \overline{\boldsymbol{f}}\left(\boldsymbol{p}(t)\right) \mid \boldsymbol{g}_1\left(t, \boldsymbol{p}(t)\right) = \boldsymbol{0} \forall t \in]t_0; t_0 + t_h] \; ; \; \boldsymbol{g}_2\left(t, \boldsymbol{p}(t)\right) \leq \boldsymbol{0} \forall t \in]t_0; t_0 + t_h] \right\} . (5.1)$$

$\overline{\boldsymbol{f}}\left(\boldsymbol{p}(t)\right) \in \mathbb{R}^{n_f}$ is a vector of normalized objective functions, each of which should be minimized by a suitable choice of the time-varying components of the parameter vector $\boldsymbol{p}(t)$. $\boldsymbol{p}(t)^*$ denotes the point, where $\overline{\boldsymbol{f}}\left(\boldsymbol{p}(t)\right)$ has a minimum under the given constraints.

The equality constraints $\boldsymbol{g}_1\left(\boldsymbol{p}\right) = 0 \in \mathbb{R}^{n_{g1}}$ are constituted by the equations of motion of the respective plant model, Eq. 3.17 or Eq. 3.19, and their respective initial conditions given by the driver's momentary perception of the vehicle's state of motion.

The vector $\boldsymbol{g}_2\left(\boldsymbol{p}(t)\right) \in \mathbb{R}^{n_{g2}}$ of inequality constraints is explained in section 5.1.3

5.1.1   Optimization parameters

The inputs provided by the driver to control the vehicle are:

$\varrho(t) \in \mathbb{R}$ Longitudinal input: $\varrho \in [-1; 1]$ defines the driver's input to the accelerator and brake pedal. According to Eq. 3.1 $\varrho \geq 0$ gives the normalized throttle position, which is proportionally related to the accelerator pedal position. $\varrho < 0$ gives a normalized measure for the force exerted to the brake pedal.

$\varphi(t) \in \mathbb{R}$ Steering input: $\varphi(t)$ is the steering angle, measured at the steering wheel. The driver adjusts $\varphi(t)$ by turning the steering wheel.

$\eta(t) \in [1, 2, \ldots, 5]$:   Gear number: $\eta(t)$ is manually chosen by the driver through manual gearshift operations. $\eta(t)$ determines the gear ratio between engine and wheel. In contrast to ϱ and φ, η is usually a discrete variable with a fixed domain.

The vector $\boldsymbol{p}(t)$ of optimization parameters is then

$$\boldsymbol{p}(t) = \left[\begin{array}{ccc} \varrho(t) & \in & \mathbb{R} \\ \varphi(t) & \in & \mathbb{R} \\ \eta(t) & \in & \mathbb{N} \end{array} \right] \quad \begin{array}{l} \text{throttle/brake signal} \\ \text{steering angle} \\ \text{gear sequence} \end{array} \tag{5.2}$$

5.1.2   Objective functions

The driver performs his optimization with respect to certain objective functions. Several objectives are defined in this section. They have to be balanced versus each other by an appropriate choice of weighting factors.

Maximize travel distance (time-optimal)

The basic goal of vehicle driving is to transport passengers or goods from one point to another in an efficient manner. Efficiency means mostly speed. Thus, a driver would always try to maximize the distance he travels in a given time.

The travel distance $s_R(t)$ is defined along the center line of the road, see Fig. 5.1. $s_R(t_0 + t_h) - s_R(t_0)$ is the distance traveled between the current time t_0 and the time $t_0 + t_h$, with t_h being the optimization horizon or the prediction time. Since the travel distance should be maximized, its inverse is taken as an optimization criterion:

$$f_1 = \frac{1}{s_R(t_0 + t_h) - s_R(t_0)} . \tag{5.3}$$

Minimize horizontal accelerations (acceleration-optimal)
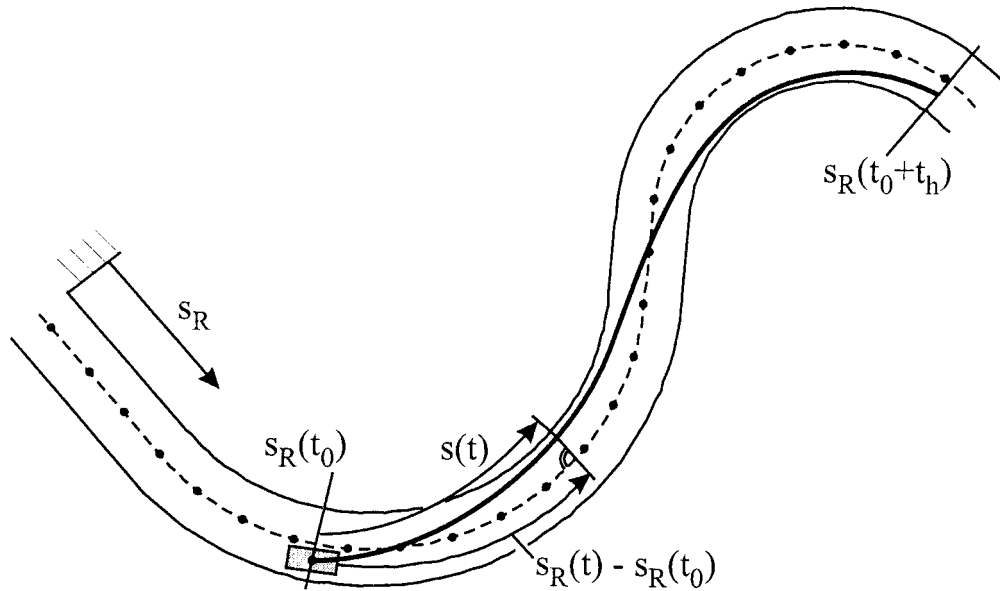
Figure **5.1:** Travel distance with respect to road middle line

For a comfortable ride, inertial forces exerted on the passengers in all three directions should be as small as possible. When cornering, however, or during accelerating and braking the passengers are exposed to horizontal accelerations. Vertical accelerations can not be directly influenced by the driver and are usually taken care of by the suspension. The driver can minimize horizontal accelerations by a correct timing of accelerating, braking and cornering, as well as by choosing large curve radii.
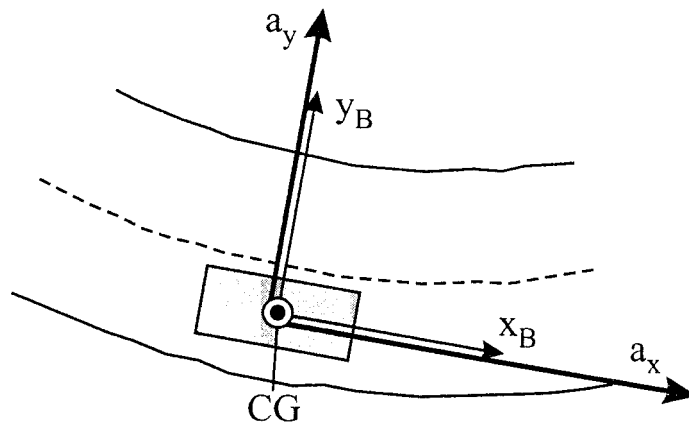
Figure *5.2:* Longitudinal and lateral accelerations

To formulate the acceleration criteria, longitudinal $a_x(t)$ and lateral $a_y(t)$ accelerations at the center of gravity (CG) are considered, see Fig. 5.2:

$$a_x(t) = \ddot{s}(t) \qquad , \qquad a_y(t) = K(t)\dot{s}^2(t) \,. \tag{5.4}$$

For the optimization, quadratic integral criteria over time from t_0 to t_h are used:

$$f_2 = \int a_x^2(t)\, dt \qquad\qquad f_3 = \int a_y^2(t)\, dt\, . \qquad\qquad (5.5)$$

Minimize brake usage (brake-optimal)

The main goal of minimizing brake usage during driving is to prevent kinetic energy from being dissipated by the brake discs. On the other hand, people are instructed by driving schools to spare the brakes when going downhill to prevent them from overheating. Thus, there are situations, where this criterion plays a significant role.

A penalty function $p_b\left(\varrho(t)\right)$ is defined to penalize brake usage, which is indicated by $\varrho(t) < 0$, see Fig. 5.3:

$$p_b\left(\varrho(t)\right) = -\varrho^-(t)\, , \qquad\qquad (5.6)$$
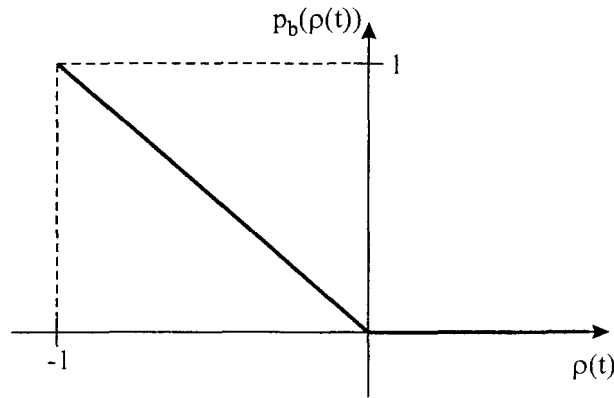
Figure **5.3:** Penalty function for brake usage

The criterion f_4 is then formulated as the integral of the penalty function over the prediction period:

$$f_4 = \int_{t_0}^{t_h} p_b\left(\varrho(t)\right)\, dt \qquad\qquad (5.7)$$

Stay in middle of lane (keep right)

An important issue during highway driving is to stay in one lane and to avoid uncontrolled lane changes. Thus, we define a quadratic function $p_l\left(\Delta w(t)\right)$, which penalizes the lateral deviation from the center of the lane:

$$p_l\left(\Delta w(t)\right) = \left(\Delta w(t) - \Delta w_0\right)^2\, , \qquad\qquad (5.8)$$
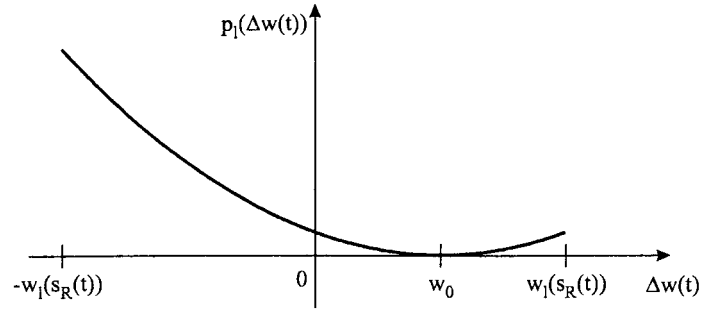
Figure **5.4:** Penalty function for lane keeping

where Δw_0 denotes the desired lateral position on the road: according to its definition in Fig. 2.9.

The respective objective function is then again the integral of the penalty function over the prediction period:

$$f_5 = \int_{t_0}^{t_h} p_l\left(\Delta w(t)\right) dt \tag{5.9}$$

Minimize deviation **of** optimal engine speed (rpm-optimal)

Most drivers involuntarily try to keep a certain engine speed, at which they are feeling comfortable with respect to engine noise on one hand, and possible engine torque on the other hand. Assuming a perfect rolling constraint to be fulfilled at the driven wheels, the engine speed $n_e(t)$ is:

$$n_e(t) = \frac{60}{2\pi} i_{diff} i_{gear}\left(\eta(t)\right) \frac{\dot{s}(t)}{R}, \tag{5.10}$$

We define again a penalty function $p_e\left(n_e(t)\right)$ for the engine speed, see Fig. 5.5:

$$p_e\left(n_e(t)\right) = \left(n_e(t) - n_{e,0}\right)^2, \tag{5.11}$$

with $n_{e,0}$ being the engine speed felt optimal by the driver.

The criterion to be minimized is again the integral of $p,\left(n_e(t)\right)$ over the prediction period.

$$f_6 = \int_{t_0}^{t_h} p_e\left(n_e(t)\right) dt \tag{5.12}$$

Minimize deviation **of** given velocity (velocity-optimal)
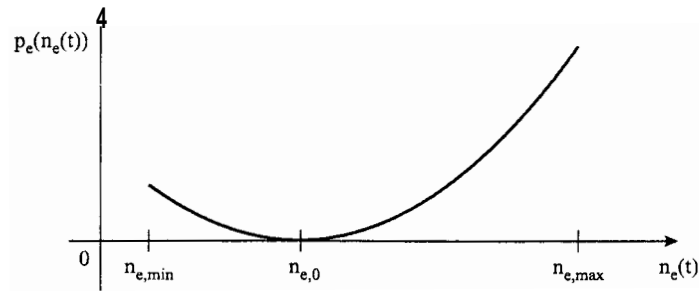
Figure *5.5:* Penalty function for engine speed

The velocity criterion is important in two possible situations: first, on almost every road speed limits apply, which influence the driver's behavior in a sense that he tries to minimize the deviation of his vehicle's speed from the posted limit. Second, in certain situations he may think that a certain speed is appropriate for safety reasons. Making the appropriate speed zero and imposing all weight on this objective function causes the driver model to brake suddenly, e. g. to simulate an emergency situation.

Speed deviations are penalized by the penalty function $p, (\dot{s}(t))$, see Fig. 5.6:

$$p_s\left(\dot{s}(t)\right) = \left(\dot{s}(t) - \dot{s}_0\right)^2 \ . \tag{5.13}$$

is a given (desired) velocity.
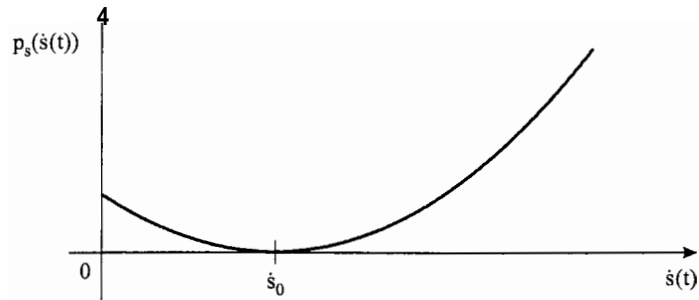
Figure *5.6:* Penalty function for velocity

The objective function f_7 is again formulated as the integral of $p, (\dot{s}(t))$ over the prediction period:

$$f_7 = \int_{t_0}^{t_h} p_s\left(\dot{s}(t)\right) \ dt \tag{5.14}$$

Normalization of objectives

To form a vector optimization problem, where a sensible trade-off between the objectives can be made, the objective functions f_i, $i = 1, \ldots, 7$ have to be normalized. This is to ensure, that equal qualities in different criteria result in equal values of their respective objective functions.

We define threshold values f_{i0}, $i = 1, \ldots, 7$ for each of the criteria, where the driver finds the behavior only just comfortable. The normalized objective functions $\overline{f}_i = f_i/f_{i0}$ have a value of 1 when the behavior becomes uncomfortable for the driver.

$$
\boldsymbol{f} = \begin{bmatrix} f_1 \\ f_2 \\ \vdots \\ f_7 \end{bmatrix} \quad ; \quad \overline{\boldsymbol{f}} = \begin{bmatrix} \overline{f}_1 \\ \overline{f}_2 \\ \vdots \\ \overline{f}_7 \end{bmatrix} = \begin{bmatrix} f_1/f_{10} \\ f_2/f_{20} \\ \vdots \\ f_7/f_{70} \end{bmatrix} \tag{5.15}
$$

Table 5.1: Normalization of objective functions

criterion	f_{i0}	$\overline{f}_i$
time-optimal	$f_{10} = \dfrac{1}{\overline{s}\,(t_h - t_0)}$	$\overline{f}_1 = \dfrac{\overline{s}\,(t_h - t_0)}{s_R\,(t_h)}$
acceleration-optimal	$f_{20} = \overline{a}\,(t_h - t_0)$ $f_{30} = \overline{a}\,(t_h - t_0)\,,$	$\overline{f}_2 = \dfrac{1}{\overline{a}\,(t_h - t_0)} \int\limits_{t_0}^{t_h} a_x(t)\,dt$ $\overline{f}_3 = \dfrac{1}{\overline{a}\,(t_h - t_0)} \int\limits_{t_0}^{t_h} a_y(t)\,dt$
brake-optimal	$f_{40} = \overline{\varrho}\,(t_h - t_0)$	$\overline{f}_4 = \dfrac{1}{\overline{\varrho}\,(t_h - t_0)} \int\limits_{t_0}^{t_h} p_b\,(\varrho(t))\,dt$
keep right	$f_{50} = \overline{\Delta w}^2\,(t_h - t_0)$	$\overline{f}_5 = \dfrac{1}{\overline{\Delta w}} \int\limits_{t_0}^{t_h} (\Delta w(t) - \Delta w_0)^2\,dt$
rpm-optimal	$f_{60} = \overline{\Delta n_e}^2\,(t_h - t_0)$	$\overline{f}_6 = \dfrac{1}{\overline{\Delta n_e}^2\,(t_h - t_0)} \int\limits_{t_0}^{t_h} (n_e(t) - n_{e,0})\,dt$
velocity-optimal	$f_{70} = \overline{\Delta \dot{s}}^2\,(t_h - t_0)$	$\overline{f}_7 = \dfrac{1}{\overline{\Delta \dot{s}}^2\,(t_h - t_0)} \int\limits_{t_0}^{t_h} (\dot{s}(t) - \dot{s}_0)^2\,dt$

Table *5.2:* Quantities used for objective normalization

$\dot{\bar{s}}$	:	given travel speed desired by the driver
$\bar{a}$	:	comfortable acceleration
$\bar{e}$	:	comfortable brake input
$\overline{\Delta w}$	:	comfortable lane deviation
$\overline{\Delta n_e}$	:	comfortable deviation in engine speed
$\dot{\bar{s}}$	:	comfortable speed deviation

5.1.3   Constraints

The vector $\overline{\boldsymbol{f}}(\boldsymbol{p})$ of objective functions, see Eq. 5.15 must be minimized under the equality constraints $\boldsymbol{g}_1(t,\boldsymbol{p}) = 0$ and inequality constraints $\boldsymbol{g}_2(t,\boldsymbol{p}) \le 0$, according to Eq. 5.1.

$\boldsymbol{g}_1(t,\boldsymbol{p})$ is constituted by the dynamic equations of motion Eq. 3.17, Ey. 3.19 of the driver's plant model imagination.

$$\boldsymbol{g}_2(t,\boldsymbol{p}) = \begin{bmatrix} g_{2,1}(t) \\ g_{2,2}(t) \\ \vdots \\ g_{2,6}(t) \end{bmatrix} \tag{5.16}$$

is the vector of inequality constraints coming from the following considerations.

Stay on road
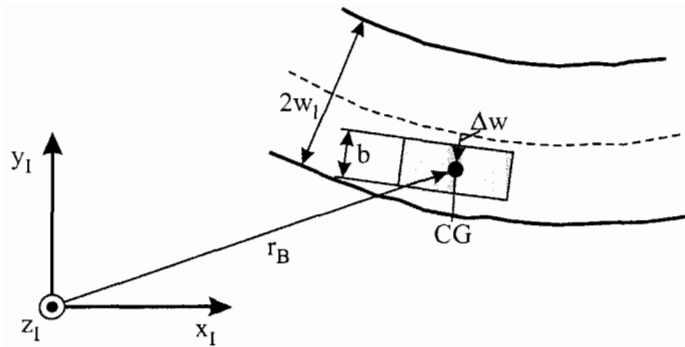
Figure *5.7:* Definition of quantities describing the relative
position of vehicle to road; w_l: lane width; Δw:
lateral vehicle position; b: vehicle width

The most important constraint during driving is to keep the vehicle on the road under all circumstances. Fig. 5.7 shows all quantities needed to determine the vehicle's relative

position on the road. $\Delta w(t)$ is the vehicle's lateral offset with respect to the middle line of the road. The constraints to be fulfilled are:

$$
\begin{aligned}
g_{2,1}(t) &= \Delta w(t) + \frac{b}{2} - w_l \leq 0 \\
\\
g_{2,2}(t) &= -\Delta w(t) + \frac{b}{2} - w_l \leq 0
\end{aligned}
\tag{5.17}
$$

Limit horizontal accelerations

If the driver employs a prediction model with kinematic rolling constraints between wheels and road, he has no measure for the contact forces, which can be transmitted through the tire latch. On the other hand, it takes very little experience to know that only limited accelerations can be tolerated in both longitudinal and lateral directions. The maximal values thereof depend heavily on the road conditions and on the accuracy of the prediction model employed.
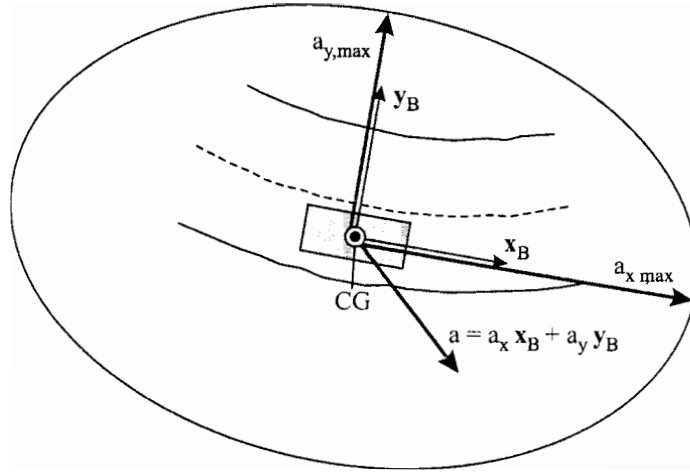
Figure *5.8:* Maximal and actual accelerations acting on the vehicle; *a:* overall horizontal accelera- tion; $a_{x,max}$: maximal longitudinal accelera- tion; $a_{y,max}$: maximal lateral acceleration

Fig. 5.8 shows the accelerations acting on the vehicle in a body fixed coordinate system. The maximal allowable longitudinal and lateral accelerations depend on each other. They are assumed to be situated on an ellipse, the main axes of which are the vehicle's roll and pitch axes:

$$
g_{2,3}(t) = \left(\frac{a_x(t)}{a_{x,max}} \right)^2 + \left(\frac{a_y(t)}{a_{y,max}} \right)^2 - 1 \leq 0
\tag{5.18}
$$

$a_x(t)$ and $a_y(t)$ are the components of the resulting absolute acceleration of the vehicle's center of gravity, in the body fixed coordinate system, see Fig. 5.8.

Limit engine speed

When using manual gear shifting, the driver is responsible for the proper choice of his engine speed. Particularly, he must not exceed the vehicle's maximal engine speed $n_{e,max}$. On the other hand, he has to keep the engine speed higher than a minimal limit value $n_{e,min}$ to prevent the engine from stalling.

The respective constraints are:

$$
\begin{aligned}
g_{2,4}(t) &= n_e(t) - n_{e,max} &\leq 0 \\
\\
g_{2,5}(t) &= -n_e(t) + n_{e,min} &\leq 0
\end{aligned}
\tag{5.19}
$$

Ability to decelerate to zero velocity within half sight distance

In many situations, especially on winding narrow roads, where there is oncoming traffic, the driver must adjust his speed, so that he can stop within half of the sight distance d_s, if necessary.

To formulate the respective constraint, we assume a brake maneuver with the highest possible longitudinal deceleration:

$$
g_{2,6}(t) = \dot{s}(t) - \sqrt{2a_{x,max}\frac{d_s}{2}} \leq 0.
\tag{5.20}
$$

Avoid obstacles

5.2   Implementation

5.2.1   Problem reduction

For a possible numerical treatment with standard parameter optimization algorithms the problem Eq. 5.1 must be suitably reduced. In particular, the control inputs, which finally have to be given as functions of time, must be parameterized, the inequality constraints $g_2(t,p(t)) \leq 0 \forall t$ E $[t_0;t_0 + t_h]$ have to be discretized.

Moreover, the continuous/discrete optimization problem must be suitably addressed. This is accomplished by separating the problem into three steps, see Fig. 5.9:

- Solve the optimization problem Eq. 5.1 assuming all variables (throttle/brake $\varrho \in \mathbb{R}$, steering φ E $\mathbb{R}$, gear η E $\mathbb{R}$) as real numbers.

- Discretize the gear numbers ($\eta \in \mathbb{IN}$), such that a certain error criterion is minimized.

$$
\begin{array}{c}
\boxed{\text{problem 1} \ \begin{vmatrix} {}^1\rho \in \mathbb{R} \\ {}^1\varphi \in \mathbb{R} \end{vmatrix}} \\[2mm]
\Big\downarrow \ \begin{array}{l} {}^1\rho^* \in \mathbb{R} \\ {}^1\varphi^* \in \mathbb{R} \\ {}^1\eta^* \in \mathbb{R} \end{array} \\[2mm]
\boxed{\text{problem 2} \ \begin{vmatrix} {}^2\eta \in \mathbb{N} \end{vmatrix}} \\[2mm]
\Big\downarrow \ {}^2\eta^* \in \mathbb{N} \\[2mm]
\boxed{\text{problem 3} \ \begin{vmatrix} {}^3\rho \in \mathbb{R} \\ {}^3\varphi \in \mathbb{R} \end{vmatrix}} \\[2mm]
\Big\downarrow \ \begin{array}{l} {}^3p^* \in \mathbb{R} \\ {}^3\varphi^* \in \mathbb{R} \\ {}^3\eta^* \in \mathbb{N} \end{array}
\end{array}
$$
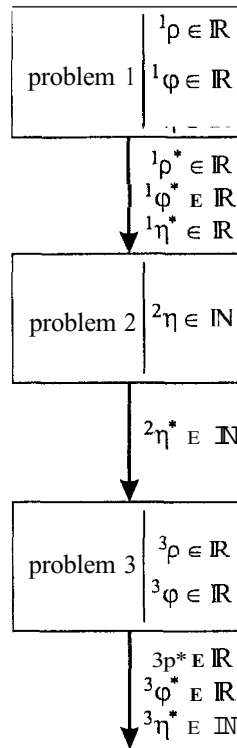
Figure 5.9: Implementation of the continuous/discrete optimization problem for the trajectory planning task

- Solve the continuous part of the problem ($\varrho \in \mathbb{R}$, $\varphi \in \mathbb{R}$) assuming the gear sequence to be fixed at the result of the second step.

As a result of these three consecutive steps we obtain a suboptimal solution of the problem Eq. 5.1. The simulations in chapter 8 show however, that our solution is close enough to the optimum to provide sensible results.

Problem 1: Optimization with real parameters

In the first step the parameters are assumed to be real functions of time:

$$
{}^1\boldsymbol{p}({}^1\overline{\boldsymbol{p}}, t) = \begin{pmatrix} {}^1\varrho({}^1\overline{\boldsymbol{p}}, t) \in \mathbb{R} \\ {}^1\varphi({}^1\overline{\boldsymbol{p}}, t) \in \mathbb{R} \\ {}^1\eta({}^1\overline{\boldsymbol{p}}, t) \in \mathbb{R} \end{pmatrix} \quad ; \qquad t_0 \leq t \leq t_0 + t_h \,. \tag{5.21}
$$

Since standard numerical optimization algorithms deal mostly with optimization parameters instead of functions over time, the input vector ${}^1\boldsymbol{p}(t)$ must be parameterized. We do this using x linear interpolation:

The time range $[t_0; t_0 + t_h]$ is divided into n intervals by an equally spaced vector t of interval boundaries:

$$t := \begin{bmatrix} t_0 & t_1 & \dots & t, \end{bmatrix} \in \mathbb{R}^{n+1}. \tag{5.22}$$

The parameter vector used for the optimization consists of the function values at the interval boundaries:[1]

$$^1\overline{p} := \begin{bmatrix} {}^1\varrho(t_0) & \dots & {}^1\varrho(t_{n-1}) & | & {}^1\varphi(t_0) & \dots & {}^1\varphi(t_{n-1}) & | & \dots \\ & {}^1\eta(t_0) & \dots & {}^1\eta(t_{n-1}) \end{bmatrix}^T \in \mathbb{R}^{3n}. \tag{5.23}$$

linear interpolation   interpolation with zero-order hold
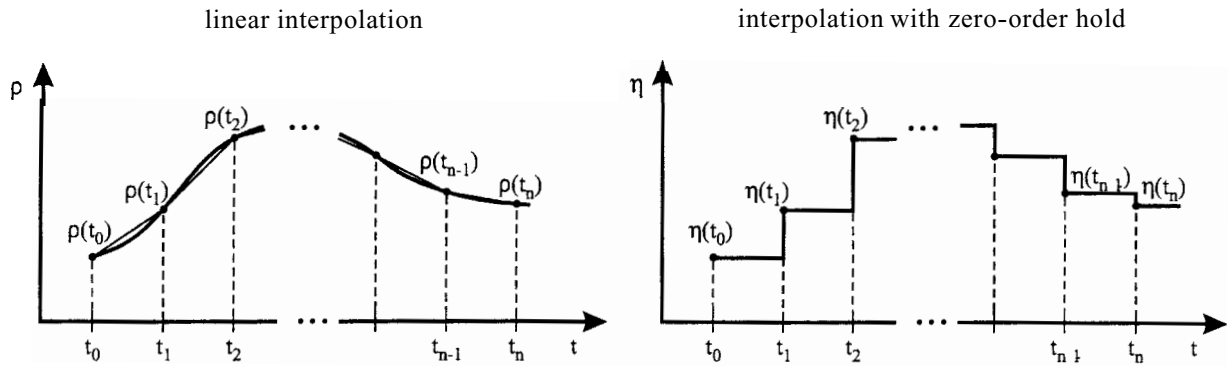
Figure 5.10: Interpolation of driver inputs

Linear interpolation is used to determine the function values within the intervals, see Fig. 5.10:

$$^1\xi(^1\overline{p}, t) = \begin{pmatrix} {}^1\varrho(^1\overline{p}, t) \\ {}^1\varphi(^1\overline{p}, t) \\ {}^1\eta(^1\overline{p}, t) \end{pmatrix} = \begin{pmatrix} {}^1\varrho(t_i) + \dfrac{{}^1\varrho(t_{i+1}) - {}^1\varrho(t_i)}{t_{i+1} - t_i}(t - t_i) \\ {}^1\varphi(t_i) + \dfrac{{}^1\varphi(t_{i+1}) - {}^1\varphi(t_i)}{t_{i+1} - t_i}(t - t_i) \\ {}^1\eta(t_i) + \dfrac{{}^1\eta(t_{i+1}) - {}^1\eta(t_i)}{t_{i+1} - t_i}(t - t_i) \end{pmatrix} ; \ t_i \le t \le t_{i+1}. \tag{5.24}$$

The differential equations of motion describing the prediction model, which are included in the vector $g_1(p(^1\overline{p}, t))$ of equality constraints, are solved in continuous time. Consequently, $g_1(p(^1\overline{p}, t))$ and the cost function vector $\overline{f}(p(^1\overline{p}, t))$ are evaluated in continuous time. The vector $^1\overline{g}_1(^1\overline{p}, t)$ for the modified problem 1 is then:

$$^1\overline{g}_1(^1\overline{p}, t) = \begin{pmatrix} g_1(^1p(^1\overline{p}, t)) \\ {}^1p(t) - {}^1\xi(^1\overline{p}, t) \end{pmatrix}. \tag{5.25}$$

---

[1] System inputs at the time $t_n = t_h$ do not influence the behavior in the regarded time range $[t_0; t_h]$.

The discretized vector ${}^1\overline{\boldsymbol{g}}_2({}^1\boldsymbol{p}(t))$ of inequality constraints for problem 1 is:

$$
{}^1\overline{\boldsymbol{g}}_2({}^1\boldsymbol{p}({}^1\overline{\boldsymbol{p}},t)) =
\begin{bmatrix}
\boldsymbol{g}_2({}^1\boldsymbol{p}({}^1\overline{\boldsymbol{p}},t),t_1) \\
\boldsymbol{g}_2({}^1\boldsymbol{p}({}^1\overline{\boldsymbol{p}},t),t_2) \\
\vdots \\
\boldsymbol{g}_2({}^1\boldsymbol{p}({}^1\overline{\boldsymbol{p}},t),t_n)
\end{bmatrix}
\qquad \in \qquad \mathbb{R}^{n_{g2}n} .
\tag{5.26}
$$

The optimization problem solved in problem 1 is then

$$
{}^1\overline{\boldsymbol{p}}^* = \min_{{}^1\overline{\boldsymbol{p}} \in \mathbb{R}^{3n}} \left\{ \overline{\boldsymbol{f}}(\boldsymbol{p}({}^1\overline{\boldsymbol{p}},t)) \mid {}^1\overline{\boldsymbol{g}}_1({}^1\overline{\boldsymbol{p}},t) = 0 \ \forall \ t \in [t_0;t_h] \ ; \ {}^1\overline{\boldsymbol{g}}_2({}^1\boldsymbol{p}({}^1\overline{\boldsymbol{p}},t)) \leq 0 \right\} .
\tag{5.27}
$$

Problem 2: Combinatorial optimization of gear sequence

In the next step the gear sequence ${}^1\boldsymbol{\eta}^* := \begin{bmatrix} {}^1\eta^*(t_0) & \ldots {}^1\eta^*(t_{n-1}) \end{bmatrix} \in \mathbb{R}^n$ is discretized to obtain an integer sequence

$$
{}^2\overline{p} := {}^2\boldsymbol{\eta} := \begin{bmatrix} {}^2\eta(t_0) & \ldots {}^2\eta(t_{n-1}) \end{bmatrix} \in \mathbb{N}^n
\tag{5.28}
$$

of gear numbers. The optimization variable ${}^2\eta({}^2\overline{p},t)$ can be an integer number only. Therefore, we interpolate between the interval boundaries using a zero order hold:

$$
{}^2\xi({}^2\overline{p},t) :={}^2\eta(t) ={}^2\eta(t_i) \qquad ; \qquad t_i \leq t < t_{i+1} .
\tag{5.29}
$$

Assume the same velocity profile ${}^1\dot{s}^*(t)$ as in problem 1, the engine speed n_e is solely a function of the gear sequence and of time: $n_e({}^2\overline{p},t)$. The vector ${}^2\overline{\boldsymbol{g}}_1({}^2\overline{p},t)$ of equality constraints for problem 2 is then:

$$
{}^2\overline{\boldsymbol{g}}_1({}^2\overline{p},t) =
\begin{pmatrix}
n_e({}^2\overline{p},t) - \dfrac{{}^1\dot{s}^*(t)}{R} i_{diff} \dfrac{60}{2\pi} i_{gear}({}^2\eta({}^2\overline{p},t)) \\[4mm]
{}^2\eta({}^2\overline{p},t) -{}^2\xi({}^2\overline{p},t)
\end{pmatrix} .
\tag{3.30}
$$

In problem 2 the driver must assure that for the given velocity ${}^1\dot{s}^*(t)$ the lower and upper engine speed limits are not exceeded. Thus, the inequality constraints ${}^2\overline{\boldsymbol{g}}_2({}^2\overline{p})$ applicable for problem 2 are

$$
{}^2\overline{\boldsymbol{g}}_2({}^2\overline{p}) =
\begin{bmatrix}
g_{2,4}({}^2\overline{p},t_1) \\
\vdots \\
g_{2,4}({}^2\overline{p},t_n) \\
\hline
g_{2,5}({}^2\overline{p},t_1) \\
\vdots \\
g_{2,5}({}^2\overline{p},t_n)
\end{bmatrix}
\qquad \in \qquad \mathbb{R}^{2n} .
\tag{5.31}
$$

The objective in problem 2 is to keep the deviation from the gear ratio $i_{gear}\left({}^1\eta^*(t)\right)$, which is given by the solution of Eq. 5.27, low:

$$
{}^2\overline{f} = \sum_{j=0}^{n-1}\left(\left(\frac{i_{gear}\left({}^2\eta(t_j)\right)}{i_{gear}\left({}^1\eta^*(t_j)\right)}\right)^{\alpha_j} - 1\right) \quad ; \quad \alpha_j = \mathrm{sgn}\left(\frac{i_{gear}\left({}^2\eta(t_j)\right)}{i_{gear}\left({}^1\eta^*(t_j)\right)} - 1\right). \tag{5.32}
$$

The combinatorial optimization problem for problem 2 is then:

$$
{}^2\overline{p}^* = \min_{{}^2\overline{p}\in\mathbb{N}^n}\left\{\overline{f}\left(p\left({}^2\overline{p},t\right)\right) \mid {}^2\overline{g}_1\left({}^2\overline{p},t\right) = 0 \;\forall\; t \in [t_0;t_h] \;;\; {}^2\overline{g}_2\left({}^2p\left({}^2\overline{p},t\right)\right) \le 0\right\}. \tag{5.33}
$$

Problem 3: Final optimization with fixed gear sequence

After selecting an optimal gear sequence, the throttle/brake signal and steering angle are adjusted to the changed gear ratios by a third (continuous) optimization step.

The vector ${}^3p(t)$ of optimization variables for problem 3 is

$$
{}^3p(t) = \begin{pmatrix} {}^3\varrho(t) \\ {}^3\varphi(t) \end{pmatrix} \in \mathbb{R}^2. \tag{5.34}
$$

Discretizing ${}^3p(t)$ with respect to time under usage of Eq. 5.22 yields the parameter vector

$$
{}^3\overline{p} := \begin{bmatrix} {}^3\varrho(t_0) & \cdots & {}^3\varrho(t_{n-1}) \mid {}^3\varphi(t_0) & \cdots & {}^3\varphi(t_{n-1}) \end{bmatrix}^T \in \mathbb{R}^{2n}. \tag{5.35}
$$

The input variables at time t are gained by linear interpolation:

$$
{}^3\boldsymbol{\xi}\left({}^3\overline{p},t\right) := \begin{pmatrix} \quad \\ \quad \end{pmatrix} \begin{pmatrix} {}^3\varrho\left(t_i\right) + \dfrac{{}^3\varrho\left(t_{i+1}\right) - {}^3\varrho\left(t_i\right)}{t_{i+1}-t_i}(t-t_i) \\ {}^3\varphi\left(t_i\right) + \dfrac{{}^3\varphi\left(t_{i+1}\right) - {}^3\varphi\left(t_i\right)}{t_{i+1}-t_i}(t-t_i) \end{pmatrix} \quad t_i \le t < t_{i+1}. \tag{5.36}
$$

The equality and inequality constraints for problem 3 are:

$$
{}^3\overline{g}_1\left({}^3\overline{p},t\right) = \begin{pmatrix} g\left({}^3p(t)\right) \\ \eta(t) - {}^2\eta^* \\ {}^3p(t) - {}^3\boldsymbol{\xi}\left({}^3\overline{p},t\right) \end{pmatrix} \tag{5.37}
$$

$$
{}^3\overline{g}_2\left({}^3p\left({}^3\overline{p},t\right)\right) = \begin{bmatrix} g_2\left({}^3p\left({}^3\overline{p},t\right),t_1\right) \\ g_2\left({}^3p\left({}^3\overline{p},t\right),t_2\right) \\ \vdots \\ g_2\left({}^3p\left({}^3\overline{p},t\right),t_n\right) \end{bmatrix} \quad \in \quad \mathbb{R}^{n_{g2}n} \tag{5.38}
$$

The optimization problem, which is solved in problem 3 is then

$$
{}^3\overline{p}^* = \min_{{}^3\overline{p}\in\mathbb{R}^n}\left\{\overline{f}\left(p\left({}^3\overline{p},t\right)\right) \mid {}^3\overline{g}_1\left({}^3\overline{p},t\right) = 0 \;\forall\; t \in [t_0;t_h] \;;\; {}^3\overline{g}_2\left({}^3p\left({}^3\overline{p},t\right)\right) \le 0\right\}. \tag{5.39}
$$

5.2.2   Solution of **the** vector optimization problem

It is known from the theory of vector optimization, that there exists no unique solution for the problems Eq. 5.27 and Eq. 5.39, if at least two of the objective functions are competing. In general this is the case, so that the solution of the problems Eq. 5.27 and Eq. 5.33 span an $n_f - 1$dimensional subspace – the functional efficient set of solutions – in criterion space. Functional efficiency is reached, if none of the objective functions can be reduced further without increasing at least one of the other objectives.

To obtain a unique solution the vector problems are reduced to a scalar substitute problem using the method of objective weighting, [4]. Thus, we introduce a scalar preference function P representing a weighted sum of the components of $\overline{f}$. A row vector $w \in \mathbb{R}^{n_f}$ of weighting factors is defined such that

$$0 \leq w_i \leq 1 \qquad ; \qquad \sum_{i=1}^{n_f} w_i = 1 \, , \tag{5.40}$$

is fulfilled. The preference function P is then defined as[2]

$$P\left(\overline{f}(\overline{p}), w\right) = w\overline{f}(\overline{p}) \, , \tag{5.41}$$

such that the scalar substitute problem is

$$\min_{\overline{p}} \left\{ P\left(\overline{f}\left(\overline{p}\right), w\right) \mid \overline{g}_1\left(\overline{p}\right) = 0 \, ; \, \overline{g}_2\left(\overline{p}\right) \leq 0 \right\} \, . \tag{5.42}$$

By solving Eq. 5.42 repeatedly with a systematic variation of the components in w, one could calculate the functional efficient set of solutions. In our case: we are only interested in a single solution point for a given w. w is determined in the cognitive decision layer using the driver's expert knowledge.

For the optimization a Sequential Quadratic Programming (SQP) method is used, where the Hessian of the Lagrangian function is updated at every iteration by a quasi-Newton approximation (BFGS), see [9, 10, 14].

---

[2]Defining the preference function as in Eq. 5.41 is to some extent arbitrary. The different objective functions are weighted using a 1-norm (algebraic sum). Different formulations of preference functions using other norms together with their geometric interpretation can be found e. g. in [11].

Chapter 6

The vehicle control task

Having the trajectory planned for the next couple of seconds the driver employs then strategies to follow that path as accurately as possible. This stabilization update has to be done at a much higher sampling rate (time increment δt) than the trajectory update, which is done at increments of At, see Fig.6.1[1]. For the following mathematical description, we introduce an integer number k to count the trajectory updates, and an integer number i for the stabilization updates between k and $k+1$:

$$^{k}t_0 \quad = \quad {}^{k-1}t_0 + \Delta t \quad = \quad {}^{k-1}t_0 + n\delta t. \tag{6.1}$$
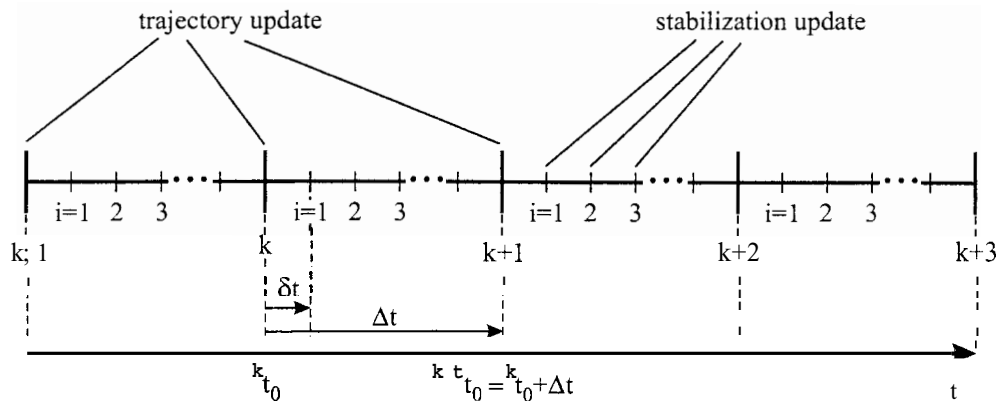
Figure 6.1: Timing of control updates at different levels;
k: counter for trajectory update, i: counter
for stabilization update, At trajectory update
time, bt: stabilization update time.

The driver is assumed to employ a simple PID control scheme to minimize speed deviations (longitudinal) and path deviations (lateral). Longitudinal and lateral directions are decoupled in this controller.

---

[1]For convenience we choose $\frac{\Delta t}{\delta t} = n \in \mathbb{N}$. Typically δt is about 10 times smaller than At: $n \approx 10$.

6.1 Reference trajectory filtering

At each trajectory update ${}^k t_0$ the actual perceived state of motion $\tilde{z}\left({}^k t_0\right)$ is taken as the initial condition contained in the vector $\boldsymbol{g}_1$ from Eq. 5.1. Due to controller errors $\tilde{z}\ ('t_0)$ differs from the desired state of motion ${}^{(k}-1)z\left({}^k t_0\right)$ predicted at time ${}^{(k}-1)t_0$.

Consequently, if at the time $t \geq {}^k t_0$ the trajectory ${}^k z(t)$ is solely taken as the new reference, the desired trajectory would become unsteady on position level at the trajectory updates. This would result in unsteady driver input signals, i. e. jumps in throttle position and steering angle. Therefore, an appropriate filtering is necessary.

This is done by weighting the precedent ν trajectory updates against each other using a vector 'forgetting factors' u_j.
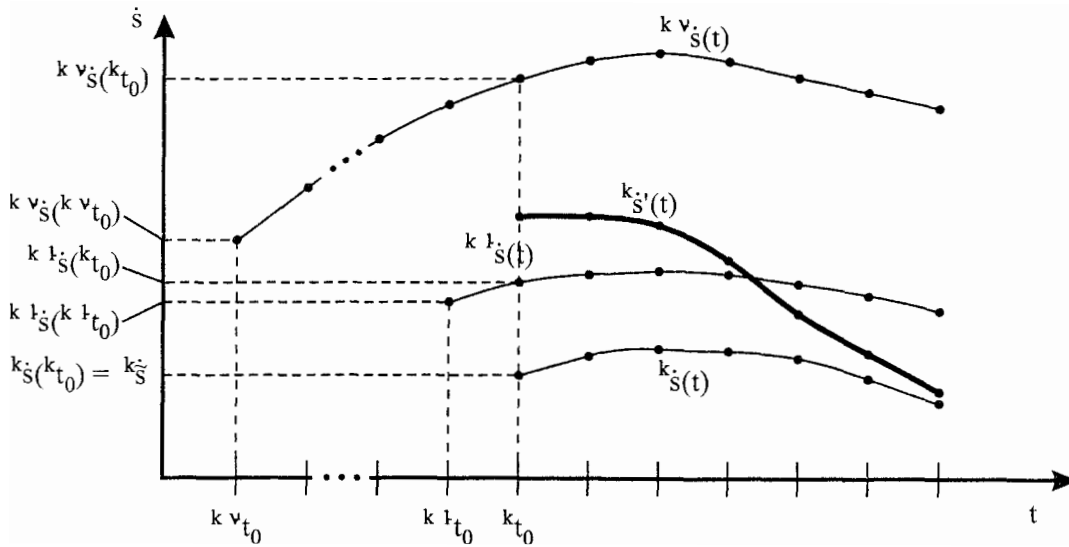
Figure 6.2: Correction of the planned velocity to produce smooth longitudinal driver inputs.

From Fig. 6.1 follows:

$${}^k t_0 = {}^{k-1} t_0 + \text{A}t = {}^{k-2} t_0 + 2At = \ldots = {}^{k-\nu} t_0 + \nu \Delta t \,. \tag{6.2}$$

According to Figs. 6.2 and 6.3 we define the quantities listed in Table 6.1.

The filtered reference trajectory ${}^k r'_{POI}(t)$ and velocity profile ${}^k \dot{s}'(t)$ are then calculated as

$$
\begin{aligned}
{}^k r'_{POI}\left({}^k t_0 + t\right) &= \sum_{j=0}^{\nu} u_j {}^{k-j} r_{POI}\left({}^k t_0 + t\right) \\
{}^k \dot{s}'\left({}^k t_0 + t\right) &= \sum_{j=0}^{\nu} u_j {}^{k-j} \dot{s}\left({}^k t_0 + t\right),
\end{aligned}
\tag{6.3}
$$
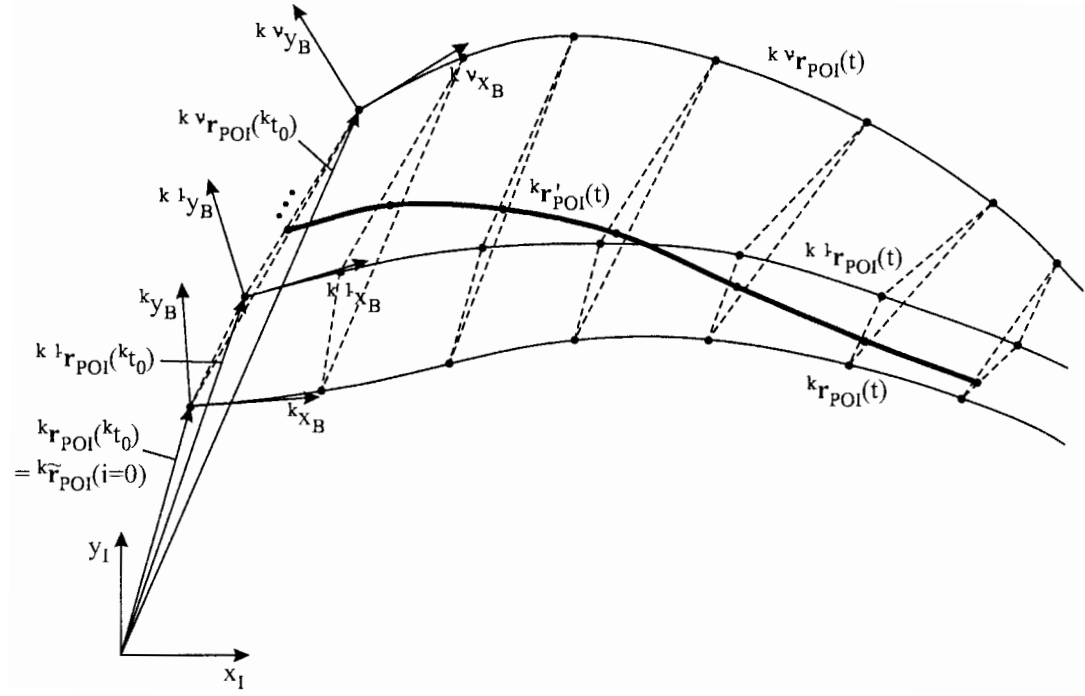
Figure 6.3: Correction of the planned trajectory to produce smooth lateral driver inputs.

Table 6.1: Quantities defined for interpolation

$^k\dot{s}(t)$	:	velocity predicted at time $^k t_0$ for time t
$^k\dot{s}'(t)$	:	filtered velocity predicted at time $^k t_0$ for time t
$^k\dot{\tilde{s}}(i=0)$	:	velocity perceived at time $^k t_0$
$^k\boldsymbol{r}_{POI}(t)$	:	POI position predicted at time $^k t_0$ for time t
$^k\boldsymbol{r}'_{POI}(t)$	:	filtered POI position predicted at time $^k t_0$ for time t
$^k\tilde{\boldsymbol{r}}_{POI}(i=0)$	:	POI position perceived at time $^k t_0$

with u_j being a weight function (forgetting factor) with the following properties:

$$u_j \geq 0 \; \forall j \in \mathbb{N} \quad ; \quad u_0 = 0 \quad ; \quad u_\nu = 0. \tag{6.4}$$

6.2   PID control

Longitudinal control

The throttle position $\varrho(t)$ is used in the control layer of the proposed driver model to control the vehicle in longitudinal direction. The equation describing the PI-control of the throttle

position is

$$\tilde{\varrho}(t) = \varrho(t) - K_{P,\varrho} \left({}_k \dot{s}'(t) - \dot{\tilde{s}}(t) \right) - K_{I,\varrho} \int\limits_0^t \left({}_k \dot{s}'(\tau) - \dot{\tilde{s}}(\tau) \right) d\tau \,, \tag{6.5}$$

with the following controller coefficients

$K_{P,\varrho}$ coefficient of proportional term of longitudinal control
$K_{I,\varrho}$ coefficient of integral term of longitudinal control

Lateral control

The steering angle $\varphi(t)$ is used to control the vehicle in lateral direction. The underlying equation for the PID-control of the steering angle is

$$\tilde{\varphi}(t) = \varphi_0(t) - K_{P,\varphi} \Delta y(t) - K_{D,\varphi} \dot{\Delta y}(t) - K_{I,\varphi} \int\limits_0^t \Delta y(\tau) d\tau \,, \tag{6.6}$$

with the following quantities

$K_{P,\varphi}$ coefficient of proportional term of lateral control
$K_{I,\varphi}$ coefficient of integral term of lateral control
$K_{D,\varphi}$ coefficient of differential term of lateral control
φ_0 nominal value of steering angle, calculated in trajectory control layer
$\Delta y(t)$ lateral deviation from the nominal trajectory.

$\Delta y(\mathbf{t})$ is calculated from

$$\Delta y(t) = \left(\tilde{\mathbf{r}}_{POI}(t) - {}^k \mathbf{r}'_{POI} \right)^T \begin{bmatrix} 0 & -1 \\ 1 & 0 \end{bmatrix} \mathbf{t}(t) \,. \tag{6.7}$$

$\mathbf{t}(t)$ is thereby the unit tangent vector along the filtered reference trajectory ${}^k \mathbf{r}'_{POI}(t)$ at time t, according to Fig. 6.4.
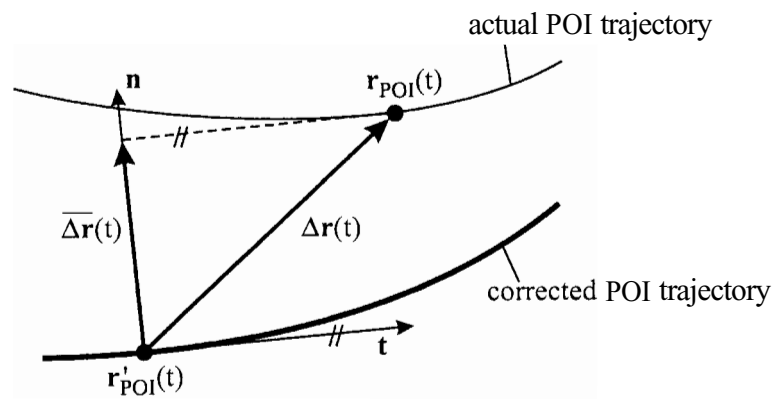
Figure **6.4:** Projection of trajectory error into lateral direction.

Chapter 7

Experimental investigations

7.1 Real world experiments

In order to compare the simulation results with human driving behavior, a real-world experiment was carried out. The experiment described in the following chapter took place at the facilities of California PATH, Richmond Field station, USA.

7.1.1 Test vehicle

The test vehicle, which was used for this experiment was a Buick Le Sabre 1997 with a four speed automatic transmission, see also Fig. 7.1. Any further specifications of the test vehicle are given in Tab. 7.1.1.

make	Buick
model	Le Sabre 1997
engine	3800 series II, V6
max power	149 kW @ 5200 1/min
max engine torque	312 Nm @ 4000 1/min
transmission	4-speed automatic
curb weight	1560 **kg**
wheelbase	2.81 m
length	5.08 m
width	1.9 m
height	1.41 m

Table 7.1: Specification of test vehicle
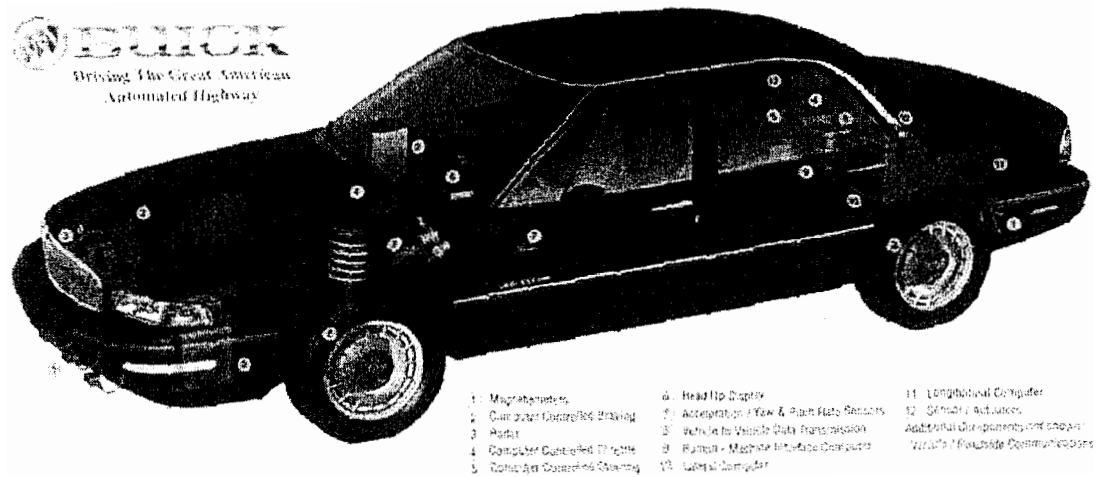
Figure 7.1: Test vehicle, Buick Le Sabre 1997, PATH,
Richmond Field Station (source: PATH)

The test vehicle was fitted with several different sensors in order to measure the driver input data as well as the vehicle behavior and position. The time was also measured with respect to the data sets mentioned before. The measured driver input data consists of

- steering angle

- throttle position

The measured vehicle data consists of

- magnetometer number

- magnetometer poles

- lateral displacement front

- lateral displacement rear

- wheel speed

- yaw rate

- longitudinal acceleration

- lateral acceleration

The longitudinal vehicle position on the test track is a function of the magnetometer number and, therefore, can be easily calculated. The vehicle orientation can be calculated using the lateral displacement of the front and rear sensor with respect to the magnetometers mounted on the test track. The sensors which read the magnetometer information are shown in

Fig. 7.2. The measurement range in which the magnetometer sensors provide sensible results is approximately 0.5 m to the left and 0.5 m to the right side of the vehicle's longitudinal axis, see also Fig. 7.2. The lateral offset is updated at every sensed magnetometer. But if the magnetometers are out of the vehicle's measurement range, the lateral offset is not updated until the magnetometers enter the measurement range again. This leads to false information about the lateral offset, which has to be taken into account during the evaluation of the results.
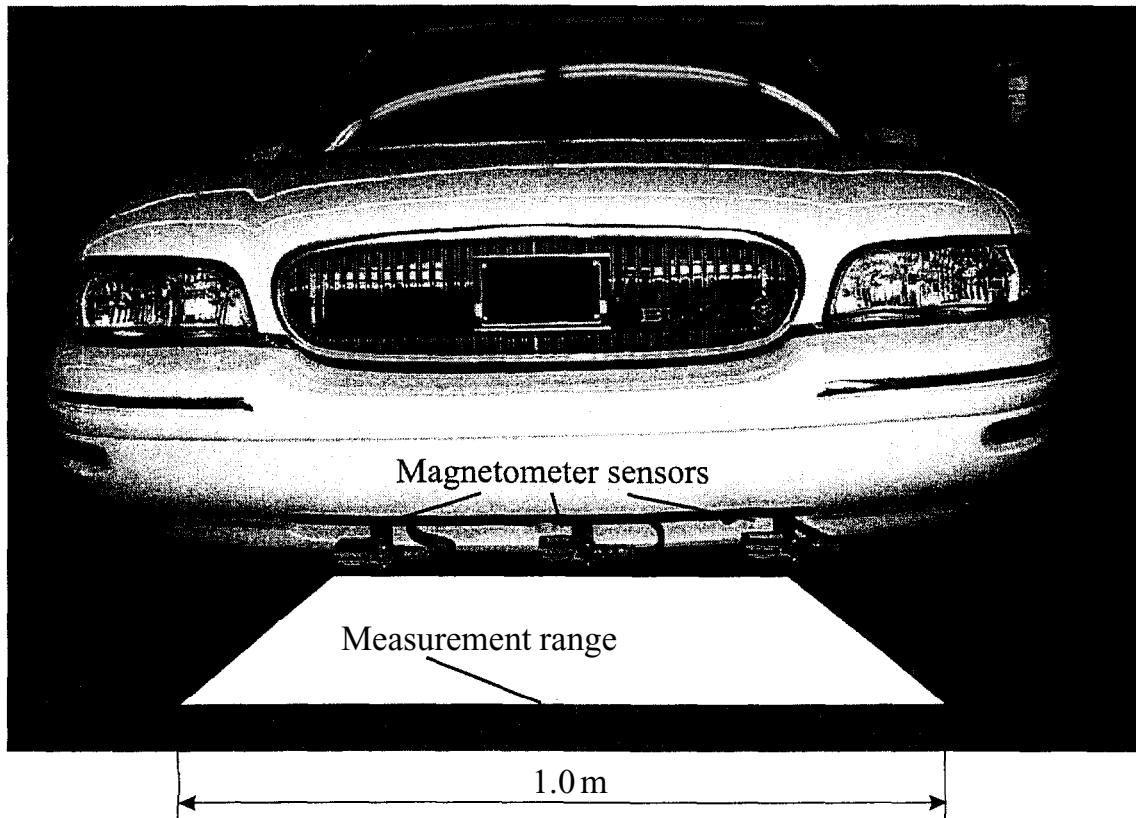
Figure 7.2: Front sensors mounted on test vehicle (source: PATH)

7.1.2 Test **tracks**

The test track which was used for the real-world experiments is shown in Fig. 7.3. It is part of the facilities of California PATH, Richmond Field Station, USA. The provided test track was used in the four different ways

- *o* straight east,

- ● straight west,

- right turn,

- left turn.

The road width differs slightly over the test track. The average road width is 3.52m. The road boundaries in the area of the right and left turn as well as in the area of the transient part turn/straight of the test, track were marked with white tape. In the remaining parts of the test track the road boundaries were not explicitly marked with white tape. The boundaries of the road sheeting were used as reference for the driver, instead. Following from that, there is no precisely defined reference of the road boundaries for the test subjects in this sections. This fact has to be taken into account in the evaluation of the driving behavior.

The test track is fitted with magnetometers which are inserted in the sheeting of the test track. The distance of the magnetometers to each other is one meter. Therefore, the longitudinal position of the test vehicle equals the number of magnetometers which are passed by the vehicle, see Fig. *7.3*. It is not possible for the used software and sensors to handle two rows of magnetometers at a time. Therefore, the magnetometers have to be inserted either for the straight section or the curved section. The consequence are jumps in the lateral offset at special parts of the test track. The magnetometers are inserted in such a way that jumps occur at position a) and b), see Fig. *7.3*. These irregularities have to be considered while evaluating the lateral offset and trajectory of the test vehicle.

The length of the part of the test track, which is used for the test runs straight east and straight west is 320m. The length of the part of the test track, which is used for the test runs right turn and left turn is 250m. The minimum sight, distance of the entire test track is 63m. Therefore, the sight distance has just little impact on the driving behavior if we consider the allowable top speed of only 30mph.

7.1.3 Experimental limitations

The experiment was limited in different ways which may have influenced the results.

- The maximum speed was set to 30mph because of safety reasons.

- An additional supervisor was sitting in the test vehicle who controlled that the speed maximum was not exceeded. This rose pressure on test subjects and the original mind set which was intended for the experiment could be influenced. It is very likely that the subjects focus was shifted to obeying the speed limit rather than concentrating on the instructions given during the course of experiments.

- No continuous test situation was possible, because the test tracks where no closed loops. In order to reach the starting point of the test tracks, the test subjects had to leave the testing area and drive short distances on public roads. Therefore, the test
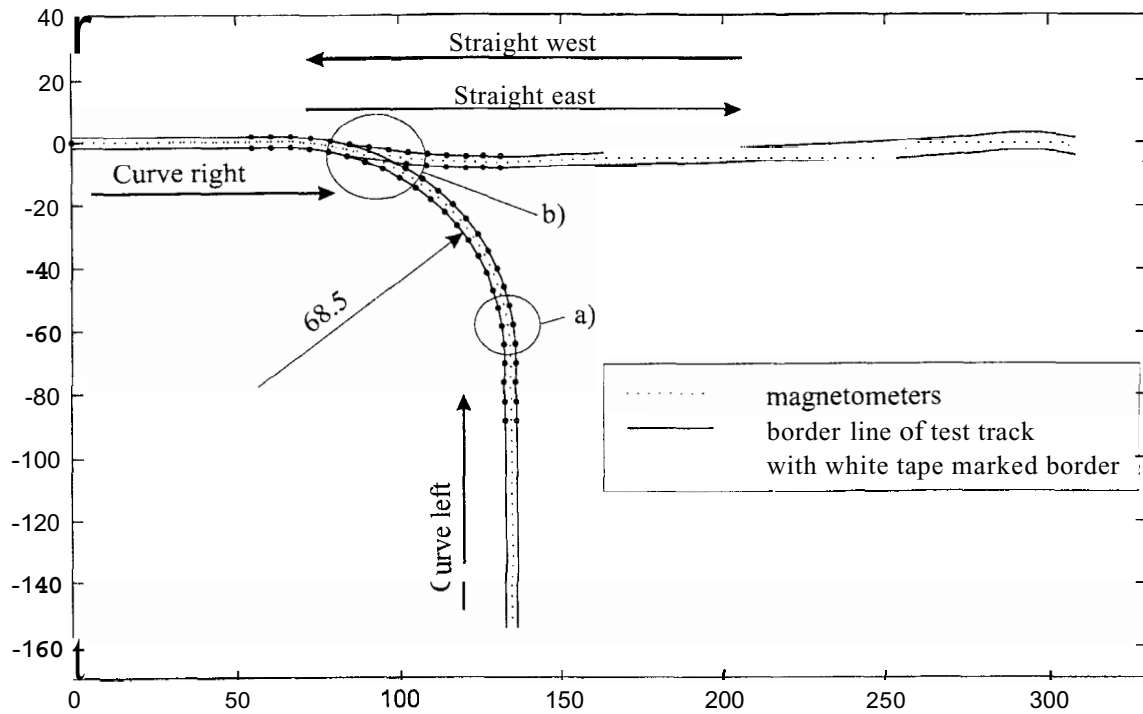
Figure **7.3:** Test ground, California PATH, Richmond
Field Station, USA. a) and b) mark the parts of
the test track where jumps in the lateral offset
and the trajectory may occur

subjects had to switch between the test situation and a real traffic situation. Possible
influences on the test subjects mind set can not be ruled out.

o The measuring range of the magnetometer sensors was not sufficient for the experi-
ments. It was possible to extrapolate the vehicle trajectory partially, but the sensor
accuracy and the accuracy of the available track data was too low in order to gain
meaningful results if the test vehicle left the measurement range for long distances.
Especially, the meaningfulness of the experiment with the driver preference keep-right
was strongly reduced, due to that limitation.

o The test run with the preference keep-right, which includes possible oncoming traffic
was carried trough without the possibility of real oncoming traffic.

o The same test sequence was used for all test subjects. Possible results may be influenced
by learning effects.

o The test vehicle has automatic transmission. Therefore, the human subject was not
able to actively influence the current gear ratio. Following from that no conclusion can
be drawn from that experiment with respect to the engine speed and engine torque.

7.1.4 Test subjects

In the course of the experiment, the test subjects had to fill out a questionnaire. All the information about the test subjects, is taken from these questionnaires. The subjects were assisted answering the questions in order to make sure, that the subject fully understood the questions.

number of test subjects	8
gender	male
age	21 - 31
profession	all subjects work or study in the field of engineering
driving experience (time)	3 - 15 years
driving experience (dist)	10,000 - 150,000 miles
driven miles within the last 12 months	5,000 - 20,000
driving skill (self-assessment)	good - very good
technical knowledge (self-assessment)	good - very good

Table 7.2: General characteristics of test subjects

For the test subject's self-assessment of their driving skill and technical knowledge about autos and driving, the subjects could choose

- very good,

- good,

- fair,

- poor

as their answer. The test subjects were also tested about their general knowledge about cornering with a vehicle. They could choose among the following questions.

a) The tighter the corner is, the more you have to turn the steering wheel.
b) The tighter the corner is, the less you have to turn the steering wheel.
c) The higher your speed is during cornering, the lower is the side force on the passengers.
d) The higher your speed is during cornering, the higher is the side force on the passengers.
e) The tighter the corner is, the lower is the side force during cornering.
f) The tighter the corner is, the higher is the side force during cornering.

All test, subjects were aware of the correlation between steering wheel angle and trajectory as well as speed and curve radius and the side force, which is exerted on the passengers. They all chose the right answers a), d) and f).

7.1.5   Course **of** experiments

The subjects were asked to fill out a questionnaire. This was independent of the driving experiment and, therefore, before or after the test runs. The subjects were assisted answering the questions in order to ensure, that the subjects understood entirely the asked questions.

The course of the driving experiment is as follows. The experiment starts, when the subject sits down on the driver's seat. Before starting the engine, the subject gets several safety instructions.

Safety instructions

- *o* The safety for all participating persons is the absolute priority for the experiment.

- *o* A safety belt is required for the test subject as well as for all other passengers in the test vehicle.

- The absolute speed limit for the experiment is 30 mph.

- *o* The test subject must not exceed his driving skills in order to fulfill the experiment.

- *o* The driver must stop immediately when other vehicles or pedestrians enter the test area.

The subject is also told, that it is possible to discontinue the experiment at any time of the experiment without giving any reason. After that the subject gets a brief overview over the ongoing experiment, the test tracks and instructions about vehicle. After each test run the subject must make a full stop at the end of each track. This is necessary to store the data. Safety reasons also require a full stop at the end of each run, because the subject has then to enter public traffic again.

After this introductions, the actual driving experiment begins and the subject is advised to start the engine. The test person has then approximately 15 rnin time in order to adjust to the test vehicle. The subject gets more time if needed. This training period includes fast acceleration of the vehicle and hard braking in order to get a feeling for the dynamics of the vehicle. During the training, all four different test routes must be driven at least once. The subject should also try to drive with the maximum allowable speed, so that the vehicle behavior at higher velocities can be experienced. No data is recorded during the training period.

After the training the instructor tries to give the subject several special scenarios. Once the instructor has given the subject a certain scenario in order generate a special mind set, the order of test tracks is for all different mind sets the same. In this phase of the experiment, the data is recorded. The safety instructions are repeated frequently to ensure that the experiment is carried through within the given safety regulations. The different scenarios and mind sets are as follows.

● Driving without any given preference
Mind set: The driver is supposed to drive as he would drive without any special constraint. Therefore, the driver needs not reckon with oncoming traffic. The subject can choose the trajectory liberally and does not have to stick to one side of the road. This scenario does also include that the driver does not need to drive particularly careful and no special speed limit is given.
Safety instructions: Independent of the given scenario, the subject must obey the maximum speed limit of $30mph$ and be aware of possible risks and the safety instructions given before. Before the driver drives the next test track, these instructions are always repeated.

● Driving comfortably, smoothly
Mind set: The driver should drive as smoothly as possible. This means that the driver is supposed to minimize the longitudinal and lateral acceleration exerted on the passengers. In this scenario, the driver does not have to expect oncoming traffic. The given situation is such, that the driver should imagine that a person who is very anxious, e.g. grand mother, is sitting beside him. The goal is not to scare this virtual person.
Safety instructions: Same safety instructions as given in the experiment before are repeated.

● Driving with a constant speed of **25**mph
Mind set: The driver is advised to keep a constant speed of $25mph$. The given scenario is a speed limit which is eagerly controlled by the police. No oncoming traffic has to be taken into account? which means that the subject can choose the trajectory liberally without staying at one side of the test track.
Safety instructions: If the speed of $25mph$ is too fast for the subject, the test person needs not to fulfill the experimental requirements. All the other safety instructions mentioned above also apply for this test run.

● Driving at the right side **of** the road
Mznd set: The instructions are that the driver should try to stay at the right side of the lane. As reference serves the right borderline of the track, which is partly marked with white tape. The given test scenario is that the driver has to take into account possible oncoming traffic. That is why he is supposed to stay on the right lane. No special speed limit except the absolute speed limit of $30mph$ is given and the driver is not advised to drive particularly smoothly.
Safety instructions: The usual safety instructions as mentioned above are also repeated so that the subject is always aware of the existing safety regulations.

7.2   Simulator experiments

In addition to the real-world experiment described in section 7.1, experiments with a driving simulator were carried out. The used driving simulator was provided by Nissan CBR, Boston, USA.

7.2.1   Driving simulator

Hardware

The used Hardware was designed and built by Product Genesis, Inc. (Cambridge, MA) The main component is the front two-thirds of a Nissan 240SX convertible which provides kinesthetic and audio feedback to the driver. The complete test setup is shown in Fig. 7.4. The dimensions of the driving simulator are given in Fig. 7.5.
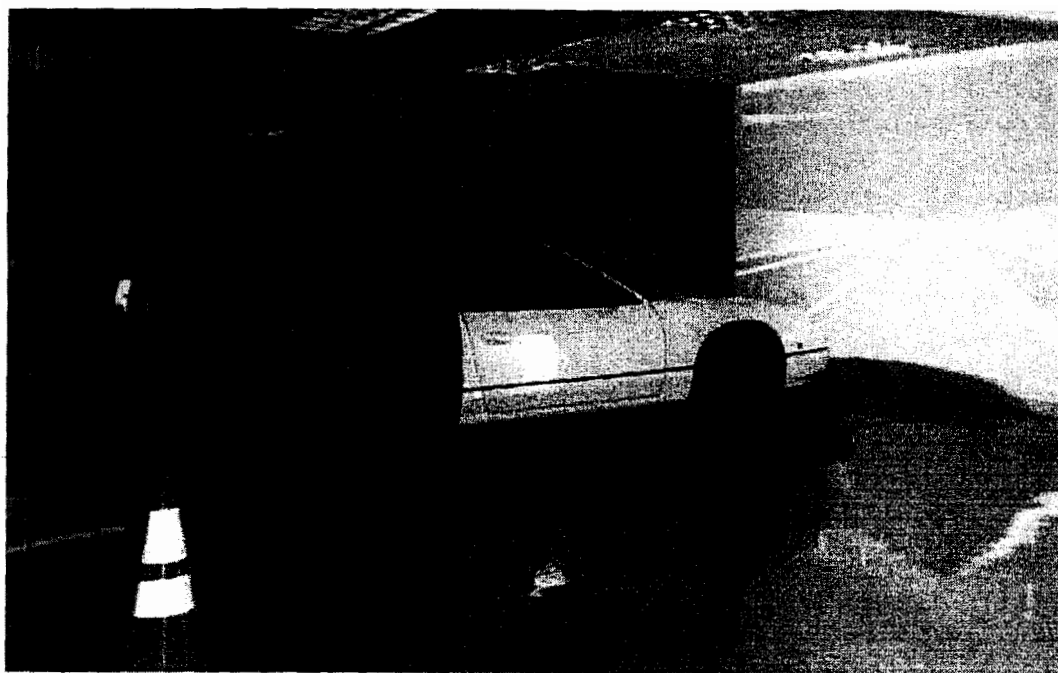
Figure **7.4:**Test set up of driving simulator, Nissan CBR, Boston

The audio feedback of the driving simulator is the engine noise which is dependent on the engine speed. The simulator also provides a force feedback in form of a steering torque. Depending on driving conditions, it generates a peak torque up to 5.67Nm and a continuous torque of 2.8Nm, which is usually sufficient under normal driving conditions. The instrument panel displays of the test setup are completely under user control.

Side view   Bird eye's view

Figure **7.5:** Dimensions of driving simulator, Nissan CBR,
Boston

A projector projects a 59" (horizontal) and 40" (vertical) color image onto the wall facing
the driver, see also Fig. 7.5. An SGI Octane/Si workstation provides for the described setup
the following update rates of the vehicle model and the virtual environment. The data frame
rate is circa 30Hz and the graphics frame rate is circa 30Hz. For more information about
the used hardware, see [13]

Software

The current software is based on a system developed by CyberGear, Inc. (Cambridge, MA).
Key features of both include precise measurement of car parameters and input devices,
control of the display devices in the car, and control over the appearance and movement of
other objects in the scene. The current vehicle position in the virtual environment is updated
on the basis of the current position, velocity, gravity, and drag. For more information about
the used software see [13].

Driving environment

The driving environment, which is provided by the driving simulator, is according to Fig. 7.6. The color of the road is grey with white borderlines. The area between the road and the walls on the left and right side of the track is colored green. Every $50m$ poles are put up in order to provide the subjects with better longitudinal reference. The pink walls on either sides of the test track are interrupted every $11.0m$ by $1.0m$ wide yellow stripes, in order to enhance the contrast of the driving environment. This makes it easier for the subjects to estimate the vehicle speed visually by the flow of texture.

Figure **7.6:** Environment of driving simulator, Nissan CBR, Boston

Vehicle model

The vehicle model used in the driving simulator is a one track model with a tire model with force saturation. The equations of motion are according to Eq. 3.35. Therefore, the one track vehicle model with tire force saturation used as prediction model is similar to the vehicle model used for the driving simulator. The driving torque M_a is according to Eq. 3.2, Eq. 3.3 and Eq. 3.4. The torque distribution factor ε is always 0. Therefore, the vehicle model of the driving simulator has according to Eq. 3.5 solely front wheel drive. The engine torque M_e is represented by a linear engine characteristics without drive train dynamics and can, therefore, be calculated according to Eq. 3.6, see also Fig. 3.3. The specific vehicle parameters, which were used for the driving simulator experiment are listed in the following tables.

Environmental parameters

g $=$ 9.81 $[m/s^2]$ gravity

ϱ $=$ 1.23 $[kg/m^3]$ density of air

Vehicle body

m	$=$	1740	$[kg]$	vehicle body mass
Θ	$=$	3214	$[kgm^2]$	rotational inertia of vehicle body around z-axis
l_F	$=$	1.058	$[m]$	horizontal distances of front axle from CG
l_R	$=$	1.756	$[m]$	horizontal distances of rear axle from CG
c_W	$=$	0.34	$[-]$	drag coefficient
A_W	$=$	1.9	$[m^2]$	projected vehicle area

Brake parameters

ζ	$=$	0.697	$[-]$	brake torque distribution, see Eq. 3.11
K_{brake}	$=$	4500	$[N/m]$	maximal brake torque

Engine characteristics

a_{M1}	$=$	434.8142	$[Nm]$
b_{M1}	$=$	-40.5741	$[Nm]$
a_{M2}	$=$	46.4208	$[Nm]$
b_{M2}	$=$	114.7832	$[Nm]$
ε_0	$=$	0.4	$[-]$

Limiting engine speed for automatic transmission

$n_{up,min}$	$=$	2500	$[1/min]$
$n_{up,max}$	$=$	6400	$[1/min]$
$n_{down,min}$	$=$	1500	$[1/min]$
$n_{down,max}$	$=$	3700	$[1/min]$

Vehicle gear ratios

1.gear   =   3.9   [-]
2.gear   =   2.4   [-]
3.gear   =   1.7   [-]
4.gear   =   1.3   [-]
5.gear   =   1.1   [-]
i_{diff} =   2.8   [-]

Vehicle wheels

R =   0.254   *[m]* tire radius of front and rear wheel
Θ_F = $2 * 1.1$ $[kgm^2]$ rotational inertia of front wheel in rolling direction
Θ_R = $2 * 1.1$ $[kgm^2]$ rotational inertia of rear wheel in rolling direction

Special parameter of HSRI tire model

f_R =   1.0   [−]   traction potential
k_R =   0.009 $[1/(m/s)]$ traction coefficient
C_S =   13 $[N]$ longitudinal slip stiffness
C_α =   22   *[N]* cornering stiffness

The experimental setup also provides the possibility to record specific test data. For this experiment the following driver input data and data of the vehicle response were recorded. The recorded driver input data consists of

- steering angle,

- brake signal,

o accelerator signal.

The recorded data representing the vehicle response consists of

o vehicle position,

- velocity,

o yaw angle,

- engine speed,

- rotational speed front wheel,

o rotational speed rear wheel,

    o longitudinal acceleration,

    o lateral acceleration.

7.2.2 Test tracks

Five different test tracks were used for this experiment. Four test tracks were similar to the tracks used for the real-world experiment and the fifth test track was the Hockenheim Motodrom (HM).

Track similar to real-world tracks
Although the meaningfulness of the test tracks, which were used for the real-world experiments is strongly reduced to simple driving tasks, they were also used for experiments with the driving simulator. The goal was to back up the results gained in the real-world experiment. In addition, the results can be used to filter out the specific effects off the driving simulator on human driving behavior. These results can then be used to evaluate further experiments without any reference to real-world experiments. The used test tracks were

    o straight east,

    o straight west,

    ● right turn,

    ● left turn.

The road width of the test tracks of the driving simulator is the average road width of the real test tracks of California PATH, Richmond Field Station, USA, which is 3.52m. The simulated test tracks are depicted in Fig. 7.7.

Mockenheim Motodrom (HM), Germany
The HM was used in order to test the subjects in a more complex driving situations, see Fig. 7.8. The HM was also used for training purpose.

7.2.3 Experimental limitations

The experimental results may be influenced by certain limitations, which are known for experiments in driving simulators, in general. The results may also be influenced by the specific characteristics of the used driving simulator.

    o Generally, test. subjects tend to drive faster and tend to risk more in a driving simulator compared to a real driving situation. This is probably caused by the lack of consequences in case of an accident or dangerous driving maneuver.
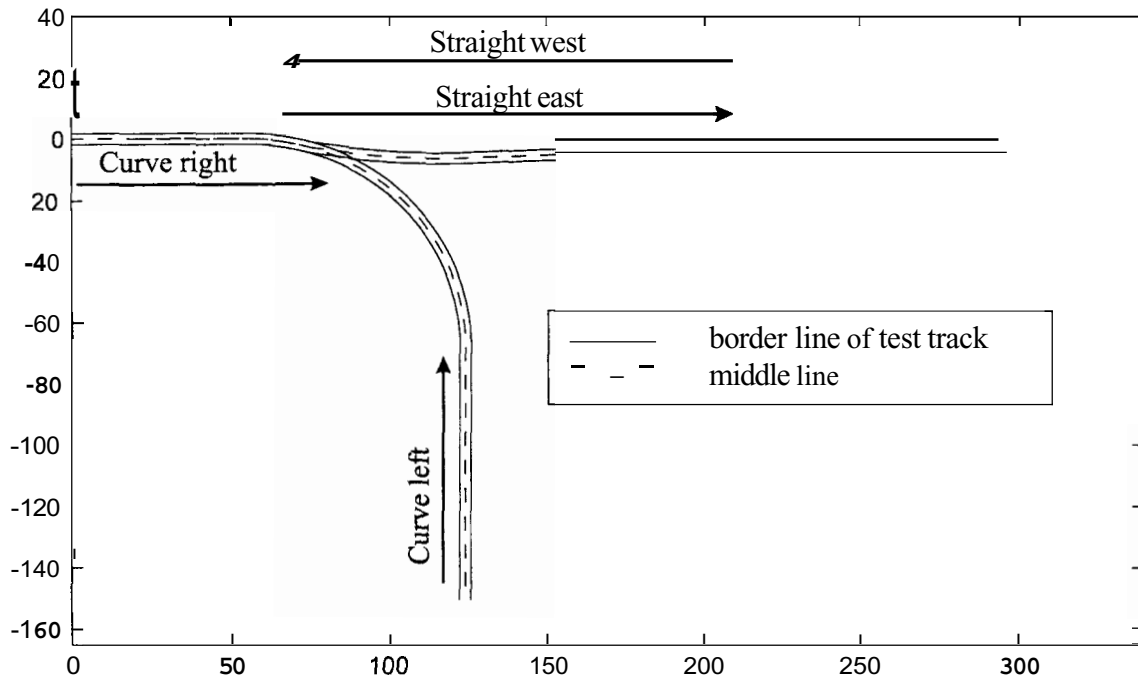
Figure 7.7: Simulated test tracks

o The virtual environment of the driving simulator is in comparison to a real environment extremely simple. The lack of contrast leads to higher velocities in general, because it is more difficult for the test subjects to estimate the vehicle speed visually.

o The driving simulator does not provide audio feedback in respect of wind noise, which makes it more difficult for the driver to estimate the current speed.

o The driving simulator does also not provide audio feedback in respect of tire noise. Therefore, the subjects do not not have any feedback of the tire saturation. Following from that, it is not possible for the driver to estimate the tire saturation. Therefore, the tire forces can be involuntarily exceeded very easily.

o The driving simulator does not provide longitudinal or lateral acceleration feedback, which also leads to difficulties in controlling the vehicle speed.

o No oncoming traffic is simulated in experiments, which actually require oncoming traffic.

o The sight distance is strongly reduced while cornering, due to the limited projection area solely in front of the driver. The driver's curve negotiation is negatively influenced by that. This makes it extremely difficult for the driver to assess the suitable velocity while cornering. Especially left curves are affected by this limitation of the driving simulator.

e The test tracks similar to real-world experiments are simplified in respect of road width. This has to be taken into account while comparing results of the real-world experiment with results gained in the driving simulator.

• The test vehicle has automatic transmission. Therefore, the human subject is not able to actively influence the current gear ratio and engine speed, respectively.

7.2.4 Test subjects

The test subjects had to fill out a questionnaire before the driving experiment. All the information about the test subjects, is taken from these questionnaires. The subjects were assisted answering the questions in order to make sure, that the subject fully understood the questions.

number of test subjects	6
gender	5 female, 1 male
age	21 - 32
profession	partly in the field of engineering, partly in other fields
driving experience (time)	5 - 14 years
driving experience (dist)	30,000 - 1,000,000 miles
driven miles within the last 12 months	0 - 10,000
driving skill (self-assessment)	fair - very good
technical knowledge (self-assessment)	poor - very good

Table 7.3: General characteristics of test subjects

For the test subject's self-assessment of their driving skill and technical knowledge about autos and driving, the subjects could choose among

• very good,

e good,

• fair,

e poor,

as their answer. As in the real-world experiment, the subjects were also questioned about their general knowledge of cornering with a vehicle. They could choose among the following questions.

a) The tighter the corner is, the more you have to turn the steering wheel.
b) The tighter the corner is, the less you have to turn the steering wheel.

c) The higher your speed is during cornering, the lower is the side force on the passengers.
d) The higher your speed is during cornering, the higher is the side force on the passengers.
e) The tighter the corner is, the lower is the side force during cornering.
f) The tighter the corner is, the higher is the side force during cornering.

Almost all test subjects were aware of the correlation between steering wheel angle and trajectory as well as speed and curve radius and the side force on the passengers. Except for one subject which chose answer b) instead of a) all other test persons chose the right answers a), d) and f).

7.2.5   Course **of** experiments

The subjects were asked to fill out a questionnaire before the actual experiment.

After answering the questions the subjects were advised in the use of the driving simulator. The subjects were also told, that they can stop the experiment at any time without giving any reason. It was also mentioned, that drivers in a driving simulator tend to drive too fast. Therefore: they were given the advice to watch the speedometer carefully. The subjects were also given the possibility to make short breaks in between the different test runs in order to maintain full concentration throughout the entire experiment, which lasts circa 2 hours.

After introducing the hardware, the subjects had approximately 20 minutes in order to adjust to the simulator. During that time, the drivers had to drive through all different test tracks at least once, with special stress on the HM. This is the most difficult track, which needs the most training. It was also suggested to try out how the vehicle behaves in extreme driving situations e.g. when the possible tire forces were exceeded. If the driver had still major problems after this training period an additional training of 10 minutes was required.

In the first part of the experiment, the subjects had to go through the same test cycle as in the real-world experiment. The instructor gave the subject several special scenarios, which were according to the scenarios used for the real-world experiment. Once the instructor has given the subject a certain scenario in order generate a special mind set, the order of test tracks is for all different mind sets the same. The test tracks were straight east, straight west, curve right and curve left. The experiment was carried through with the same order of test runs and preferences as the real-world experiment, see chapter 7.1.5. As in the real-world experiment, the vehicle must come to a stop at the end of each test run. It is also crucial, that the driver follows the given track and does not cross the right or left borderlines. The course of given scenarios and mind sets in the first part of the driving simulator experiment was as follows.

- Driving without any given preference
  No special situation should be assumed. The driver is supposed to drive without any special restrictions or preferences. The driver can choose his trajectory liberally, therefore, he neither needs to take into account oncoming traffic or any other obstacles

nor does the driver has to drive particularly careful or must obey any given speed limits.

o Driving comfortably, smoothly
The driver is advised to drive as smoothly as possible. The given mind set includes that the driver should imagine to transport a person which does not like high acceleration of any kind, e.g. grandmother. But it is also mentioned, that it in not obligatory to stay on the right side of the track. Therefore, the driver can choose the trajectory regardless of the middle line of the test track. The main stress is put on reducing the acceleration.

o Driving with a constant speed of $25mph$
In this test run, the driver has to obey a speed limit of $25mph$. As motivation to stick to the speed limit, the picture of police men who do speed checks is used. But the driver is not advised to stay strictly on the right side of the road. Therefore, the subject is still able to choose the vehicle trajectory independent of the track's middle line. No oncoming traffic is assumed.

o Driving at the right side of the road
The goal of this test run is to stay on the right side of the track. The driver should imagine possible oncoming traffic, so that it is not possible to choose liberally the vehicle trajectory without risking an accident.

Usually, the experiment was stopped after this part to give the subjects a short break of approximately 10 - 20min.

In the second part of the experiment, the HM was used as test track, see Fig. 7.8. The HM was linked together for fives times so that it appeared as continuous track. The length of the test run was at least two times the single distance of the HM. If the subjects did not, manage to stay on the track for the second time, the test run was extended until one entire part of the HM was driven through without leaving the track. The maximum driving distance was set to the absolute length of the linked track. The subject was advised to be particularly careful not to drive off the track. They were also given a set of different preferences as in the first part of the experiment. The preferences were given in random order.

The set of preferences consists of

- driving without any given preference,

- driving comfortably, smoothly,

- driving at the right side of the road,

o driving with a constant speed of $55mph$,

o minimize brake usage,

o driving time-optimally.

The instructions for the runs with the first three preferences were exactly the same as for the tracks of the first part of the experiment. The instructions for the test runs with the remaining preferences are described below.

- **Driving with a constant speed of 55**mph

  The given instructions are similar to instructions given for the preference driving with a constant speed of $25mph$. But despite of a speed limit of $25mph$ the subjects have to obey a speed limit of $55mph$. In addition, the subjects are alerted that this speed is too fast in order to drive safely through all the curves of the test track. That means, that they have to decide the appropriate speed for each corner. The subjects are also advised not to drive off the track but to stay with in the limits of the borderlines.

- *o* Minimize brake usage

  The instructions are such, that the subject should feel like on a race track and try to drive as fast as possible. But it is also given the constraint that they should use the brake as less as possible. No oncoming traffic is considered and no other restrictions apply for this test run. The driver can also choose any trajectory regardless of the middle line of the test track.

- *o* Driving time-optimally

  During this run the driver should consider himself as a race driver. The only goal is to drive as fast as possible without leaving the test track. No oncoming traffic, no speed limits and no other constraint is given. The choice of the vehicle trajectory is also unrestricted.
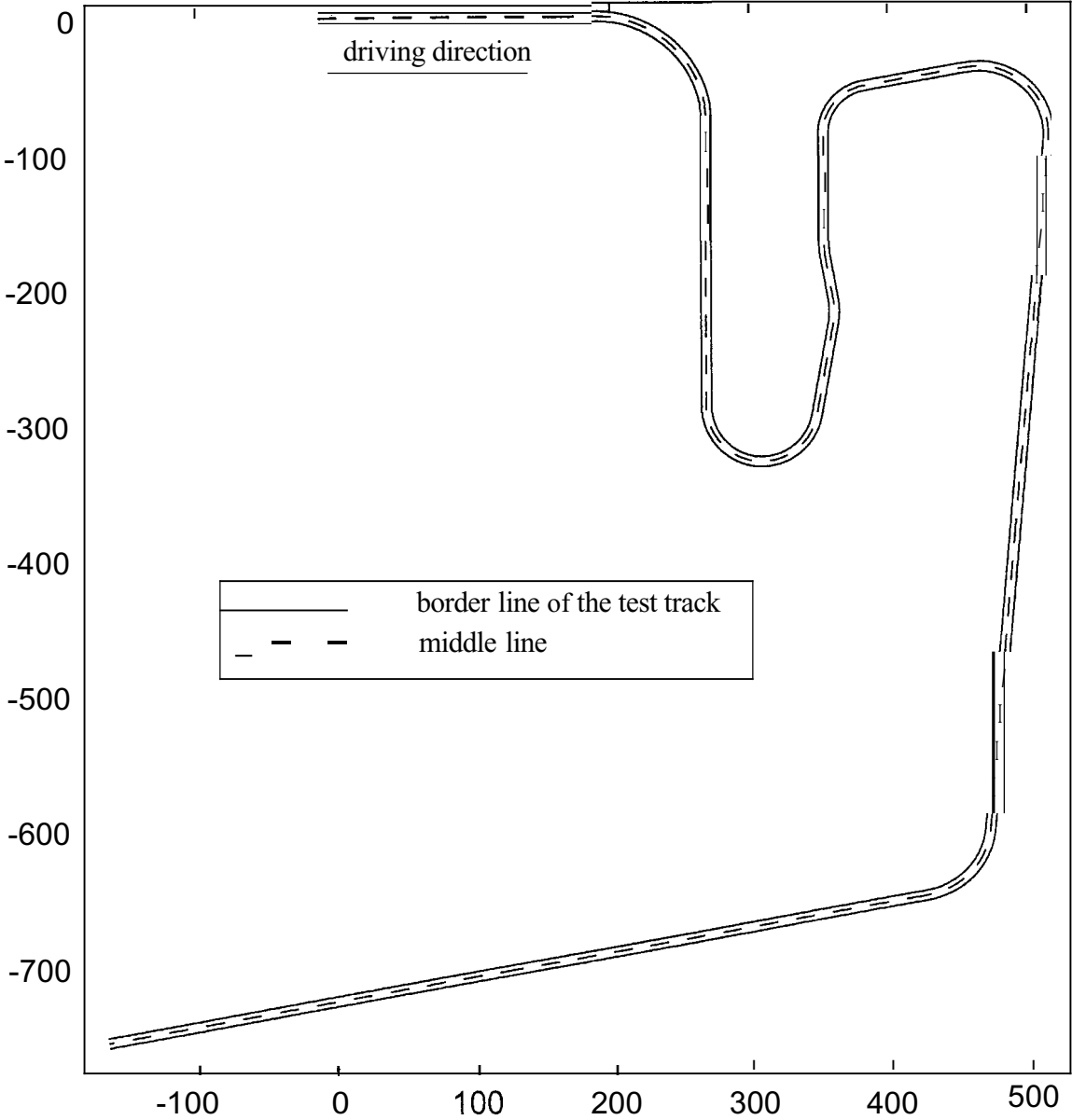
Figure **7.8:** Hockenheim Motodrom (HM), Germany

Chapter 8

Results

8.1   Parameters of simulation

8.1.1   Vehicle characteristics and parameters

The underlying kinematics and kinetics of the plant model used for the simulations are already explained in chapter 2. The specific parameters which were used for the simulations are listed below.

Table **8.1:** Vehicle parameters for simulation

Environment

g	=	9.81	$[m/s^2]$	gravity
ϱ	=	1.23	$[kg/m^3]$	density of air
v_W	=	0	$[m/s]$	velocity of wind

Vehicle body

m	=	1573	$[kg]$	vehicle body mass
Iy_B	=	2660	kgm^2	rotational inertia of vehicle body around y-axis
Iz_B	=	3214	$[kgm^2]$	rotational inertia of vehicle body around z-axis
s	=	0.3	$[m]$	height of CG above the wheel axles under static load
l_F	=	1.058	$[m]$	horizontal distances of front axle from CG
l_R	=	1.756	$[m]$	horizontal distances of rear axle from CG
b	=	1.7	$[m]$	vehicle width
c_W	=	0.34	$[-]$	drag coefficient
A	=	1.9	$[m^2]$	projected vehicle area
xyz_D	=	$[0.85\ 0\ 0.1]$	$[m\ m\ m]$	coordinates of center of pressure

Suspension system

c_F	=	$2*31392$	$[N/m]$	spring Stiffness front axle
c_R	=	$2*15113$	$[N/m]$	spring stiffness rear axle
d_F	=	$2*2300$	$[Ns/m]$	damping coefficient front axle
d_R	=	$2*2000$	$[Ns/m]$	damping coefficient rear axle

Table 8.2: Vehicle parameter for simulation

Vehicle drive and brake parameters

ε	=	0	$[-]$	drive torque distribution, see Eq. 3.5
τ	=	12 *7r	$[rad/s]$	time coefficient of vehicle engine
ζ	=	0.697	$[-]$	brake torque distribution, see Eq. 3.11
K_{brake}	=	4500	$[N/m]$	maximal brake torque

Vehicle's gear ratios

1.gear	=	3.9	[-]
2.gear	—	2.4	[-]
3.gear	=	1.7	[-]
4.gear	—	1.2	[-]
5.gear	=	1.0	[-]
differential gear ratio	=	2.8	[-]
steering gear ratio	=	17.1	[-]

Vehicle wheels

R	=	0.254	$[m]$	tire radius of front and rear wheel
m_F	=	2 * 28.58	$[kg]$	mass inertia front wheel
Iy_F	=	2 * 1.1	$[kgm^2]$	rotational inertia of front wheel in rolling direction
Ixz_F	=	2 * 0.6	$[kgm^2]$	rotational inertia of front wheel perpendicular to rolling direction
m_R	=	2 * 54.43	$[kg]$	mass inertia rear wheel
Iy_R	=	2 * 1.1	$[kgm^2]$	rotational inertia of rear wheel in rolling direction
Ixz_R	=	2 * 0.6	$[kgm^2]$	rotational inertia of rear wheel perpendicular to rolling direction
ct_F	=	2 * 192000	$[N/m]$	radial stiffness of front tire
ct_R	=	2 * 208000	$[N/m]$	radial stiffness of rear tire

Special parameter of HSRI tire model

f_R	=	1.0	$[-]$	traction potential
k_R	=	0.009	$[1/(m/s)]$	traction coefficient
C_S	=	13	$[N]$	longitudinal slip stiffness
C_α	=	22	$[N]$	cornering stiffness
l_R	=	2 * 0.05	*[m]*	length of tire contact patch
c_R	=	2 * 42950	$[N/m]$	carcass lateral stiffness

8.1.2 Driver characteristics

The different sets of parameters needed to specify the driver's knowledge and trigger the driver's actions are listed below in Tab. 8.3, Tab. 8.4, and Tab. 8.5.

The driver's skill and preferences are varied according to the intended mind set of the driver model. The driver's skill can be expressed by the use of different prediction models, see chapter 3 for details. Whereas the driver's preferences are expressed through a set of weighting factors, contained in the vector w, see Eq. 5.40. See chapter 5.2.2 how these factors influence the solution of the vector optimization problem. The investigated cases are listed in Tab. 8.3.

Table **8.3:** Weighting factors for case study

$$\text{time-optimal} \quad : \quad w = \begin{bmatrix} 1.0 & 0 & 0 & 0 & 0 & 0 & 0 \end{bmatrix}$$

$$\text{acceleration-optimal} \quad : \quad w = \begin{bmatrix} .1 & 1.0 & 0 & 0 & 0 & 0 & 0 \end{bmatrix}$$

$$\text{brake-optimal} \quad : \quad w = \begin{bmatrix} .5 & 0 & 1.0 & 0 & 0 & 0 & 0 \end{bmatrix}$$

$$\text{keep-right} \quad : \quad w = \begin{bmatrix} .1 & 0 & 0 & 1.0 & 0 & 0 & 0 \end{bmatrix}$$

$$\text{velocity-optimal} \quad : \quad w = \begin{bmatrix} .1 & 0 & 0 & 0 & 0 & 1.0 & 0 \end{bmatrix}$$

- time-optimal: The driver tries to reach the destination as fast as possible.

- acceleration-optimal: The driver mainly tries to minimize the lateral acceleration, in order to, e.g. enhance passenger riding comfort. The driver keeps a small weight on the time optimality criterion to make sure to reach the destination.

- brake-optimal: The driver minimizes the use of the brake to avoid unnecessary energy dissipation or brake disc overheating.

- keep-right: The driver's main preference is to stay on the right side of the road. This preference applies, if there is other traffic in neighboring traffic lanes or if the driver has to reckon with opposing traffic.

- velocity-optimal: The driver tries to reduce the deviation from a given vehicle speed, e.g. to meet a posted speed limit.

The investigated sets of weighting factors put extreme weight on single preferences. However, in a ordinary driving situation, a human driver would rather use a balanced mix of different weighting factors, than to put all the attention to a special one.

Further driver parameters are listed in Tab. 8.4 and Tab. 8.5.

Table **8.4:** Driver parameters for simulation

Time constants

prediction time	t_h	= 4.4	$[s]$
update sampling time	$\overline{\Delta t}$	= 0.4	$[s]$
time to hold clutch	t_{clutch}	= 0.6	$[s]$
minimal time to change gear	t_{gear}	= 2	$[s]$

Objective function formulation

desired lateral position	Δw_0	= 1.5	$[m]$
desired engine speed	$n_{e,0}$	= 2500	$[1/min]$
speed limit Richmond tracks	$\dot{s}_0$	= 25	$[mph]$
speed limit Hockenheim Motodrom	$\dot{s}_0$	= 55	$[mph]$

Objective normalization

desired speed	$\dot{\overline{s}}$	= 74.56	$[mph]$
comfortable acceleration	$\overline{a}$	= 2.5	$[m/s^2]$
comfortable brake input	$\overline{\varrho}$	= 0.2	$[-]$
comfortable lane deviation	$\overline{\Delta w}$	= 1.5	$[m]$
comfortable engine speed deviation	$\overline{\Delta n_e}$	= 2000	$[1/min]$
comfortable velocity deviation	$\overline{\Delta \dot{s}}$	= 12.42	$[mph]$

Constraint boundaries

maximal long. acceleration	$a_{x,max}$	= 6	$[m/s^2]$
maximal lat. acceleration	$a_{y,max}$	= 4	$[m/s^2]$
maximal lat. acceleration for change gear in curve	$a_{gear,max}$	= 2	$[m/s^2]$
minimal engine speed	$n_{e,min}$	= 900	$[1/min]$
maximal engine speed	$n_{e,max}$	= 6100	$[1/min]$
maximal steering torque	$M_{steer,max}$	= 300	$[Nm]$

The time, which is necessary for calculating the simulation is dependent on the test track and the driver preference, see Tab. 8.6.

Table **8.5:** Driver parameters for simulation

Constants for lateral and longitudinal control

proportional factor long.	$K_{P,\varrho}$	$=$	0.3	$[s/m]$
integral factor long.	$K_{I,\varrho}$	$=$	0.1	$[1/m]$
proportional factor lat.	$K_{P,\phi}$	$=$	8	$[rad/m]$
integral factor lat.	$K_{I,\phi}$	$=$	3.5	$[rad/m/s]$
differential factor lat.	$K_{D,\phi}$	$=$	6.5	$[rads/m]$

Table **8.6:** Calculation time for simulation

Test track	Calculation time (hours)
straight east	2.5 - 3.5
straight west	2.5 - 3.5
curve right	2.0 - 3.0
curve left	2.0 - 3.0
Hockenheim Motodrom	8.0 - 10.0

8.2   Driver behavior during cornering

The results gained from the test runs on the tracks right bend and left bend can be summarized to behavioral patterns of drivers while cornering. All diagrams shown in this section refer to the right, bend.

8.2.1   Acceleration-optimal case

Fig. 8.1 shows the different driver behavior while driving through a right bend with the requirement to keep the lateral and longitudinal acceleration as low as possible. The set of

weighting factors, which was used for this experiment, was according to Tab. 8.3

$$w = [\, .1 \quad 1.0 \quad 0 \quad 0 \quad 0 \quad 0 \quad 0 \,]\,. \tag{8.1}$$

System input: Steering angle

In order to compare better the steering angles with reference to the longitudinal vehicle position on the road, the road curvature of the right bend has been added (dashed line) to the course of steering angles, see Fig. 8.1. The road curvature is scaled with factor 2, for convenience.
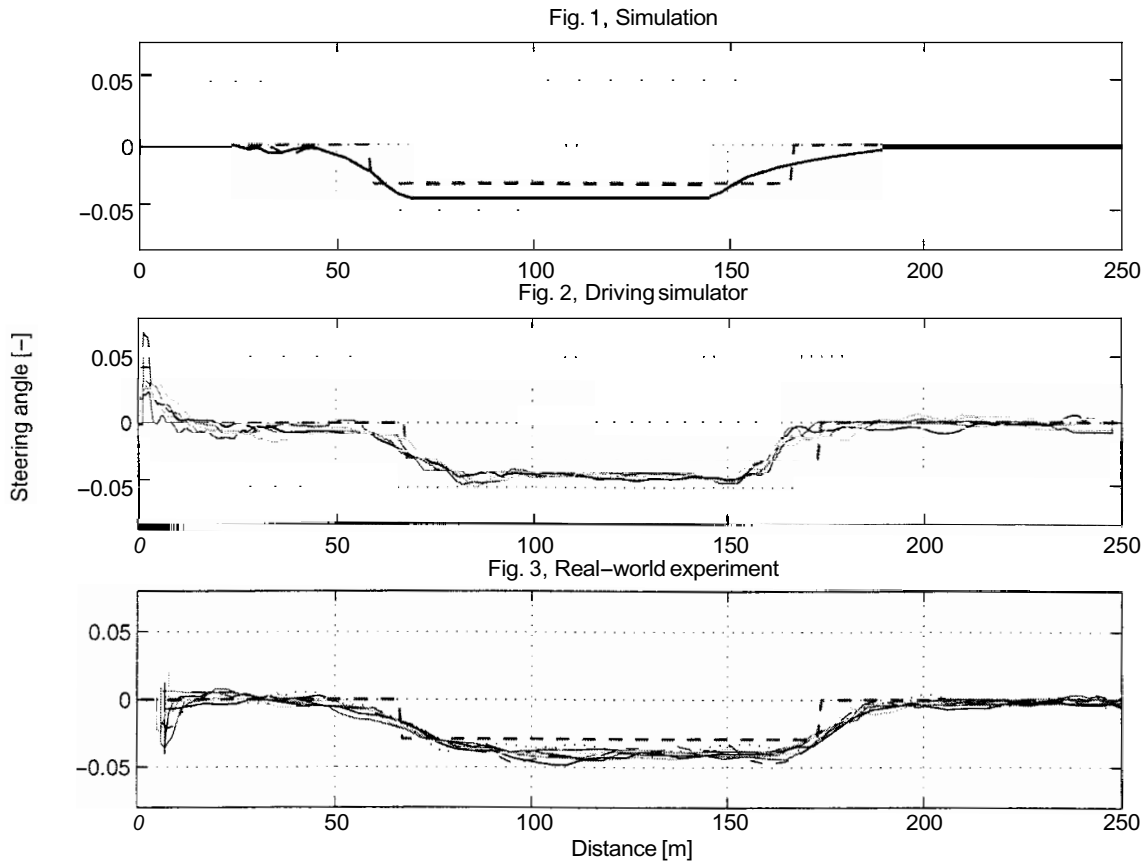

Figure 8.1: Preference: acceleration-optimal, Steering angles while cornering a right bend, with road curvature (dashed line)

- Simulation results
  The proposed driver model starts steering before the actual curve begins in order to achieve a smooth transition without any fast changes in the steering angle. While

cornering the steering wheel angle is kept constant. Therefore, the lateral acceleration is reduced to only the minimum lateral acceleration due to cornering. No additional acceleration due to correction movements of the vehicle are added to the lateral acceleration, which is exerted on the passengers during the right bend. At the beginning of the last fifth of the right bend the driver steers back and reduces very slowly the steering angle to 0 again.

- Driving simulator results
  Right at the beginning, the majority of the test subjects steer to the left in order to position the vehicle more in center of the road, see Fig. 8.4 to compare the different vehicle trajectories. Like the in the simulated results, the subjects also start adjusting the steering angle for the right bend before the actual curve begins. Because of that,, they also reduce the lateral acceleration due to a very smooth transition phase of the steering angle from 0 to the value which is necessary to drive through the right bend. But at the end of the turn all the test subjects steer back quite fast to the initial steering angle of 0. It seems that it is more important for the drivers to have a smooth increase of lateral acceleration rather than a smooth decrease. But since the test subjects can not feel any acceleration in the static driving simulator it is difficult to derive a general pattern from that characteristic. Oscillations of the steering angles in the transition areas may indicate, that the test subjects have difficulties in curve negotiation. Therefore, the steering angles seem to be adjusted by trial and error rather than by an accurate action.

- Real-world experiment results
  The little peak at the beginning of the steering angle profiles is not represented in the vehicle trajectories, see Fig. 8.4 and is caused by a initial alignment of the wheels at the beginning of the test runs. The following behavioral pattern is similar to the driver behavior shown in Fig. 8.1.2. The steering angle profiles are also characterized by smooth transitions. The stress lies also in a very smooth increase of the steering angle before and at the beginning of the right bend. Although the test subjects in the real-world experiment steer back later compared to the drivers in the driving simulator experiment, they also reduce the steering angle and with it the lateral acceleration much faster than the results gained in the simulation. The steering angle profiles are also characterized by slight oscillations.

- Conclusion
  Obviously human drivers seem to consider a increase in lateral acceleration much more uncomfortable as a comparatively fast decrease of lateral acceleration, see also Fig; 8.5. This human preference is reflected in the steering angle characteristics, which is not shown in the behavior of the proposed driver model. The slight oscillations, which occur in the driving simulator experiment as well as in the real-world experiment may be caused due to difficulties of human drivers in curve negotiation which makes it, hard to estimate an appropriate steering angle for longer distances in advance. But it can also be caused by a certain play in the joints of the vehicle's steering gear or external

disturbances, which do not occur in the simulated test runs. Since no exact data is know about the steering gear or any external disturbances no further conclusion can be drawn from that.

System input: throttle position
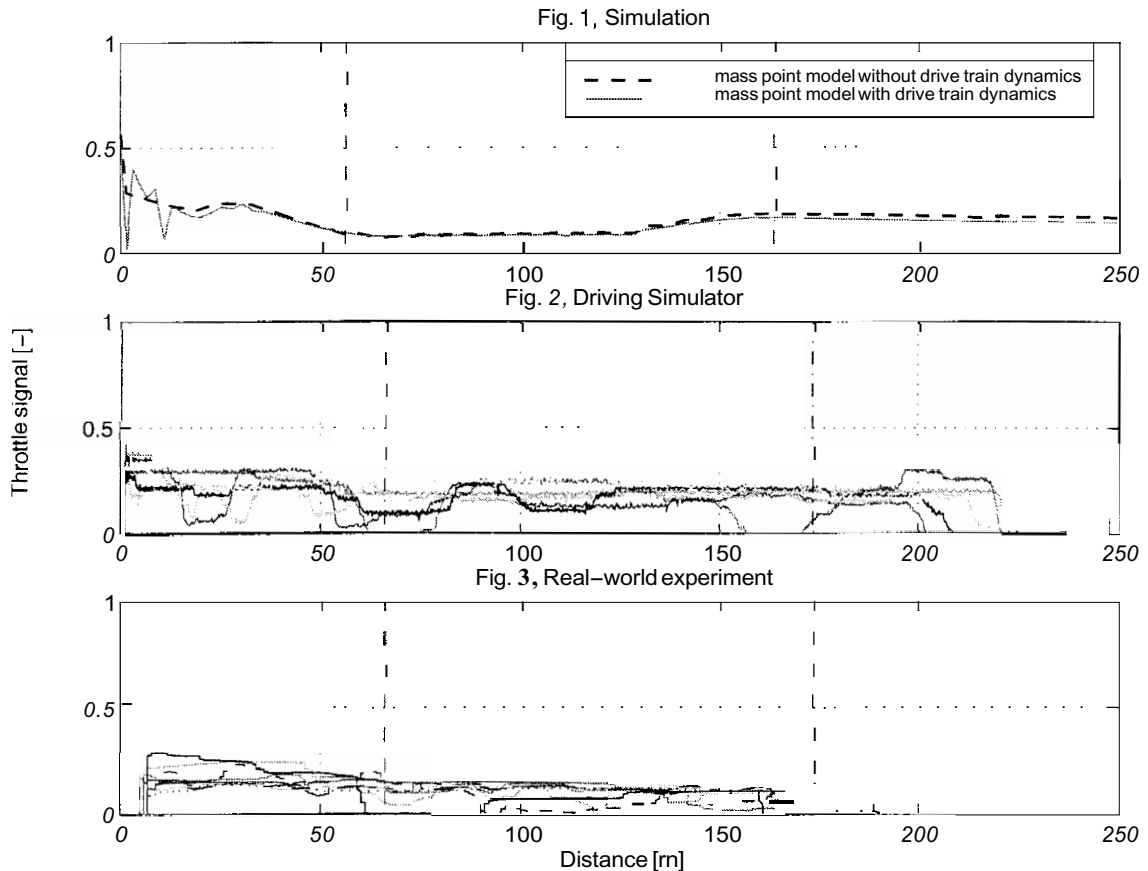
Figure **8.2:** Preference: acceleration-optimal, Throttle positions while cornering a right bend, with starting point and end point of the right bend (dash-doted line)

- Simulation results
  Moderate initial acceleration with approximately half throttle, which drops dramatically within the first few meters to a throttle position of below 0.3. Then smooth decrease of the throttle angle until the beginning of the turn. Throughout the turn a constant very small throttle angle until the last fourth of the right bend. Then increases the throttle angle again very smoothly until the very end of the turn. After

the turn, the throttle angle stays on an almost constant low value of below 0.2. The course of the test track is, therefore, represented in the course of the throttle angle, see also Fig. 8.2.1. Therefore, the longitudinal acceleration of the vehicle, which is directly connected with the throttle position is very low while cornering. Following from that, the absolute acceleration, which is exerted on the passengers during the turn is reduced to only the inevitable lateral acceleration.

- Driving simulator results
  The throttle angle value is mostly in the interval of 0.1-0.3, see Fig. 8.2.2. Therefore, the subjects try to fulfill the driving task by using an almost constant low throttle position. No special connection of the throttle angle and the road curvature is shown by subject's behavior in order to reduce specifically the longitudinal acceleration while cornering. But this may be explained by the lack of acceleration feedback of the driving simulator. The course of the different throttle angles is characterized by sudden drops. This behavior may be explained by the difficulties of the subjects to maintain a constant speed, which leads to sudden reactions. See the diagram of the velocity profiles Fig. 8.3.2 for the uneven velocity profiles. The sudden drops of the throttle angles are also accumulated at the beginning of the turn, which may be caused by the reduced sight distance due to the characteristics of the driving simulator. Following from that, the subjects have major problems in curve negotiation, which leads to a reduced velocity at the curve entrance and, therefore, to a reduction of the throttle angle, too.

- Real-world experiment results
  The behavior of the subjects can be characterized by a slightly higher initial throttle angle at the beginning of the test track, which approaches a more or less constant value after the first fifth of the test track. Irregularly oscillations of the throttle angle values within the interval of 0.0-0.2 may indicate, that the subjects do not plan the desired throttle angle in advance or according to the actual road curvature to fulfill the driving task. However, they try to reach the goal of this experiment by maintaining a more or less low constant throttle signal within the mentioned interval.

- Conclusion
  Similar to the simulation, all the subjects try to reach the goal of this experiment by using small throttle angles throughout the test run. But none of the subjects shows a similarly planned behavior like the simulation. In this test, the connection between road curvature and throttle position does not become obvious in the subjects behavior. Seemingly the subjects do not plan their behavior in advance, they rather react according to the current needs.

System response: Velocity profile

- Simulation results
  The speed constantly increases until the beginning of the right turn. During the first
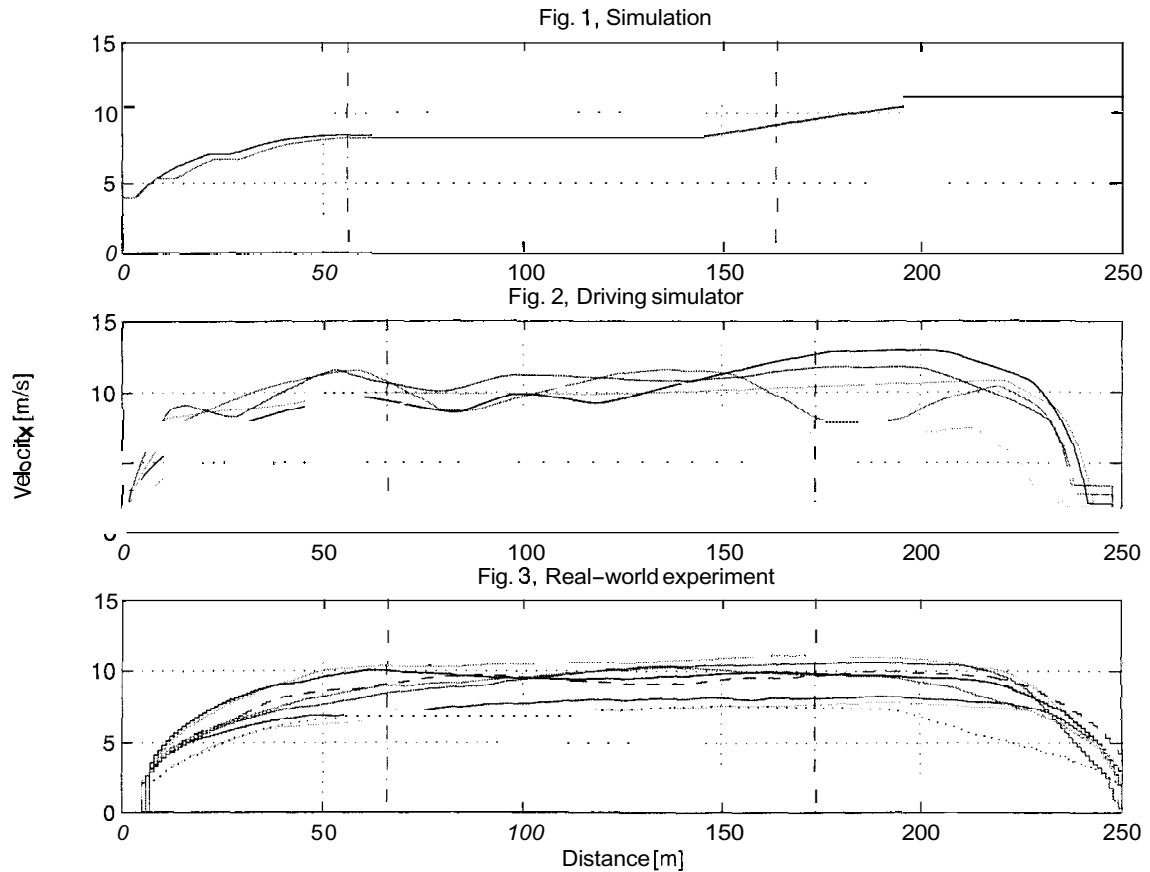
Figure **8.3:** Preference: acceleration-optimal, Velocity pro-
file while cornering a right bend, with starting
point and end point of the right bend (dash-
doted line)

three quarters of the turn, the vehicle velocity stays almost constant, with the very
slight tendency to get slower. From there on, the speed starts to increase very smoothly
again, until the end of the track. There is no stopping condition at the end of the track
in the simulation. Due to this, the vehicle velocity increases until the very end of the
test run.

- Driving simulator results
  The velocity profiles are characterized by a first acceleration phase, within the first
  $25m$ of the test track. This first acceleration is in respect of the simulation results
  much faster. This may be caused by the lack of acceleration feedback, which makes it
  impossible for the driver to sense the actual acceleration. After that, the additional
  increase of speed becomes less. The acceleration phase ends at about $10m$ before the
  beginning of the curve. Then, half of the drivers seem to be able to maintain a almost
  constant speed while cornering, whereas the other half of the drivers show a more of

less oscillating velocity profile. The difference of the velocity profiles is probably caused by the driving simulator. A lack of acceleration feedback and visual aids like the flow of texture of the surrounding environment, makes it difficult for the test subjects to control their speed. Soon after the turn, the subjects start to break, because of the stopping condition at the end of the turn. This restriction does not apply to the simulation. Therefore, no further conclusions can be drawn from that behavior.

- Real-world experiment results
  As in the simulation, the velocity profiles show a constant increase of speed until the beginning of the turn. The desired top speed is seemingly depended on individual preferences. The average values are slightly higher than the simulation results. Throughout the turn, the drivers maintain an almost constant speed with the very slight tendency to get faster towards the end of the turn, see Fig. 8.3.3. Because of the requirement to come to a full stop at the end of the track the subjects start to decrease the vehicle velocity in the second half of the last fifth of the test track. This requirement does not apply for the simulation and no conclusions can be drawn from that.

- Conclusion
  Regardless of the different restrictions and, therefore, different velocities at the end of the test track, the test subjects and the simulation show similar behavior before and while cornering. Especially, the results from the real-world experiment match very well the simulation results. The differences of the driving simulator results with respect to the simulation results are very likely to be caused specifically by the driving simulator. Obviously, it is very difficult in the driving simulator to control the vehicle speed precisely, without any acceleration feedback.

System response: Vehicle trajectory

- Simulation results
  The trajectory calculated by the simulation, starts in the middle of the lane. For a while the driver stays in the middle of the lane. About $20m$ for the bend, the driver starts to initiate the turn. The trajectory leads smoothly to the right side of the track, where it stays throughout the turn. Shortly before the end of the turn the trajectory leads smoothly to the left side of the track and the driver changes slowly lanes. From thereon the trajectory stays at the left side of the test track until the end. The result achieved by this behavior is that the trajectory curve radius is maximized and, therefore, the lateral acceleration is minimized, see Fig. 8.4.

- Driving simulator results
  The initial position of the test vehicles is the right lane of the test track. Right from the beginning, the test subjects steer to the left side of the track. Once the drivers reach the left side of the test track, they stay there for the remaining test run. There is only a slight tendency to drive more in the middle of the road towards the end of the
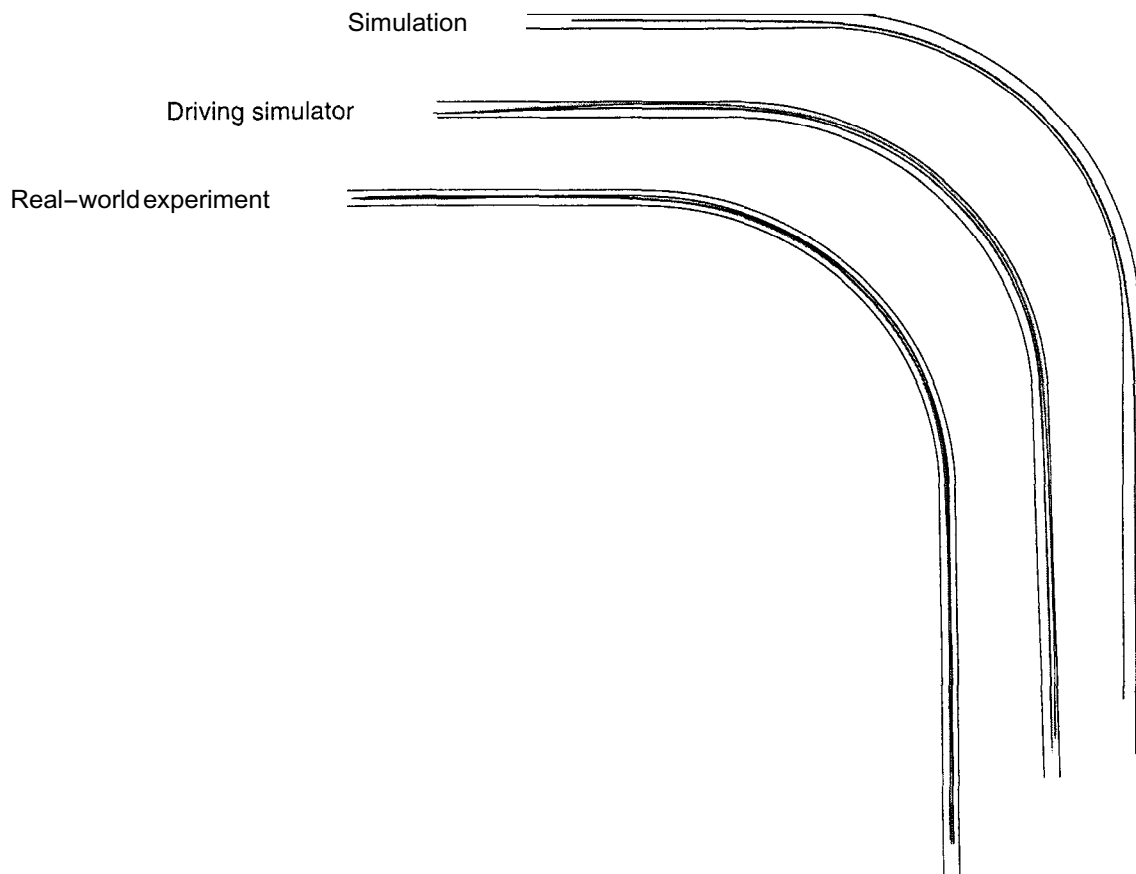
Simulation

Driving simulator

Real–world experiment

Figure **8.4:** Preference: acceleration-optimal, Trajectories
while cornering a right bend

test track. None of the drivers changes lanes again when they are on the left side of the
road. The result of this behavior is only a little reduced lateral acceleration. The radius
of the outside lane is slightly bigger than the radius of the inside lane. Therefore, the
lateral acceleration exerted on the passengers is slightly smaller on the outside lane,
than on the inside lane, if the turn is carried out with the same speed. None of the test
subjects sees the possibility of a behavior as calculated in the simulation, which would
lead to a even bigger curve radius and, therefore, to a smaller lateral acceleration, see
Fig. 8.4.

• Real-world experiment results
  The starting point of the experiment is on the middle line of the test track. In general
  most of the subjects stay relatively close to the centerline of the test track. There is
  only a slight tendency to drive to the left side of the track at the beginning. Most
  of the subjects initiate the turn approximately 35m for the right turn and tend then
  to stick more to the right side of the track. Towards the end of the turn, until the
  end of the test track, the trajectories are then grouped around the middle line of the

track without any special tendency, see Fig. 8.4. This behavior is not sufficient to significantly reduce the lateral acceleration.

- Conclusion

  Basically, the subjects seem to know and understand the connection between road radius and lateral acceleration, but they do not behave optimally as shown in the simulation, see Fig. 8.4. The behavior of the subjects in the driving simulator helps to reduce the lateral acceleration but it does not show the same pattern as in the simulation. This behavior is very likely to be motivated by the driving simulator and its provided environment, because the behavior of the subjects in the real-world experiment is principally the same as in the simulation but just not as optimal. The reason why the subjects only show the tendency to behave optimally may be caused by the relatively small test track, which does not allow a wide range of different tracks. The optimal or close to optimal behavior probably would have become far more obvious by the use of a wider test track.

System response: Lateral acceleration profile

In order to compare better the lateral acceleration with reference to the longitudinal vehicle position on the road, the road curvature of the right bend has been added (dashed line) to acceleration profiles, see Fig. 8.5. The road curvature is scaled with factor 150, for convenience.

- Simulation results

  The course of the lateral acceleration is very smooth and even, during the entire test run. The lateral acceleration increases slowly already before the curve and reaches its maximum a short distance after entering the right bend. While driving through the curve, the lateral acceleration is constant. In the last fifth of the turn, the lateral acceleration decreases again. The reduction of the lateral acceleration at the end of the turn is even slower and smoother as the increase before and at the beginning of the turn, see Fig. 8.5.1.

- Driving simulator results

  The recorded test data of the lateral acceleration is passed through a butter worth filter 2nd order with the cut off frequency 0.08 in order to reduce the noise in the test data.

  Principally, the course of the lateral acceleration is similar in a way with the results gained from the simulation. The lateral acceleration profiles are represented by two smooth transition phases which start before the curve and at the end of curve, see Fig. 8.5.2. In between the lateral acceleration is oscillating within a certain interval, which is basically similar to the constant lateral acceleration phase of the simulation. The lateral acceleration shows a slight tendency to reach a maximum in the second half of the right turn. Since the driving simulator does not provide any acceleration
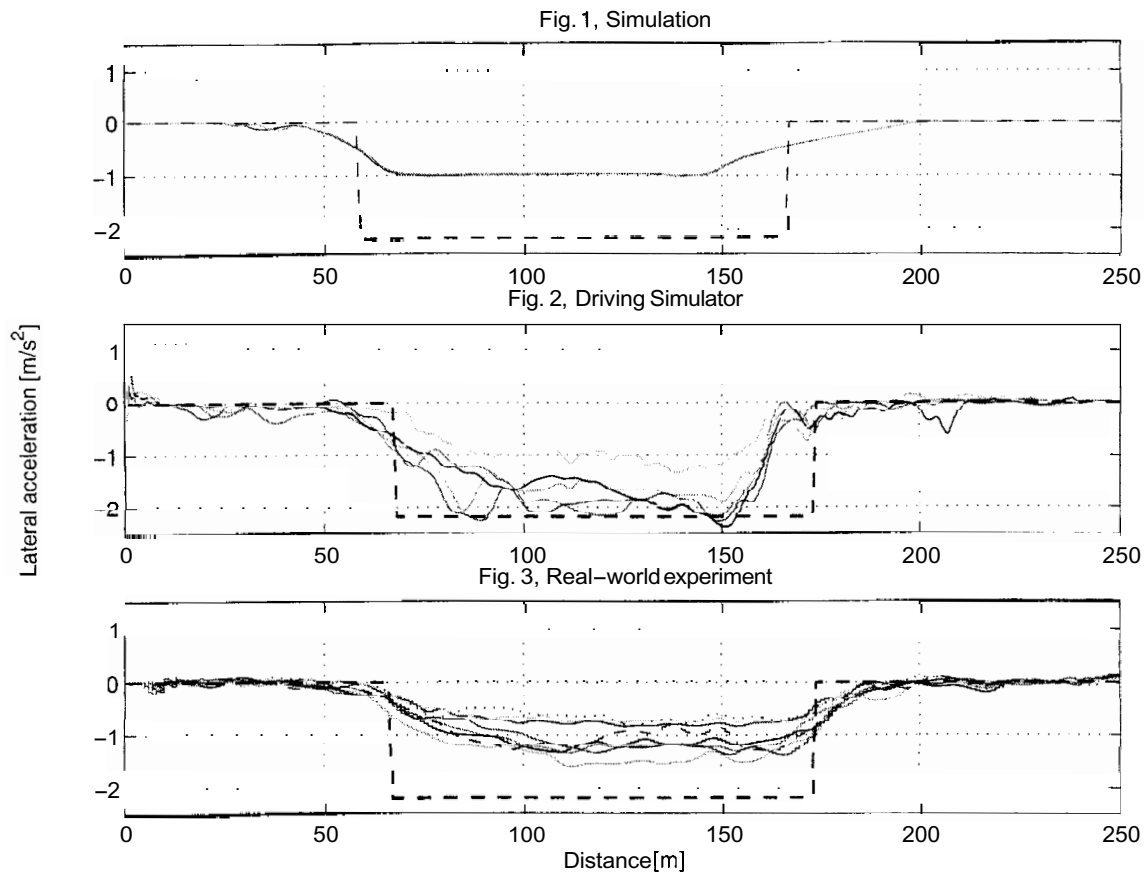
Figure **8.5:** Preference: acceleration-optimal, Lateral ac-
celeration while cornering a right bend, with
road curvature (dashed line)

feedback; it is not surprising that the subjects have difficulties in maintaining a constant
lateral acceleration and estimating the lateral acceleration, in general. There is only
one obvious difference in the driver behavior between the simulation and the driver
simulator experiment. It is, that even if human subjects are not able to sense any
acceleration, they increase the lateral acceleration much slower than they decrease it.

- Real-world experiment results
  The recorded test data of the lateral acceleration is passed through a butter worth
  filter 2nd order with the cut off frequency 0.02 in order to reduce the noise in the test
  data.
  The course of the lateral acceleration in the real-world experiment is similar to the
  course of lateral acceleration calculated in the simulation. It is characterized by a
  very smooth transition phase, which already starts before the actual beginning of the
  right turn. The lateral acceleration is slowly increased over a long distance. *Most* of
  the drivers reach the maximum lateral acceleration not until the second half of the

right turn. The majority of the subjects is then able to maintain an almost constant, lateral acceleration until they start to reduce the lateral acceleration again in the last fifth of the turn. The decrease of lateral acceleration is compared to the very smooth transition phase at the beginning of the turn much faster. Apparently, the subjects consider a fast increase of lateral acceleration more uncomfortable than a fast decrease of lateral acceleration, see Fig. 8.5.3.

- Conclusion
  Similar to the simulation results, the course of the lateral acceleration is characterized by smooth and long transition phases. The difference between the experimental results and the simulation are such, that human drivers stress a very slow increase of lateral acceleration rather than a slow decrease. Applying a force or acceleration, respectively on a human being is, therefore, considered as less comfortable than releasing it. This show even the driving simulator experiments, in which the subjects are not able to sense any acceleration. A similar behavior is not represented by the simulation. In the simulation, the lateral acceleration is faster increased than decreased.

System response: Longitudinal acceleration profile

- Simulation results
  The simulation starts with an initial acceleration of $1.3 m/s^2$ and is then constantly decreased to zero until the beginning of the right turn. The sudden drops of the longitudinal acceleration during this phase are due to shifting into another gear. Therefore, the clutch has to be opened and no power transmission is possible during this action. The longitudinal acceleration is zero while cornering and is smoothly increased again in the last quarter of the right bend. At the end of the turn, the acceleration reaches a positive maximum and is then almost constant until the end of the test track. No negative acceleration occurs at the end of the test track, because their is no requirement to stop implemented in the simulation, see also Fig. 8.6.1.
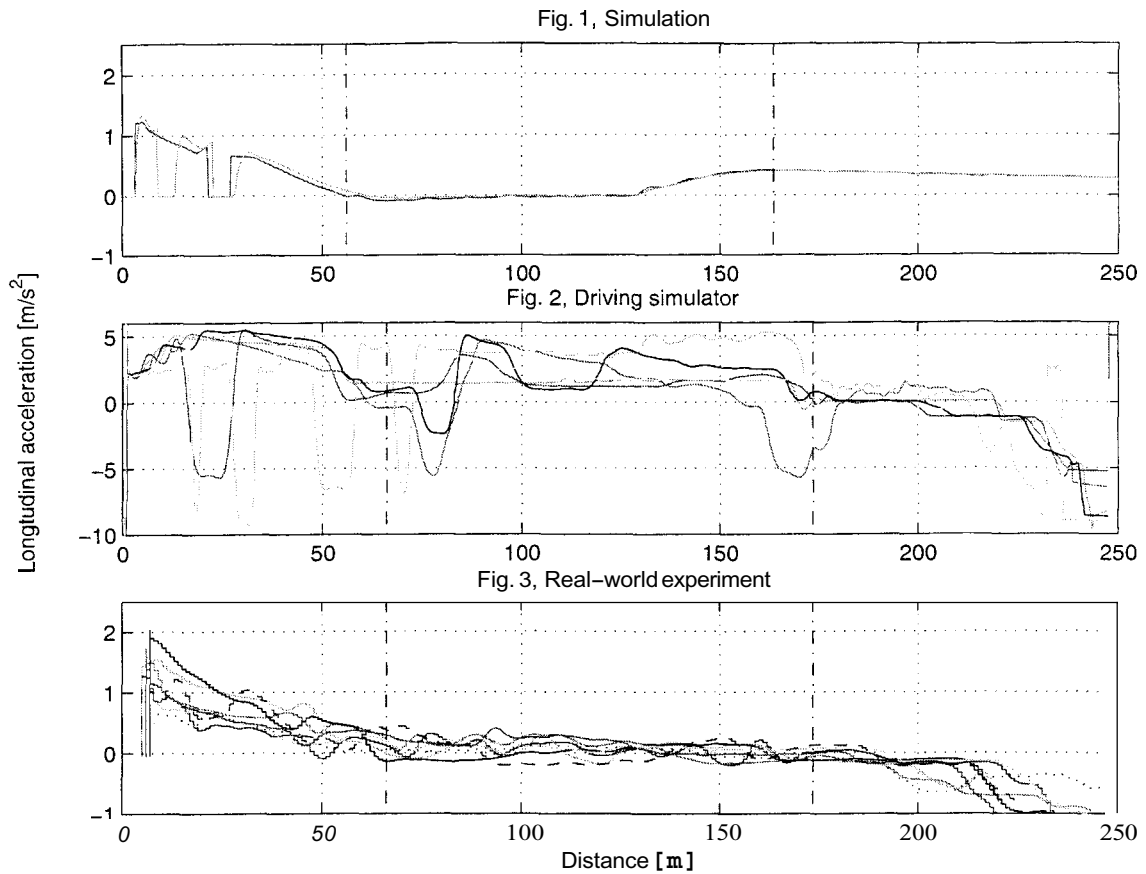
o Driving simulator results
  The recorded test data of the longitudinal acceleration is passed through a butter worth filter 2nd order with the cut off frequency 0.02 in order to reduce the noise in the test data.
  However, the longitudinal acceleration is not representative for real driving behavior, due to the lack of acceleration feedback of the driving simulator. The longitudinal acceleration is much too high, see the scale of Fig. 8.6.2 compared to the scale of Fig. S.6.1and Fig. 8.6.3which may also be caused by problems of the data processing. The course of the longitudinal acceleration is also not very steady, which also does not represent a realistic driving behavior. Therefore, no further conclusions can be drawn from this set of test data.

e Real-world experiment results
  The recorded test data of the longitudinal acceleration is passed through a butter worth

Figure **8.6:** Preference: acceleration-optimal, Longitudinal
acceleration while cornering a right bend, with
starting point and end point of the right bend
(dash-doted line)

filter 2nd order with the cut off frequency 0.02 in order to reduce the noise in the test
data.

The drivers start with a relatively high initial longitudinal acceleration, which lies in
the interval of $1.0 - 2.0m/s^2$. This initial acceleration is then reduced continuously
until the beginning of the right bend. Then, the subjects drive through the right turn
with a constant low acceleration of less than $0.5m/s^2$. Therefore, the subjects try
to reduce intentionally the longitudinal acceleration in driving situations with high
lateral acceleration. Because the subjects have the requirement to come to a full stop
at the end of the test track, none of drivers accelerate after the right bend again. The
deceleration at the end of the test track is also caused by this requirement.

- Conclusion
  The driving behavior of the subjects match the simulation results quite well. An initial
  acceleration phase with values of $1.0 - 2.0m/s^2$, then the reduction of the longitudinal

acceleration until the beginning of the turn and then cornering with a very low or without any longitudinal acceleration. Therefore, the subjects connect the longitudinal and lateral acceleration in such a way, that they try to reduce one of them if the other is increased. This behavior also represented in the simulation results. The different behaviour starting at the last forth of the right turn is due to different stopping conditions for the simulation and the real-world experiment.

8.2.2   Velocity-optimal case

The set of weighting factors, which was used for this experiment was according to Tab. 8.1

$$w = \begin{bmatrix} .1 & 0 & 0 & 0 & 0 & 1.0 & 0 \end{bmatrix}. \tag{8.2}$$

System input: throttle signal

- e **Simulation results**
  The initial value of the throttle signal is full throttle for approximately the first $15m$ of the test track, see Fig. 8.7.1. After this phase, the throttle position is dramatically decreased to a value of about 0.1 for the remaining distance of the test track. The oscillation of the throttle position is probably caused by the low update rate of the proposed driver model. In order to keep the calculation time needed for the simulation low, a low update rate of the driver model was chosen. Therefore, the deviations from the nominal system behavior and the actual system behavior become to big, which leads to problems in the control layer and an oscillating throttle angel profile. These problems become more apparent the more complex the prediction models are. Therefore, is the oscillation in the test run with the prediction model with drive train dynamics is stronger than of the model without any drive train dynamics.

- e **Driving simulator results**
  The initial values of the throttle signal are in the area of 0.35-0.55 and not full throttle as in the simulation. After the initial phase, the subjects try to maintain a lower, constant throttle position throughout the run, see Fig. 8.7. Drivers who exceed the speed limit, see Fig. 8.8.2, control their speed by reducing the throttle position to 0. Therefore, the subjects do not plan or know, respectively the optimal throttle position in advance, but readjust the throttle angle as needed.

- e **Real-world experiment results**
  In the real-world experiment, we can also see a initial acceleration phase, in which the subjects show a higher throttle signal than in the rest of the test run. Two of the subjects give even full throttle or close to full throttle, but all the others are more careful and so are the initial throttle signals in general below 0.4. After the initial phase all the subjects have different throttle signals over the test track. They differ

Fig. 1, Simulation

Fig. 2, Driving Simulator

Fig. 3, Real–world experiment
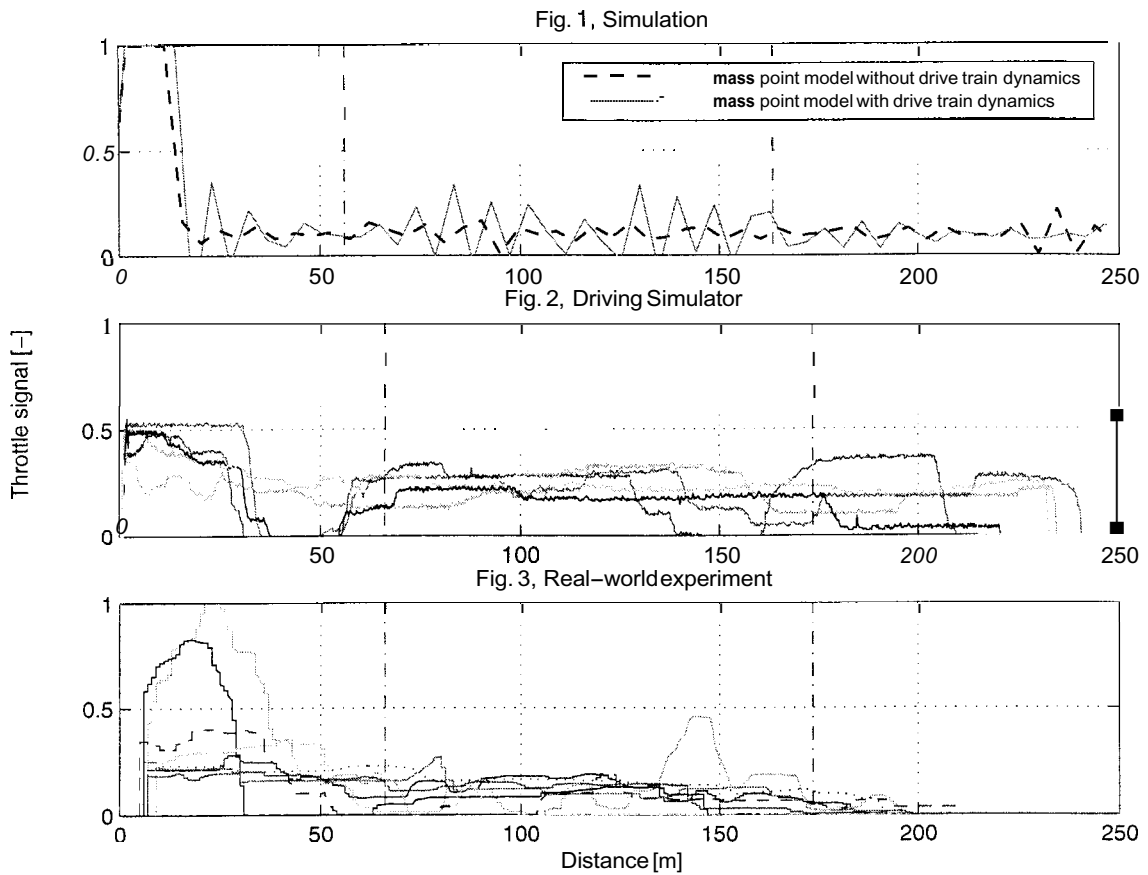
Figure **8.7:** Preference: velocity-optimal, Throttle position while cornering a right bend, with starting point and end point of the right bend (dash-doted line)

from constant values over longer periods to oscillating. But no mean value around which the signals oscillate can be determined, see Fig 8.7.3. Therefore, the drivers do not plan or do not know the appropriate throttle position to maintain exactly a given speed. The throttle position is adjusted frequently as needed. No special pattern can be determined from that behavior.

- Conclusion
  The majority of the drivers do not accelerate with full throttle at the beginning of the test track. Although no special restrictions are given with respect to minimizing the acceleration exerted on the passengers, the subjects do not accelerate as fast as possible to reach the given speed of $25mph$. In addition, the test drivers do not show the same behavior as calculated in the simulation in the remaining course of the test run. There is an optimal throttle signal being determined in the simulation and it is tried to keep this optimal value. This behavior is not represented in the experiments. The drivers

apparently do not plan or know the optimal value, they have to readjust the throttle position frequently in irregular intervals in order to control the vehicle speed.
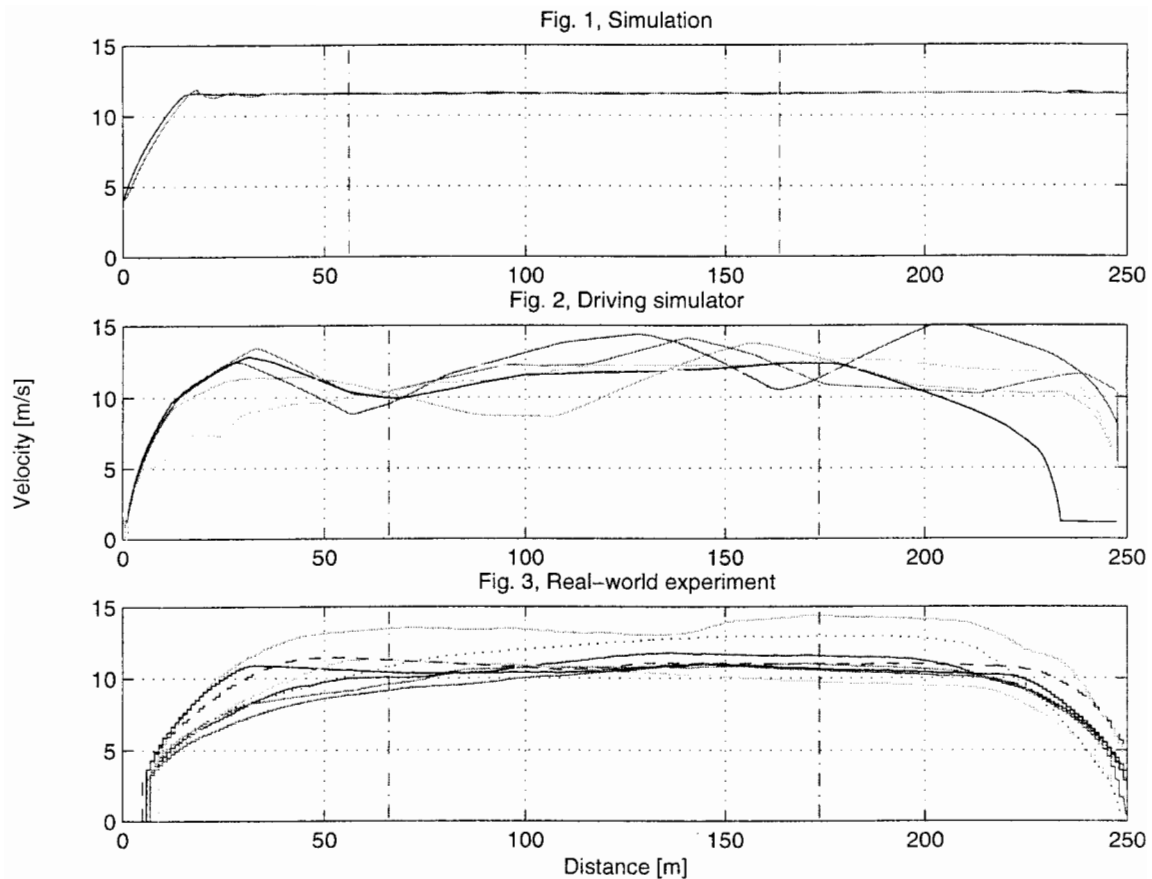
System response: velocity profile

Figure **8.8:** Preference: velocity-optimal, Velocity while cornering a right bend, with starting point and end point of the right bend (dash-doted line)

o Simulation results
The speed is rapidly increased to the required value of $25mph$. After only $18m$ the vehicle reaches its desired speed. From then on, the vehicle speed is hold perfectly constant throughout the remaining test track, see Fig. 8.8.1.

o Driving simulator results
The different courses of velocities gained in this experiment start with a varying behavior to approach the given speed limit. Some of the subjects approach the desired speed very carefully trying not to exceed the limit of $25mph$. These subjects need more than

$50m$ to reach finally the desired speed. The other subjects accelerate their vehicle much faster and reach, therefore, the speed limit earlier, but most of them severely exceed the limit after reaching it. Either way, the subjects have great difficulties in reaching and then maintaining the given speed according to the given preferences. After the initial acceleration, peaks of $13m/s$ and more are followed by minima of $10m/s$ and lower, see Fig. 8.8.2. The problems of the subjects to fulfill this task can be explained by the driving simulator characteristics. Since the driving simulator does not provide acceleration feedback, the subjects can not use the usually sensed acceleration to control the vehicle speed. In addition, the driving environment is only poorly fitted with visual aids in order to help estimating the velocity by the flow of texture. Therefore, the only preference is the speedometer, which is apparently not sufficient to control the vehicle speed very precisely.

o **Real-world experiment results**
In general, the subjects need a longer distance to reach the given speed than the simulation results show. Even if keeping the horizontal acceleration low is not an issue to fulfill successfully the task, the individual preferences are mostly such that a high longitudinal acceleration is avoided. After the test drivers have reached the desired speed, they are mostly able to maintain a constant speed of approximately $25mph$ over the remaining test track. The differences of the absolute speed which is kept constant is probably due to the imprecise speedometer of the test vehicle.

o **Conclusion**
Human drivers are able to maintain precisely a given speed in a real driving situation, as shown in Fig. 8.8.3. The results gained by the driving simulator are not representative because of the experimental restrictions of the driving simulator, see chapter 7.2.3. The slight deviations from the vehicle speed in the real-world experiment compared to the perfectly constant course of vehicle speed calculated in the simulation are probably caused by a imprecise speedometer of the test vehicle as well as probable external disturbances like e.g. wind which do not occur in the simulation. In addition, most, of the subjects do not try to reach the given speed as fast as possible. Seemingly, high longitudinal acceleration are considered to be uncomfortable, even if the given preferences do not imply special conditions or restrictions with respect to the vehicle acceleration.

System response: vehicle trajectory

o **Simulation results**
The trajectory starts on the middle line of the test track. The shortest possible trajectory is then chosen to drive through the test track. Therefore, the vehicle trajectory leads to the right lane before the turn. The vehicle stays then on the right lane or inside lane of the test track while cornering. And then, the vehicle does not change
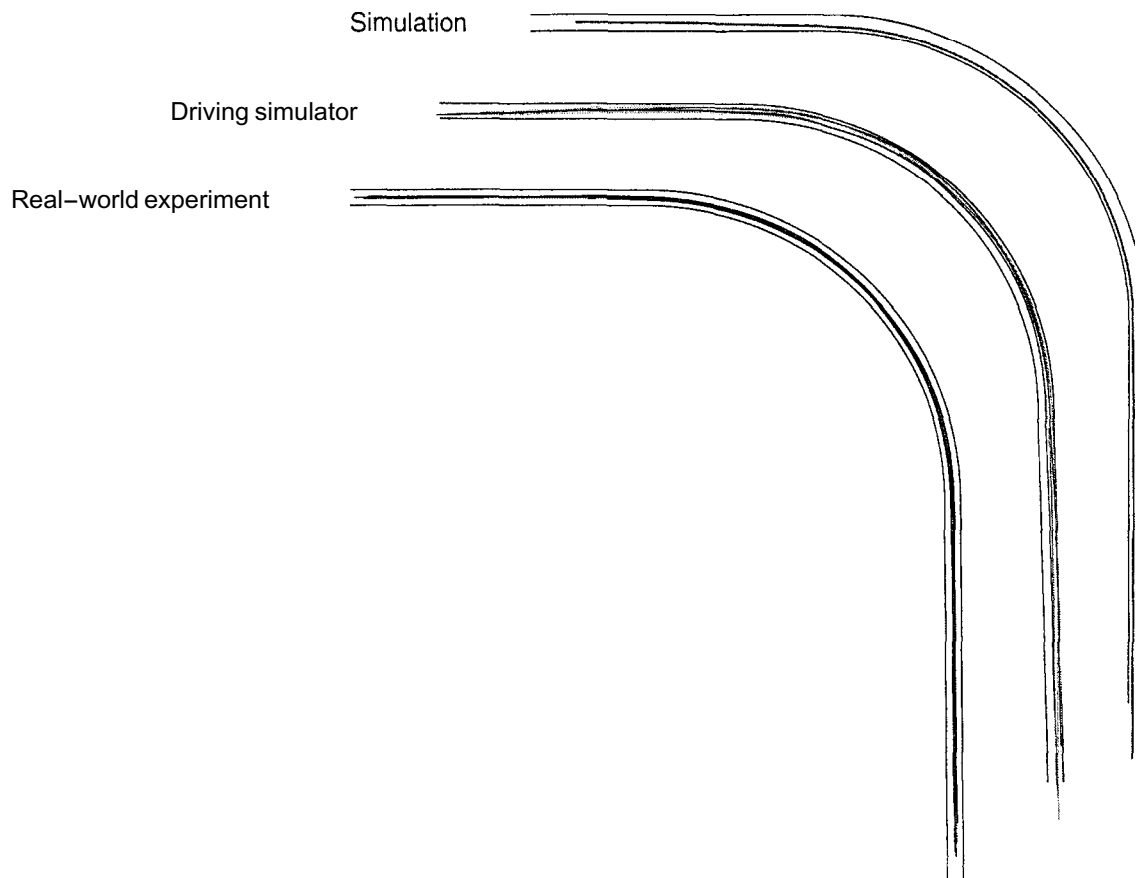
Figure **8.9:** Preference: velocity-optimal, Trajectory while
cornering a right bend

lanes again after the right turn. This behavior is caused by the little weight of the
driver preference to drive time-optimally.

- Driving simulator results
  The given preference *to* drive with a constant speed of $25mph$ does not include auto-
  matically for the test drivers to drive time optimally through the test run. Therefore,
  they do not chose the shortest possible trajectory but the trajectory they consider to
  be the most comfortable. Apparently, the subjects prefer to drive on the left lane of
  the test track, which also means the outside lane while cornering. The trajectories are
  such, that starting from the right lane of the test track, all subjects switch lanes or
  drive at least to the middle of the lane within the first $50m$ of the test track, see Fig.
  8.9. This behavior is perhaps caused by the very restricted sight distance in the driving
  sirnulator. Therefore, the subjects try to increase their sight distance by choosing the
  left lane or outside lane, respectively in this experiment,.

- **Real-world experiment results**
  In general, the subjects stay close to the middle line of the test track. But while cornering a slight tendency to drive closer to the left border of the test track becomes obvious. Although the given preference to drive with a constant speed does not include to drive time-optimally or to choose the shortest trajectory, respectively, the subjects try to shorten their way by driving more on the inside lane while cornering. This is basically the same behavior, which is also shown in the simulation results. This similarity would perhaps become more obvious by the use of wider test tracks. The average width of the used test track is just $3.52m$ and, therefore, the choice of the possible trajectories is very restricted. Especially if we consider, that a driver usually keeps a certain safety margin to the border of the track, which constrict the choice of possible trajectories even more.

- **Conclusion**
  The behavior of the test subjects in the driving simulator can not be seen as representative for a real driving situation, since the simulation results principally match the results of the real-world experiment. The similarity of the simulation results and the real-world experiment are such, that in both cases, the drivers choose a short trajectory, although in the experiment, no special restriction was given with respect to choose a short trajectory. Therefore, it seems to be a general behavior to drive always a little bit time-optimally, which means that the drivers tend to prefer a shorter distance over a longer distance.

8.2.3   Keep-right case

The set of weighting factors, which was used for this experiment was according to Tab. 8.1

$$w = \begin{bmatrix} .1 & 0 & 0 & 1.0 & 0 & 0 & 0 \end{bmatrix}. \tag{8.3}$$

System input: steering angle

In order to compare the steering angles with reference to the longitudinal vehicle position of the road, the road curvature of the right bend is added (dash-doted line).The road curvature is scaled with the factor 2, for convenience.

- **Simulation results**
  Starting from the middle line, the vehicle steers to the right lane of the test track right from the beginning, see also the course of the trajectory Fig. 8.11. This behavior results in strong oscillation of the steering angle at the beginning of the test run, see Fig. 8.10.1. The oscillation of the steering angle is probably caused by the low update rate of the proposed driver model. In order to keep the calculation time needed for the simulation low, a low update rate of the driver model was chosen. Therefore, the
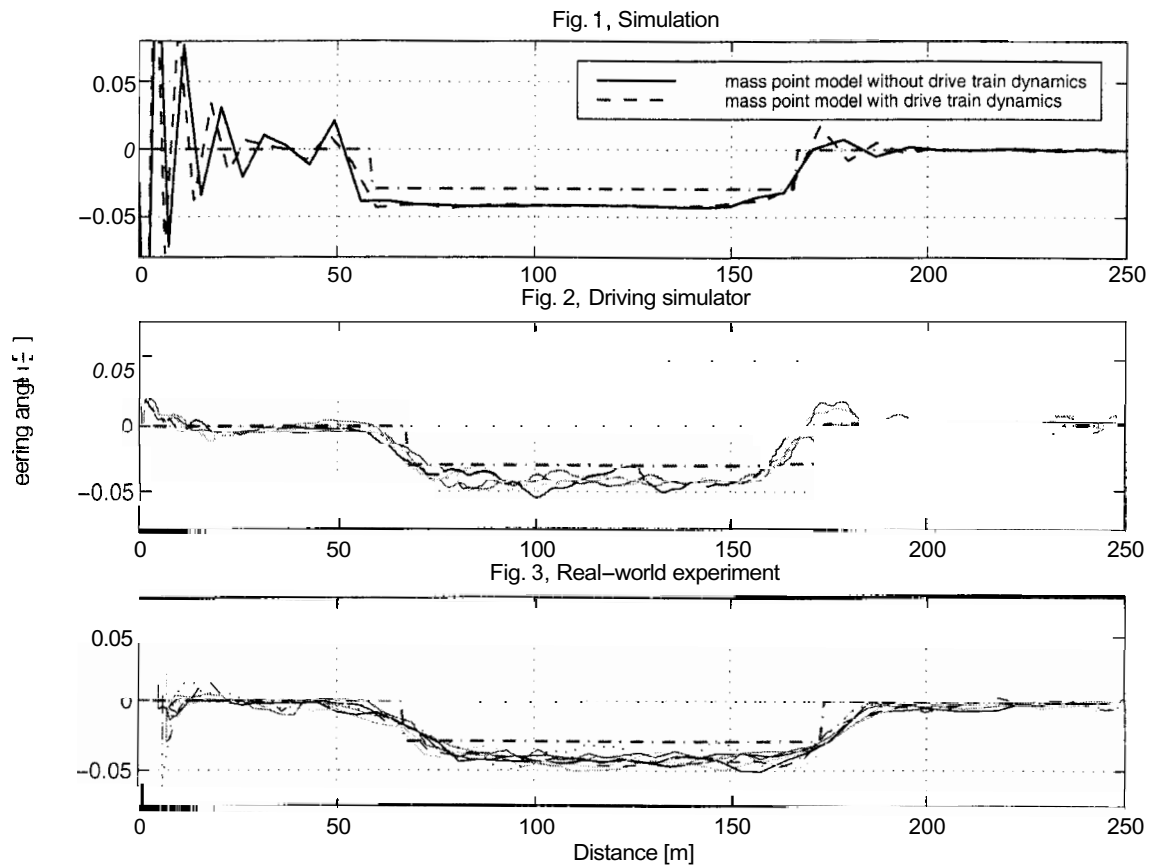
Figure **8.10:** Preference: keep-right, Steering angle while
cornering a right bend, with road curvature
(dash-doted line)

deviations from the nominal system behavior and the actual system behavior become
to big, which leads to problems in the control layer and an oscillating steering angle
profile. The proposed driver model needs the whole distance to the beginning of the
right bend in order to reduce this oscillations. From thereon, the steering angle is
according to the road curvature with sharp transitions at the beginning and the end
of the right bend. The steering angle is constant from the beginning to the end of the
turn.

• Driving simulator results
The general course of the steering angle over the test track is, that all subjects starting
from the right side steer in the direction of the middle line. Then are the steering angles
according to the road curvature, see Fig. 8.10.2. Although it is not implied in the given
preferences to reduce the lateral acceleration, the subjects show long transitions phases
at the beginning and the end of the test track. This leads to the conclusion, that abrupt
changes of the steering angle, which cause high lateral acceleration are considered

to be uncomfortable for the subjects. While cornering, is the course of the steering angles not very constant. This behavior can mean, that the drivers have difficulties in curve negotiation and must, therefore, readjust the steering angle frequently. Another possibility would be, that the drivers do not plan the appropriate steering angle in advance. They prefer to readjust the steering angle as needed in the current situation. If we just see the trajectories, this behavior is also successful to keep the vehicle close to the right side of the test track as it is required, see Fig. 8.11.

- Real-world experiment results
  As in the driving simulator experiment, the steering angles are according to the road curvature. The course of the steering angles is also similar in respect, that the subjects tend to drive in the direction of the middle line at the beginning of the test track, see Fig. 8.10.3 (positive steering angles). The transitions phases initiating and ending the right turn are smoother than in the simulation. The course of the steering angles recorded in the real-world experiment are not constant over greater distances. This can be caused by multiple reasons. One effect is probably the play of the joints in the steering gear and environmental influences like e.g. wind, rough road sheeting. Therefore, the steering movements of the driver are not directly transmitted to the wheels and in addition externally disturbed . This leads to imprecise steering which makes frequent corrections necessary. Another explanation is that the subjects have problems in curve negotiation and need, therefore, to correct the steering angle often in order to fulfill the driving task. It is also possible, that human drivers do not plan the appropriate steering angle in advance, so that they would be able to keep it constant throughout the turn. They adjust it as required due to the current situation.

o Conclusion
  Although the test subjects are all able to fulfill the driving task which requires to stay on the right side of the test track, see Fig. 8.11, they do not behave optimally as calculated in the simulation. They do not adjust an appropriate steering wheel angle at the beginning of the turn which they keep constant until the end of the right bend. They probably look just a short distance in advance and adjust then the steering angle as the actual driving situation requires. In addition, it would be too costly for the driver to plan a steering angle a too long distance in advance. Because a lot of factors like external disturbances and precise curve negotiation would have to be taken into account.

System response: vehicle trajectory

o Simulation results
  Starting from the middle line of the test track, the trajectory leads immediately to the right side of the track, where it stays throughout the remaining test run, see Fig. 8.11.

o Driving simulator results
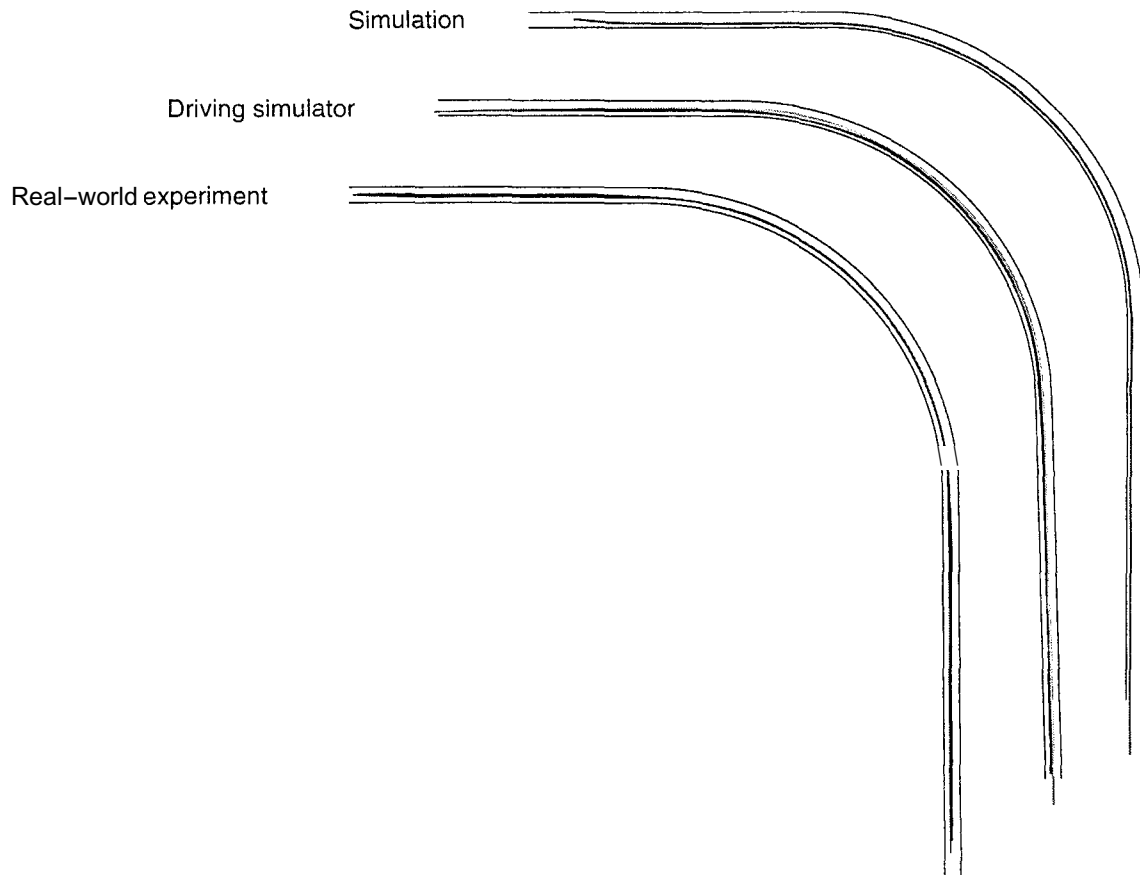 The trajectories start on the very right side of test track, but the subjects have the

Figure **8.11:** Preference: keep-right,, Trajectory while cornering a right bend

tendency to drive slightly to the middle of the test track. After entering the right bend they stay closely to the right border. From there on, all subjects maintain a constant distance *to* the right border until the end of the test track, see Fig. 8.11.

- Real-world experiment results
  In the real-world experiment, the vehicles start in the middle of the test track. Before the right bend the drivers have also the slight tendency to drive a little bit left from the middle line rather the staying close to the right side of the track, which is actually required by this experiment. After entering the right bend, all subjects stay on the right lane and maintain a certain constant distance to the right border of the test track. The subjects kept this constant distance until the end of the test track, see Fig. 8.11.

- Conclusion
  Human drivers are able to stay on the right lane of the test track and they are also able to maintain a constant distance to the right border of the test track. This behavior is also represented by the simulation results. But the tendency that the subjects in both

experiments tend to drive slightly more in the middle of the track before entering the right, bend has no similarity in the simulation results. The reason for this behavior rnay be, that the subjects increase their safety margin to the right. side before entering the turn because they feel uncomfortable to enter a bend at the very right side of a track. It may be also facilitates the curve negotiation for the subjects driving more in the middle of a road than on the very right side. Perhaps is this behavior be caused by the unintentional desire to increase the sight distance before entering a right bend, which results in a trajectory more in the middle of the test track.

8.3   Driver behavior on straight **track**

The results gained from the test runs on the tracks straight east and straight west can be summarized to behavioral patterns of drivers on straight tracks. All diagrams shown in this section refer to the test track straight east.

8.3.1   Acceleration-optimal case

Fig. 8.12 shows the different driver behavior while driving over an almost straight test track with the requirement to keep the lateral and longitudinal acceleration as low as possible. The set of weighting factors, which was used for this experiment was according to Tab. 8.1

$$w = \begin{bmatrix} .1 & 1.0 & 0 & 0 & 0 & 0 & 0 \end{bmatrix}. \tag{8.4}$$

System input: Steering angle

In order to compare better the steering angles with reference to the longitudinal vehicle position on the road, the road curvature of the test has been added (dash-doted line) to the course of steering angles, see Fig. 8.12. The road curvature is scaled with factor 2, for convenience.

- Simulation results
  The course of the steering angle levels out the road curvature and, therefore, minimizes changes in the steering angle, see Fig. 8.12.1. Due to that behavior, the lateral acceleration is reduced to a minimum.

- Driving simulator results
  No tendency to level out intentionally the road curvature becomes obvious, see Fig. 8.12.2. Seemingly, the subjects do not reduce the steering angle to a minimum, and, therefore, do not minimize the resulting lateral acceleration. The course of steering angles is also superimposed by oscillations, which may be caused by the steering angle error function of the driving simulator. This error function is thought to make the feeling of the driving simulator more realistic with respect to the steering behavior. Seeing that the driving simulator does not provide acceleration feedback, it is not possible for the subjects to adjust their driving behavior with respect to minimizing the lateral and longitudinal acceleration.

- Real-world experiment results
  The recorded steering angle profiles are very smooth and have soft transition phases in parts of the test track, where the road curvature changes significantly. The subjects also even out the road curvature where possible and, therefore, keep an almost constant steering angle over the whole test track, see Fig. 8.12.3. Following from that, it
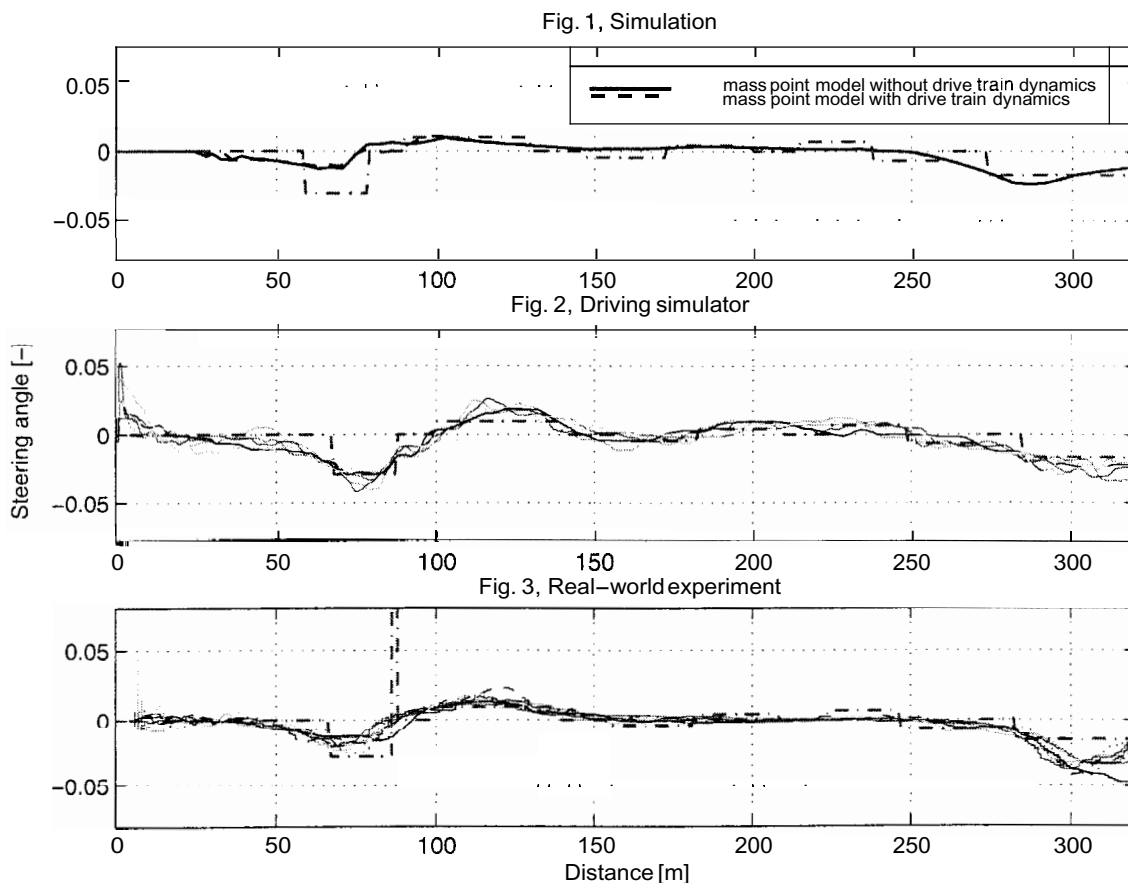
Fig. 1, Simulation

Fig. 2, Driving simulator

Fig. 3, Real-world experiment

Figure **8.12:** Preference: acceleration-optimal, Steering
angles, with road curvature (dash-doted line)

becomes apparent, that the subjects connect slow changes of the steering angle and
small steering angles with low lateral acceleration.

o Conclusion
If the subjects are provided with acceleration feedback as in the real-world experiment,
then they behave optimally with respect to minimizing deviations from the steering
angle. This behavior leads automatically to a low lateral acceleration of the vehi-
cle, which is the goal of this experiment. But if the subjects are not provided with
acceleration feedback, this optimal behavior does not become apparent.

System input: throttle position

o Simulation results
After an initial high throttle signal right at the beginning of the test track, the throttle
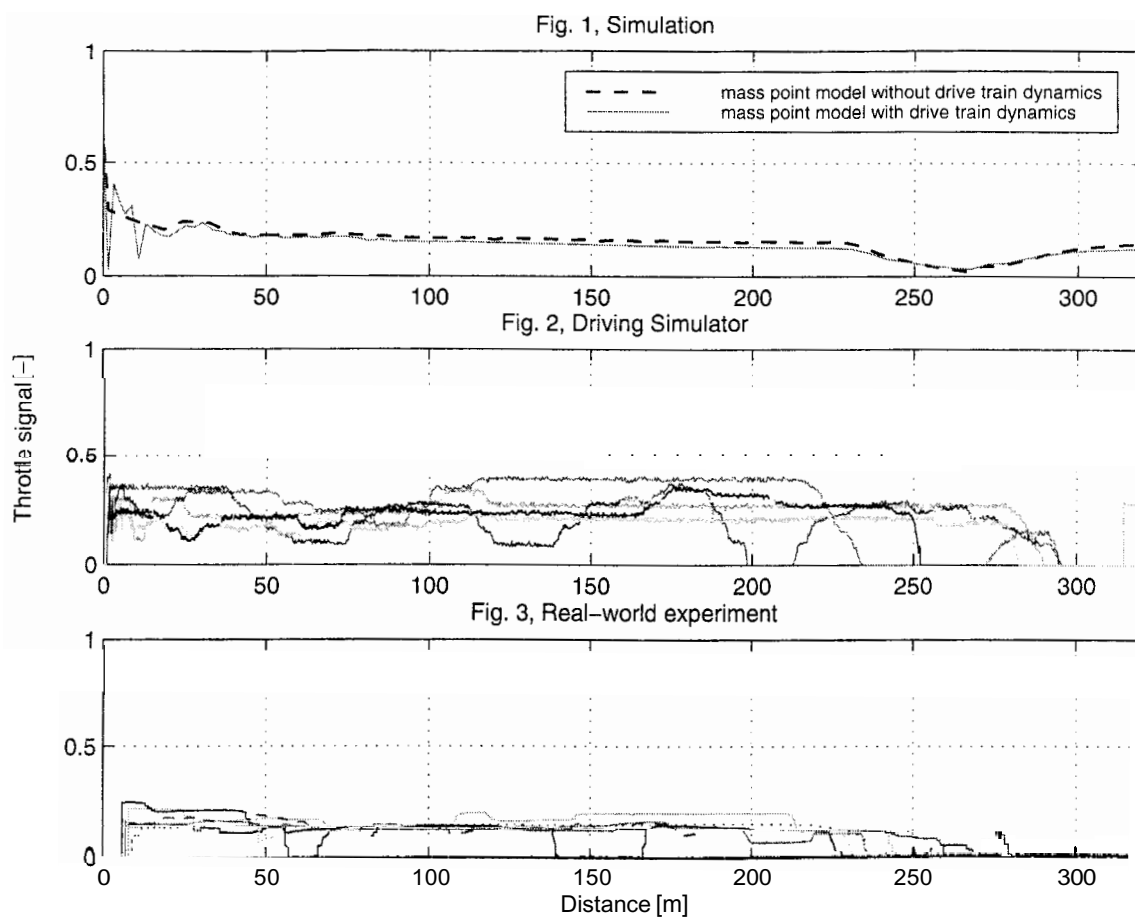angle stays almost constant (<0.2) until the end of the test track, see Fig. 8.13.1. The

Figure **8.13:** Preference: acceleration-optimal,   Throttle
position

only significant deviation from the constant value is the reduction of the throttle angle
before the final right bend of the test track, see Fig. 7.7 for the test, track straight east.
This behavior is caused by the missing condition to stop at the end of the test track.
Therefore, the vehicle gains speed until the last bend, independent of the close end of
the test track. In order not to drive too fast through this turn, the vehicle speed must
be reduced, which is carried out by reducing the throttle angle.

- Driving simulator results
  The course of the throttle signals does not show any specific initial phase as in the
  simulation. Right from the beginning of the test run, most of the subjects strive for
  a constant throttle position, see Fig. 8.13.2. But undirected attempts with large
  deviations in order to adjust the throttle position, leads to the conclusion, that the
  subjects have major difficulties in estimating the vehicle's future behavior. This may
  be caused by the lack of acceleration feedback of the driving simulator, which leads to
  unrealistic high throttle signals compared to the simulation results or the real-world

experiment.

o Real-world experiment results
The course of throttle angles is characterized by a initial phase with slightly higher throttle angle values than during the rest of the test run. After this initial phase, the subjects try to maintain small constant throttle angles. Over the entire test run, the throttle angles are in the interval 0.1-0.2, with only little deviations, see Fig. 8.13.3. The small deviations are probably caused by external disturbances, which have to be taken into account by the subjects.

o Conclusion
Similar to the simulation results, the subjects in the real-world experiment maintain a constant throttle position over the entire test run. The continuity of the throttle position leads to a minimal longitudinal acceleration, which is the goal of this experiment. The results from the driving simulator experiment are not representative, due to the lack of acceleration feedback of the driving simulator.

System response: Velocity profile

o Simulation results
With only an insignificant first acceleration phase, the vehicle velocity increases slowly but steadily until $70m$ before the end of the test track. The reached top speed is little below $14m/s$, see Fig. 8.14.1. The speed is then slightly reduced in order to drive through the final right bend of the test track. But seeing that there is no stopping condition for the simulation at the end of the test track, no further conclusions can be drawn from the driver behavior so close to the end of the test track.

o Driving simulator results
The velocity profiles are characterized by an initial acceleration phase, in the first $20m$ of the test track. From there on, the speed is slowly increased towards the end of the test track, see Fig. 8.14.2. The top speed reached by the subjects is individually different and is in the range from $10\text{-}18m/s$. Only one subject is not able to control the speed, which leads to an undirected behavior and an oscillating speed profile. $100\text{-}50m$ before the end of the test track, the subjects start to decelerate the vehicle and decrease the vehicle speed in order to fulfill the stopping condition at the end of the test track.

o Real-world experiment results
As in the driving simulator experiment, the velocity profiles are characterized by an initial acceleration phase. Then, the velocity is steadily increased towards the end of the test track. The top speed of the test driver is in the range of $9\text{-}14m/s$. .Approximately $60m$ before the end of the track the velocity is decreased again, because of the requirement to make a full stop at the end of the test track.
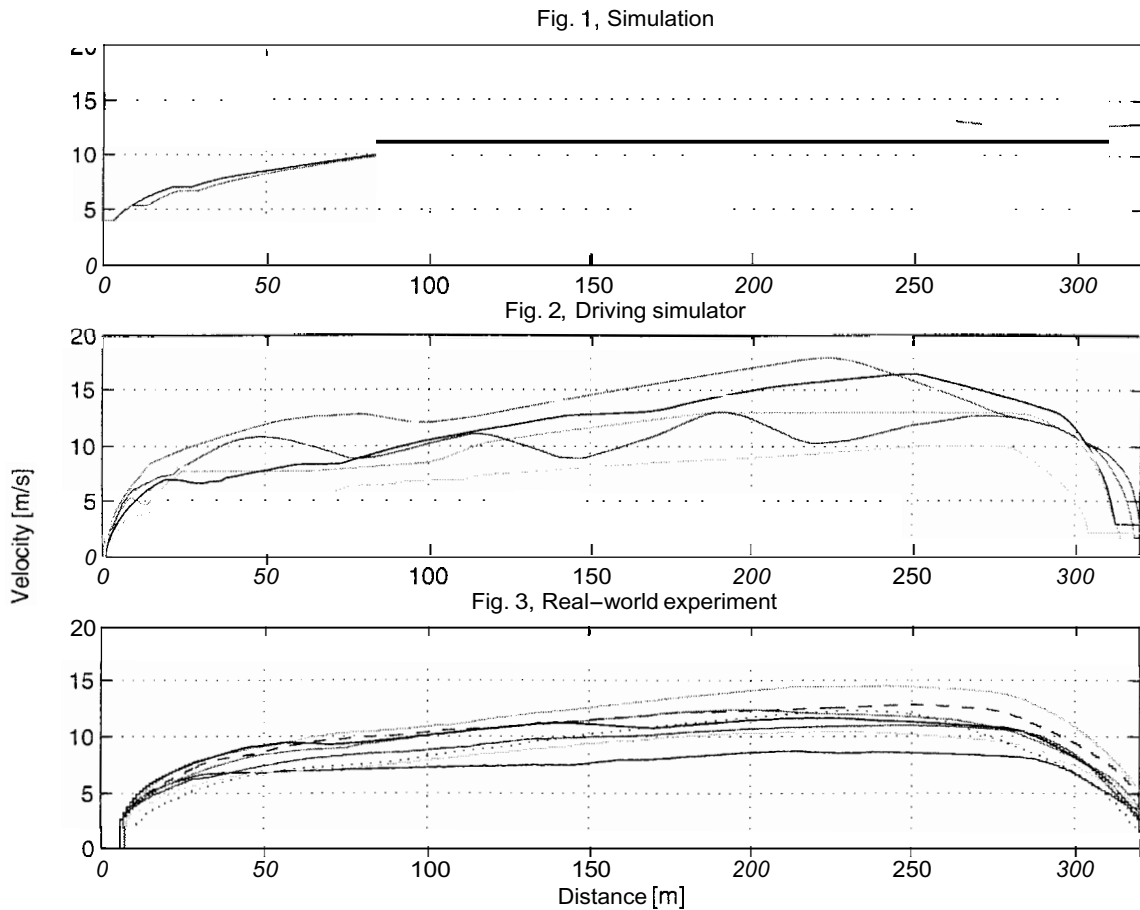
Figure **8.14:** Preference: acceleration-optimal, Velocity
profile

o Conclusion
Apart from the different stopping condition at the end of the test track, there is no
significant difference between the experiments and the simulation. Therefore, the speed
is not rapidly increased, which would cause high longitudinal acceleration exerted on
the passengers. The subjects also avoid fast changes of the vehicle velocity during
the test ride, which would also increase the longitudinal acceleration exerted on the
passengers.

System response: Vehicle trajectory

o Simulation results
The resulting trajectory of the simulation is the trajectory with the least possible
curvature. Following from that, the lateral acceleration exerted on the vehicle is also
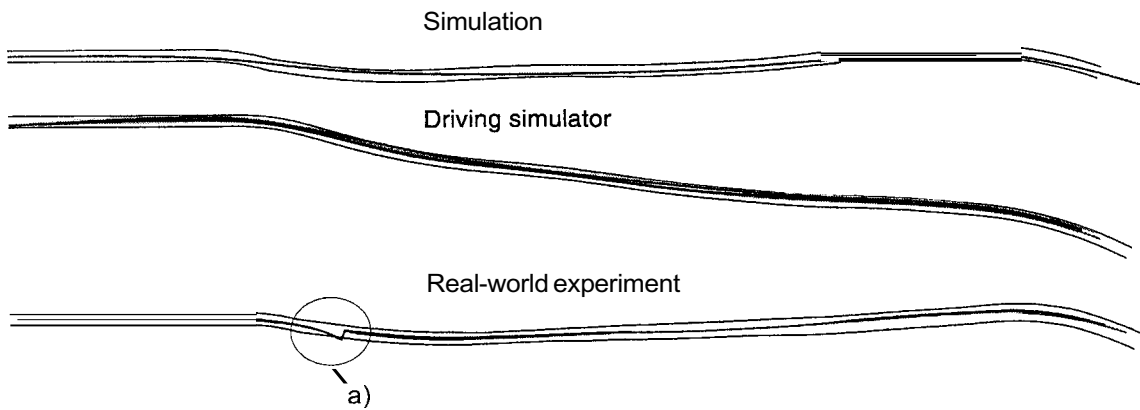very low. In order to achieve this trajectory, the vehicle changes lanes as needed and

Simulation

Driving simulator

Real-world experiment

a)

Figure **8.15:** Preference: acceleration-optimal,   Trajecto-
ries, unsteady trajectories at a) caused by
course of magnetometers in test track

does not stick to one specific lane of the test track.

- **Driving simulator results**
  Starting in the middle of the test track, the subjects steer to the left lane. All the
  subjects stay in the middle or on the left lane of test track throughout the test, run.
  They do not try particularly to even out the road curvature by choosing a trajectory
  with the biggest possible radii. Only in the section of the test, track, with a significant
  change in the road curvature, they choose a slightly bigger radius as the radius of the
  test track. Therefore, the subjects do not try to reduce the lateral acceleration exerted
  on the passengers by choosing an optimal trajectory. This behavior may be caused
  by the lack of acceleration feedback of the driving simulator. Seeing that, it is almost
  impossible for the subjects to minimize the lateral acceleration, if they can not sense
  it.

- *o* Real-world experiment results
  The unsteady course of trajectories at the point a) is caused by the characteristics of the
  test track and does not represent the real vehicle trajectories. In the remaining parts
  of the track, the subjects stay always close to the middle of the test track. However,
  they have the tendency to choose a trajectory, which evens out the road curvature.
  The resulting trajectories have a smaller curvature than the test track. Following from
  that, the subjects minimize the lateral acceleration by driving along a appropriate
 trajectory.

- *o* Conclusion
  Although the subjects in the real-world experiment, choose a trajectory with less cur-
  vature than the test track, they do not behave as optimally as calculated in the sim-
  ulation. Especially, at half distance of the test track, the subjects stay close to the
  middle line, rather than driving on the right lane. Whereas they level out bends in

high curvature sections of the test track. This leads to the conclusion, that human drivers do not plan their behavior for a long time in advance. They react as required in the current driving situation, which leads to the right behavior in high curvature sections of the test track. But the do not look enough time ahead in order to choose the optimal trajectory between the first right/left bend and the final right bend at the end of the track.

System response: Lateral acceleration profile

In order to compare better the lateral acceleratione with reference to the longitudinal vehicle position on the road, the road curvature of the right bend has been added (dashed line) *to* the course of steering angles: see Fig. 8.21. The road curvature is scaled with factor 150, for convenience.
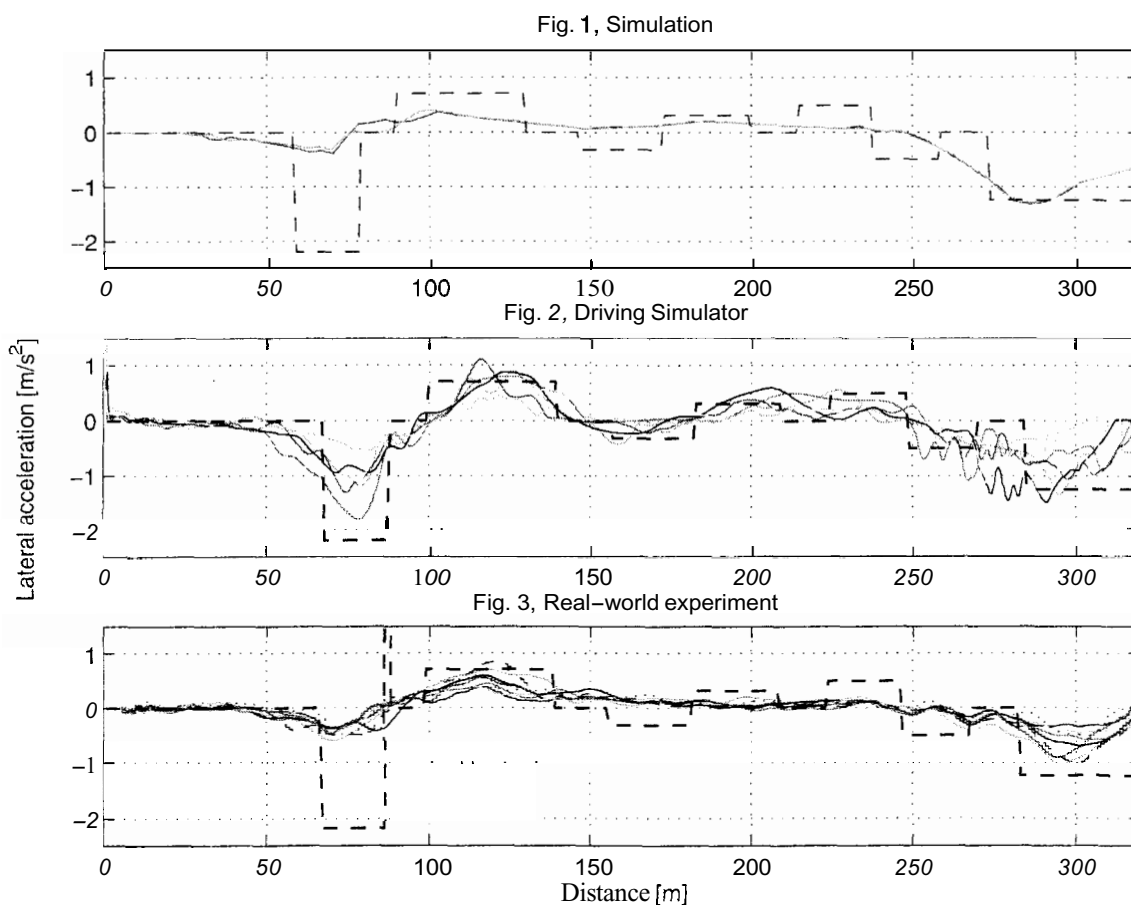
Figure **8.16:** Preference: acceleration-optimal, Lateral acceleration, with road curvature (dashed line)

o Simulation results
The course of the lateral acceleration is very smooth and even, during the entire test run. No sudden changes occur. The lateral acceleration is almost constant over most the time and never exceeds values of $0.4 m/s^2$. In the section from 120-250m of the test track the magnitude of the lateral acceleration is even below $0.2 m/s^2$. The only part, with a higher lateral acceleration is the last right turn. However this section can not be compared with the experimental results, because of the different stopping conditions at the end of the test track.

o Driving simulator results
The recorded test data of the lateral acceleration is passed through a butter worth filter 2nd order with the cut off frequency 0.08 in order to reduce the noise in the test data.
The course of lateral acceleration follows basically the road curvature profile. In general, the magnitude of the lateral acceleration profiles is higher than in the simulation. The course of the lateral acceleration profiles is also superimposed by oscillations. But changes in lateral acceleration is actually considered to be uncomfortable for human beings. Therefore, the results gained in this experiment are qualitative and quantitative not representative for real driving behavior. This is probably caused by the lack of acceleration feedback of the driving simulator. Seeing that, it is obvious that it is almost impossible for the subject to minimize successfully the lateral acceleration, if the are not able to sense it.

o Real-world experiment results
The recorded test data of the lateral acceleration is passed through a butter worth filter 2nd order with the cut off frequency 0.02 in order to reduce the noise in the test data.
The course of lateral acceleration is similar to the results calculated by the simulation. The acceleration profiles of the different subjects are smooth and even. No sudden changes in the lateral acceleration occur. Even the magnitude of the acceleration profiles are in the scale of the simulation results. Therefore, the subjects are able to minimize successfully the lateral acceleration exerted on the passengers.

o Conclusion
The results gained from the simulation match the human driving behavior. Human drivers behave almost as optimally as the simulation. They are able reduce successfully the lateral acceleration of the vehicle to a minimum. The different results of the driving simulator experiment is probably caused the lack of acceleration feedback of the driving simulator.

System response: Longitudinal acceleration profile

o Simulation results
The course of longitudinal acceleration starts with an initial value of approximately
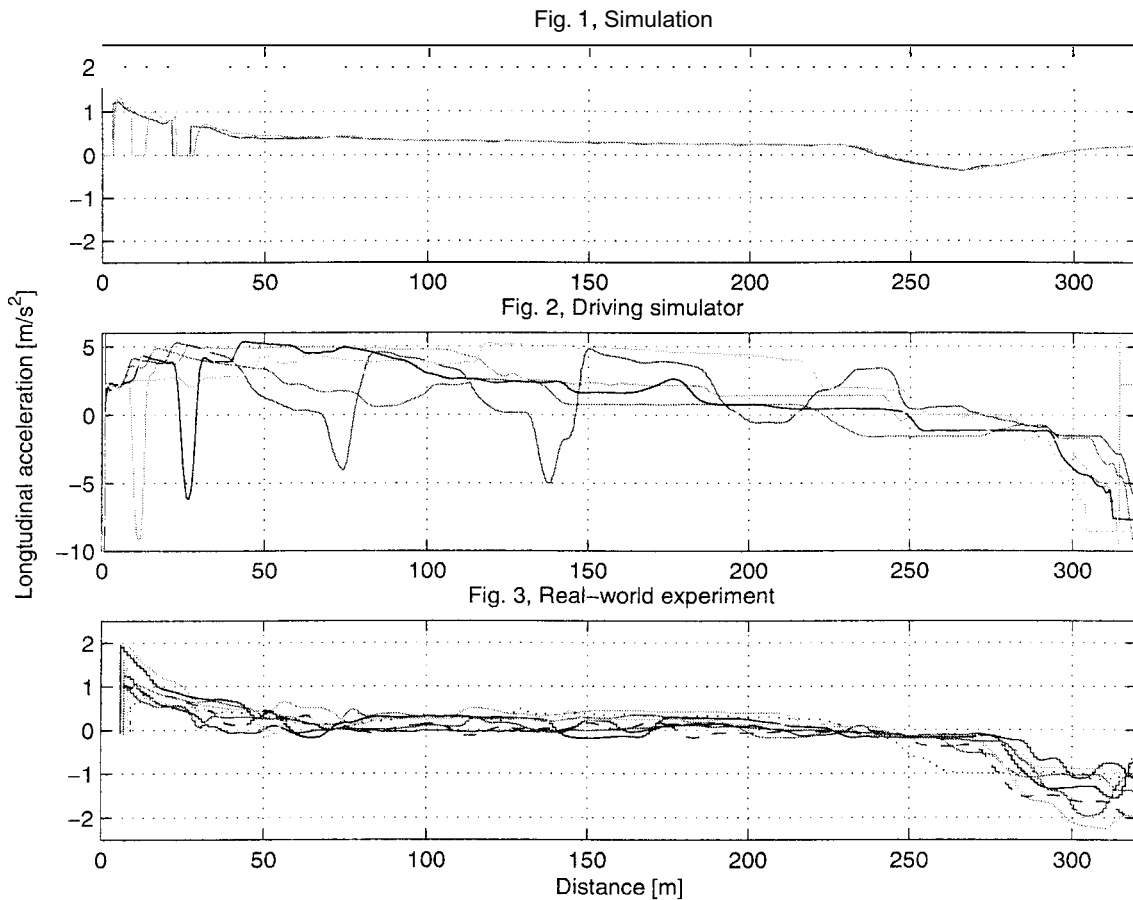
.

Fig. 1, Simulation

Fig. 2, Driving simulator

Fig. 3, Real–world experiment

Figure **8.17:** Preference: acceleration-optimal, Longitudinal acceleration

$1.3m/s^2$. The acceleration decreases smoothly in the first *50m* of the test track to a value of $0.5m/s^2$. The sudden drops of the longitudinal acceleration during this phase are due to shifting into another gear. Therefore, the clutch has to be opened and no power transmission is possible during this action. After the first $50m$ of the test track, the longitudinal acceleration is almost constant for the next $180m$. $90m$ before the end of the test track, the vehicle decelerates again in order to drive through the final right turn. But different stopping conditions apply for the simulation and the experiments at the end of the test track and, therefore; no conclusions can be drawn from the driver behavior so close to the end of the test track.

8 Driving simulator results
The recorded test data of the longitudinal acceleration is passed through a butter worth filter 2nd order with the cut off frequency 0.08 in order to reduce the noise in the test data.
However, the longitudinal acceleration is not representative for real driving behavior, due to the lack of acceleration feedback of the driving simulator. The longitudinal

acceleration is much too high, see the scale of Fig. 8.6.2 compared to the scale of Fig. 8.6.1 and Fig. 8.6.3, which may also be caused by problems of the data processing. The course of the longitudinal acceleration is also not very steady, which also does not represent a realistic driving behavior. Therefore, no further conclusions can be drawn from this set of test data.

o Real-world experiment results

The recorded test data of the longitudinal acceleration is passed through a butter worth filter 2nd order with the cut off frequency 0.02 in order to reduce the noise in the test data.

The subjects start with a high initial longitudinal acceleration, which lies in the interval of 1.0-$2.0 m/s^2$. This initial acceleration is then continuously reduced within the first $50m$ of the test track. From thereon, the subjects keep an almost constant longitudinal acceleration until about $100m$ before the end of the test track. In the last $100m$ the subjects decelerate the vehicle because of the required full stop at the end of the test track.

● Conclusion

Regardless of the different driver behavior at the end of the test track matches the simulation result the driver behavior of the real-world experiment. A higher initial acceleration followed by a smooth transition phase and than an almost constant longitudinal acceleration over a long distance of the test track. This behavior is similar in the sirnulation and the real-world experiment. The results of the driving simulator are not realistic in respect of the magnitude and acceleration profile. No conclusions can be drawn from this results, because of problems in the data processing and the fact that the driving simulator does not provide any acceleration feedback for the subjects.

8.3.2   Velocity-optimal case

The set of weighting factors, which was used for this experiment was according to Tab. 8.1

$$w = \begin{bmatrix} .1 & 0 & 0 & 0 & 0 & 1.0 & 0 \end{bmatrix}. \tag{8.5}$$

System input: throttle signal

o Simulation results

For this preference, the simulation results of the throttle signal for driving on a straight test track are similar to the simulation results for driving a right turn. The initial value of the throttle signal is full throttle for approximately the first $15m$ of the test track, see Fig. 8.18.1. After this phase, the throttle position is dramatically decreased to a value of about 0.1 for the remaining distance of the test track. The oscillation of the throttle signal is probably caused by the low update rate of the proposed driver model.
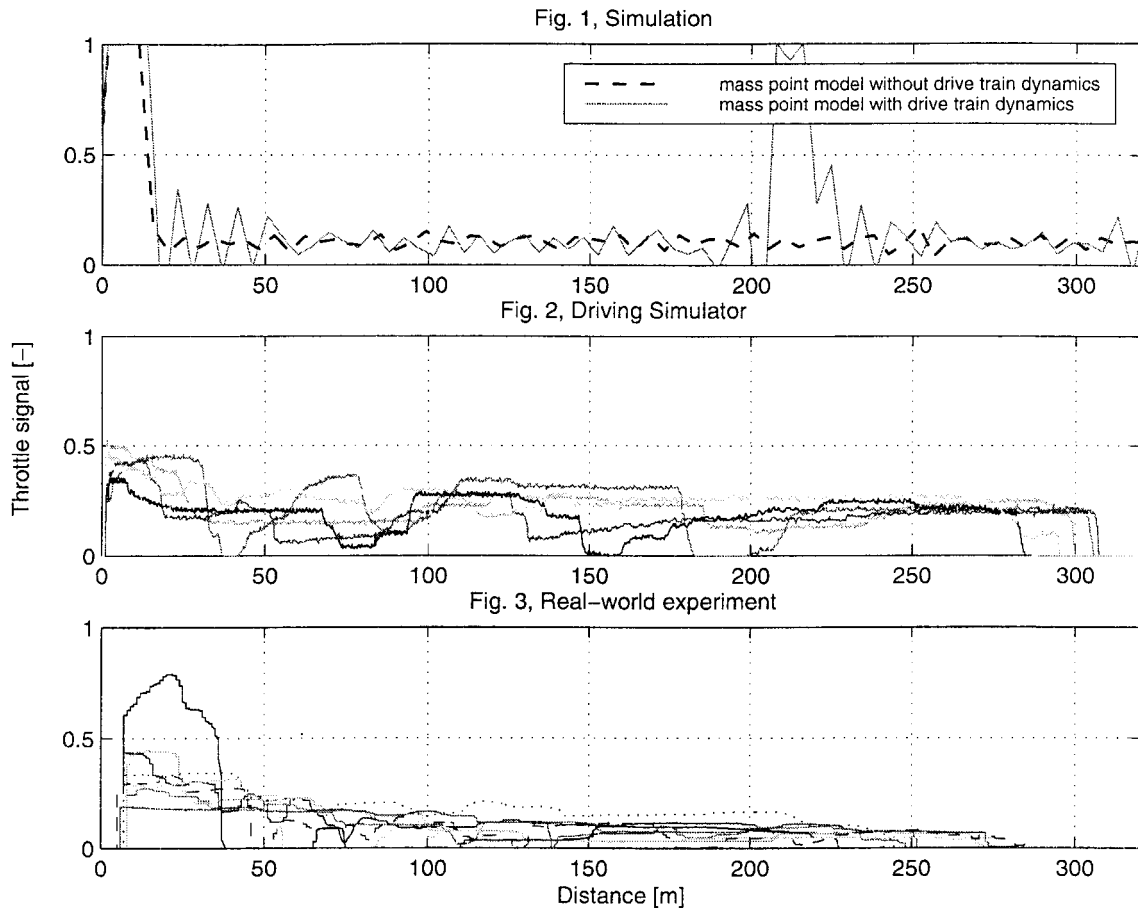
Figure **8.18:** Preference: velocity-optimal, Throttle signal

In order to keep the calculation time needed for the simulation low, a low update rate of the driver model was chosen. Therefore, the deviations from the nominal system behavior and the actual system behavior become too big, which leads to problems in the control layer and an oscillating throttle angel profile. These problems become more apparent if the driver's prediction model includes drive train dynamics.

- Driving simulator results
  Since no driver is able to approach in a directed manner the given speed of $25mph$, see Fig. 8.19.2, no directed behavior can be extracted from the course of throttle signals, see 8.18.2. No significant initial phase with higher throttle signals is shown in the recorded test data. Towards the end of the test run, most of the drivers manage finally to reach and maintain an almost constant speed of approximately $25mph$, which is also reflected by more or less constant throttle signals of the subjects.

- Real-world experiment results
  The course of throttle signals starts with different values, which are in the range of 0.2-0.8. Seemingly, the longitudinal acceleration and with it the initial throttle signal,

is strongly dependent on the different subjects and when they consider a longitudinal acceleration as uncomfortable, regardless of the given preferences. In the following course of the experiment, the subjects show various throttle angel profiles. Although all subjects try to reduce the throttle signal within the first $100m$ of the test track, no directed behavior becomes obvious. This can be caused by an imprecise picture of the vehicle dynamics, which requires to readjust the throttle position frequently. But it can also mean, that human drivers do not plan an optimal throttle signal in advance, they rather adjust it as in the current situation required.

o Conclusion

The results, calculated of the simulation are not reflected in the experimental results. The differences to the results gained from the driving simulator experiment, are probably caused by the lack of acceleration feedback and visual information (flow of texture), which usually helps the driver to adjust the vehicle speed. Without this aids it is very difficult to maintain precisely a certain speed, which is also reflected in the throttle angle profiles. But the different behavior of the subjects in the real-world experiment is rather due to an different attitude to driving than caused by problems to keep a certain speed. It seems, that human drivers rather readjust the throttle signal frequently in order to meet a certain goal, than planning the optimal throttle value in advance.

System response: velocity profile

o Simulation results

The speed is increased within the distance of $18m$ to the required speed of $25mph$ or $11m/s$. The velocity is then hold perfectly constant over the remaining distance of the test track, see Fig. 8.19.1.

o Driving simulator results

The speed is increased considerably in the first $20m$ of the test track. But then, none of the subjects is able to approach and keep the required speed not until the first half of the test run. In the second half of the test run, the subjects are finally able to reduce the huge deviations from the desired speed of $25mph$ and to keep the velocity of their vehicle constant, see Fig. 8.19.2. This problem is probably caused by the driving simulator characteristics. Without any acceleration feedback and only little contrast of the environment it is very difficult for the subjects to maintain a certain speed solely dependent on the speedometer.

o Real-world experiment results

The subjects need a considerably long time to reach the desired speed. Seemingly, even if the subject do not have to reduce the longitudinal acceleration intentionally, they avoid fast changes of the vehicle speed, which would cause a high longitudinal acceleration. After the first 50-$100m$ of the test track, maintain the subjects an almost constant speed. In the limits of the precision of the speedometer and human abilities, the drivers show optimal behavior in keeping a certain speed.
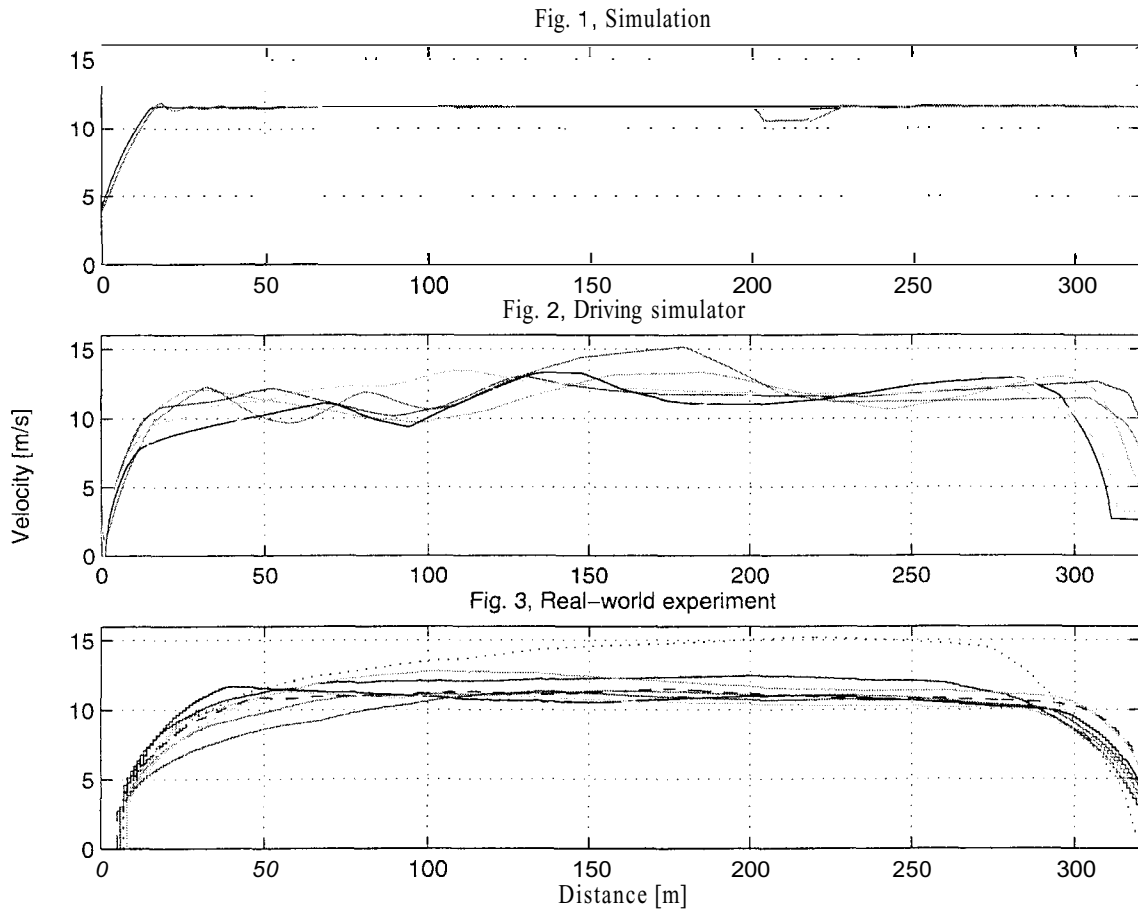
Figure **8.19:** Preference: velocity-optimal, Velocity profile

● Conclusion
Regardless of the first acceleration phase, which is much shorter in the simulation than in the real-world experiment, the simulation results match the experimental results. Human drivers are similar to the proposed driver model able to accelerate the vehicle to a certain speed and then keep this speed constant over the remaining test run. The driver behavior of the subjects in the driving simulator experiment, is not representative. The lack of acceleration feedback and the flow of texture, causes a different driving behavior as in a real environment.

System response: vehicle trajectory

o Simulation results
The resulting trajectory of the simulation is the shortest possible trajectory to drive through the test track, see Fig. 8.20.1. In this case, no other restrictions than the speed limit apply for the simulation. Therefore, the little weight on driving time-optimally

Simulation

Driving simulator

Real-world experiment

a)
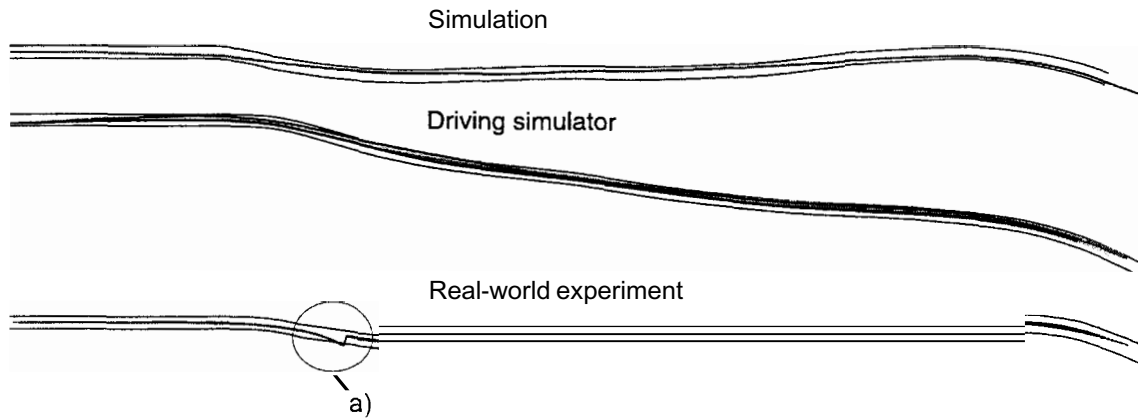
Figure 8.20: Preference: velocity-optimal,   Trajectories,
unsteady trajectories at a) caused by course
of magnetometers in test track

in this set of preferences becomes important, see Tab. 8.1. *So,* is the vehicle trajectory
the shortest possible route for this test track.

- **Driving simulator results**
Since no special attention is given to the vehicle trajectory, the subjects choose the
most comfortable one. Apparently, the left side of the test track is preferable over
the right side of the test track. The subjects change at the beginning of the test run
from the right lane to the left lane of the test track and stay there until the end, see
Fig. 8.20.2. None of the subjects makes the attempt to choose the shortest possible
trajttctory as calculated in the simulation.

- **Real-world experiment results**
The subjects tend to stay close to the middle line of the test track, see Fig. 8.20.3.
The given scenario for the subjects does not include other restrictions than the speed
limit. Therefore, the subjects pay no special attention to the vehicle trajectory. Un-
intentionally, they drive the trajectory which is the least effort to find. This means to
stay in the middle of the test track. No special attempts can be extracted from the
course of the trajectories, that the drivers try to drive the shortest possible route for
this test track.

- **Conclusion**
No special restrictions than the posted speed limit apply for this experiment'. Therefore,
the trajectory calculated in the simulation is the shortest possible, according to the
little weight of time optimality in the simulation preferences. But compared to the
simulation, the subjects put rather more weight on choosing a trajectory which they
can drive with the least effort than trying to find the shortest possible route.

8.3.3 **Keep-right** case

The set of weighting factors, which was used for this experiment was according to Tab. 8.1

$$w = \begin{bmatrix} .1 & 0 & 0 & 1.0 & 0 & 0 & 0 \end{bmatrix} . \tag{8.6}$$

System input: steering angle

In order to compare better the steering angles with reference to the longitudinal vehicle position on the road, the road curvature of the right bend has been added (dash-doted line) to the course of steering angles, see Fig. 8.21. The road curvature is scaled with factor 2, for convenience.
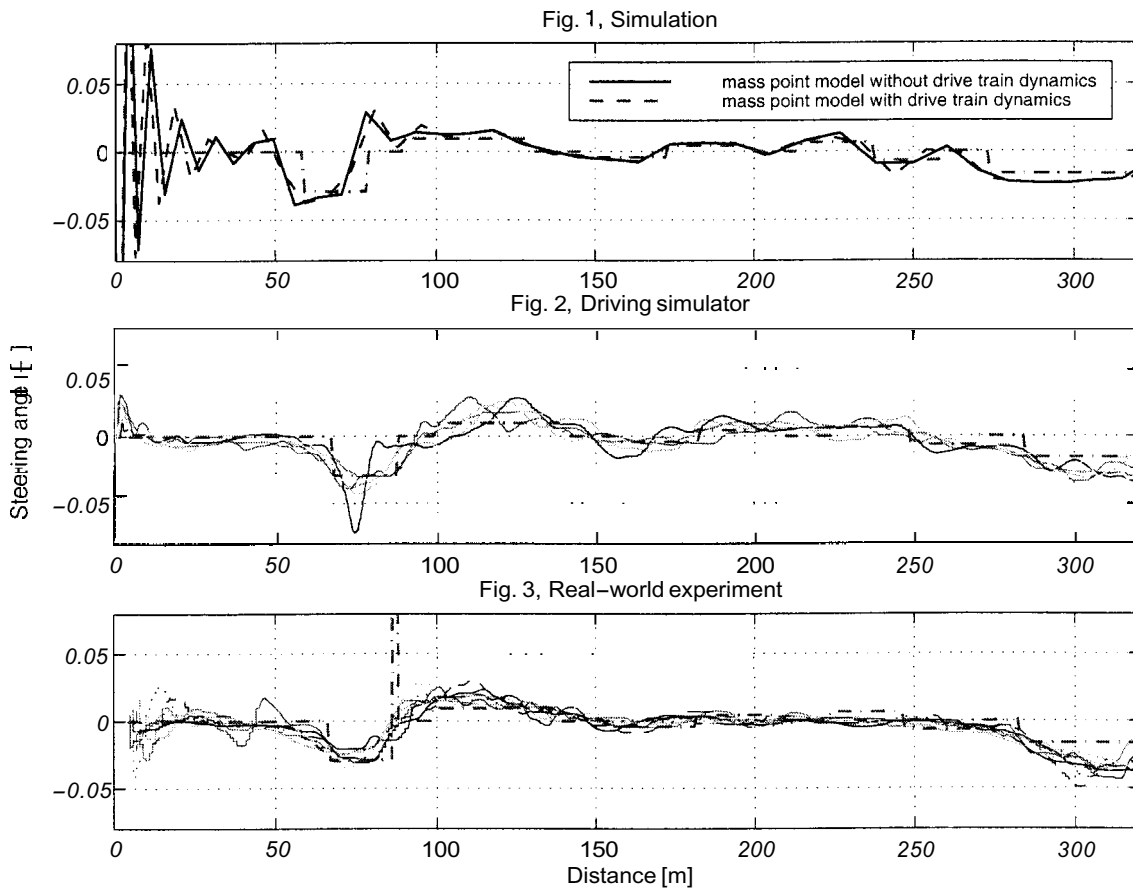

Figure **8.21:** Preference: keep-right, Steering angles, with road curvature (dash-doted line)

- Simulation results
Starting from the middle line, the vehicle steers to the right lane of the test track right

from the beginning, see also the course of the trajectory Fig. 8.22. This behavior results in strong oscillation of the steering angle at the beginning of the test run, see Fig. 8.21.1. The oscillation of the steering angle is probably caused by the low update rate of the proposed driver model. In order to keep the calculation time needed for the simulation low, a low update rate of the driver model was chosen. Therefore, the deviations from the nominal system behavior and the actual system behavior become to big, which leads to problems in the control layer and an oscillating steering angle profile. The initial strong oscillation is significantly reduced in the first $50m$ of the test track. From thereon, the steering angle follows the road curvature with sharp transitions whenever the road curvature changes.

o Driving simulator results
Principally, the steering angles follow the curvature profile of the test track, but the subjects need a lot of correction movements in order to keep their vehicle always at the right side of the test track, see Fig. 8.21.2. This behavior is probably caused by difficulties of the subjects in curve negotiation, which makes a frequent readjustment, of the steering angle necessary. Another reason for the considerably strong oscillation of the course of steering angles may be the error function implemented in the driving simulator, which is superimposed as external disturbance on the steering angles. This error function is thought to make the driving feeling in the driving simulator more realistic for the subjects.

● Real-world experiment results
As in the simulation and the driving simulator experiment, follow the steering angle profiles mainly the curvature profile of the test track, see Fig. 8.21.3. But the transitions in sections of changes in the road curvature are much smoother than in the simulation results and the steering angles do not follow as precisely the road curvature as in the simulation. This leads to the conclusion, that even if no special preference is given to reduce the lateral acceleration of the vehicle, the subjects avoid fast, changes of the steering angle, which would cause high lateral acceleration.

o Conclusion
The driver behavior of the proposed driver model is basically reflected in the driving behavior of the test subjects. But the driving behavior of the test subjects is not as extreme as the simulation results. The subjects put also always some weight on driving acceleration optimal, which results in smooth steering angle profiles. Fast changes of the steering angle are also avoided, even in sections of the test track, where the road curvature changes considerably within a short distance.

System response: vehicle trajectory

● Simulation results
Starting from the middle line of the test track, the vehicle drives immediately to the
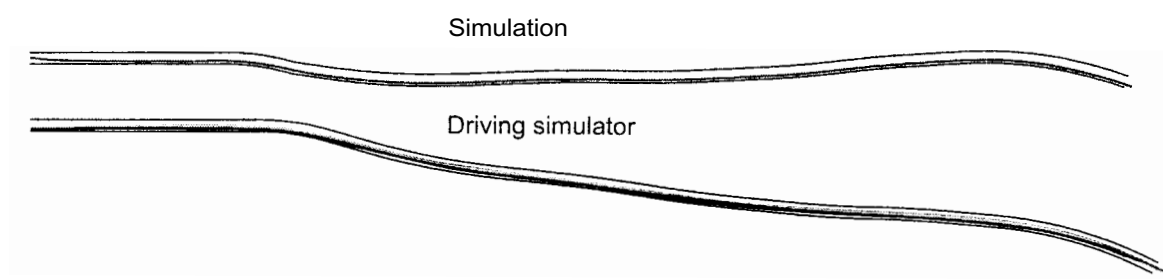
Figure **8.22:** Preference: keep-right, Trajectories

right side of the test track. From thereon, it stays close to the right border line for the remaining test run, see Fig. 8.22.

o Driving simulator results
All the subjects manage to follow exactly the right borderline of the test track throughout the test run. Only in the section with a considerably change of the road curvature after circa $75m$ from the beginning of the test track they do not keep a constant distance to the right border, see Fig. 8.22. Therefore, the subjects are able to drive exactly along a desired trajectory if it is required.

o Real-world experiment results
All the subjects were most of the time out of the measurement range of the magnetometer sensors. Therefore, no conclusions can be drawn from the trajectories recorded in this experiment.

● Conclusion
All subjects are able to fulfill the driving task, which requires to stay on the right lane of the test track, similar to the simulation results. But they do not follow exactly the road profile in sections with high changes of the road curvature. It, is probably uncomfortable for the drivers to make fast changes of the vehicle direction, which would lead to high lateral acceleration. This human preference is obviously so strong, that the subjects do not follow exactly the road curvature, even if it is required by the experiment.

8.4   Time-optimal driver behavior in the Hockenheim Motodrom

As we could show in the experiments discussed above, is the proposed driver model able to simulate human driving behavior in basic driving task, like cornering and driving on a straight track. We could also show, that the proposed driver model is able to represent different driver preferences while cornering or driving on a straight track. In the following chapter, we discuss the behavior of the proposed driver model in a more complex driving situation than just a single curve or straight section. The given preference for this simulation is to drive time optimally, see Tab. 8.1

$$\boldsymbol{w} = \begin{bmatrix} 1 & 0 & 0 & 0 & 0 & 0 & 0 \end{bmatrix}. \tag{8.7}$$

The prediction model, which is used for the simulation is a single mass point model with drive train dynamics, see Eq. 3.19. The used test track is the Hockenheim Motodrom (HM), Germany. The Motodrome is a part of the Hockenheim race track, located in Germany. For several years, Hockenheim has been used regularly for the Formula 1 Grand Prix of Germany. The HM as used for our simulations is $1870m$ long, exhibits 7 corners with their radii varying from 35 m (corner 5) up to 80 m (corner 1) and 7 straight sections.

System input: steering angle

- Simulation results
  For a time-optimal ride it is important to correlate the steering angle exactly to the points of the trajectory, where the vehicle accelerates again. This is reflected in the simulation results. Whenever the vehicle accelerates again, see Fig. 8.23, then is the steering angle reduced again. Therefore, the vehicle speed is low when the steering angle is big. This behavior reduces the lateral acceleration, and the tire forces are not exceeded while cornering.

- Driving simulator results
  The course of steering angles recorded in the driving simulator experiment, see Fig. 8.23.2 and Fig. 8.23.3 are not so optimal with respect to the given preference as the simulation. The course of steering angles is not very directed which means, that the subjects need a lot of correction movements in order to keep the vehicle on track. This leads to high peaks in the course of steering angles, which cause a high lateral acceleration. Following from that, the subjects have to reduce the vehicle speed more as actually needed in order not to exceed the tire forces. The correlation of the acceleration points, where the vehicle gains speed again, to the steering angle is not optimal. The acceleration points are distributed around areas of high steering angles but they are not placed optimally at the vertex of the turn. The recorded driver behavior may
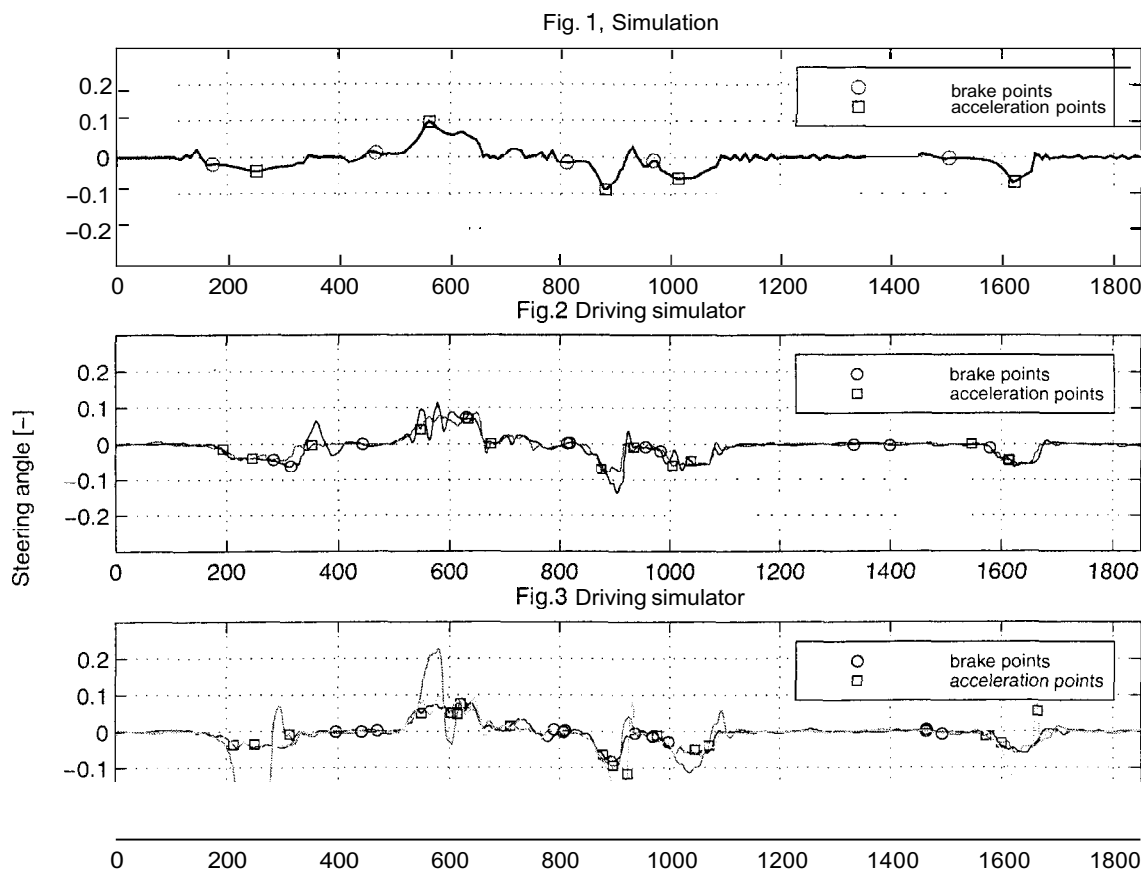
Figure **8.23:** Preference: time-optimal, Steering angles,
with brake points and acceleration points

be influenced by the characteristics of the driving simulator as described in the experiments above, like lack of acceleration feedback, lack of flow of texture and a lack of tire noise feedback, which would give the subject the possibility to estimate the current tire saturation.

- Conclusion
  The course of the steering angle calculated by the simulation, is as shown optimal with respect to the given preference. But the driving behavior of the test subjects is not optimal. The acceleration points are not placed optimally at the vertex of turns, the subjects need a lot of correction movements and the course of steering angles in general is not as directed as the simulation results. Therefore, the simulation is not able in this case to reflect the driving behavior of the subjects. This is probably caused by the driving simulator characteristics on one hand and of the lack of driving experience of the subjects on the other hand. The given preference is very extreme and never happens in a real driving situation and the subjects are no race drivers, which are specially trained to drive time-optimally. Therefore, the experiment must automatically come to the

result, that the simulation does not reflect the driver behavior of the test subjects.
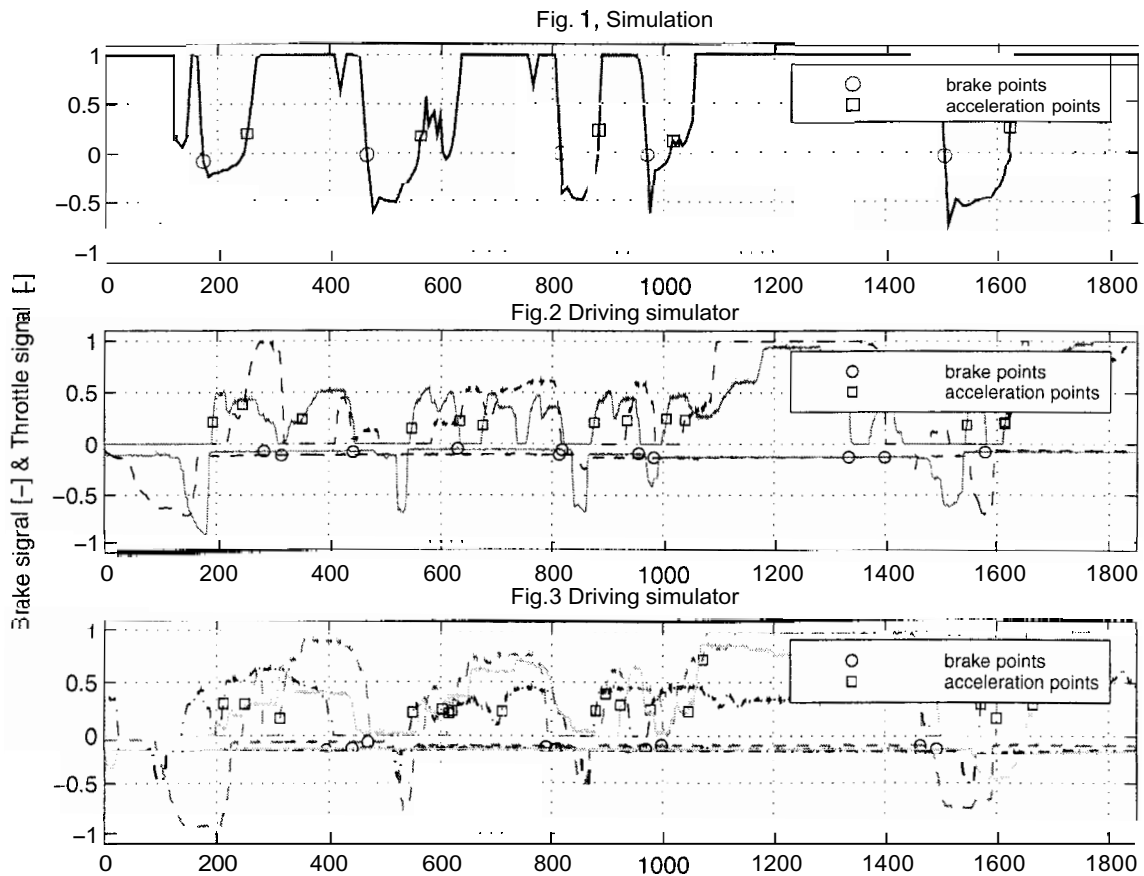
System input: throttle signal

Fig. 1, Simulation

Fig.2 Driving simulator

Fig.3 Driving simulator

Figure **8.24:** Preference: time-optimal, Throttle signals ($>$ 0) and brake signals (< 0), with brake points and acceleration points

- Simulation results
  The starting condition of the simulation is a speed of $4m/s$, which basically means stand still. This fact has to be taken into account, when comparing the simulation results with the results of the driving simulator experiment. The simulation results show, that the proposed driver model always accelerates with full throttle. Therefore the driver uses the maximum available engine power, which is optimal in respect to minimize the driving time needed to cover the whole distance of the HM. However, the driver uses the brakes carefully in order not to lose to much speed.

e Driving simulator results

The starting condition of the driving simulator experiment, differs from subject to subject, because of the course of the experiment, see chapter 7.2.5. The last successful run through the HM was taken as result of each respective subject, which causes different initial velocities of each set of recorded test data. In addition, is the initial speed much higher than the initial speed of the simulation, which starts from an almost standstill. Due to this starting condition is the subject's brake point for the first turn out of range. Therefore, is the first significant point of the course of throttle positions the acceleration point of the first turn and not the brake point of the first turn as in the simulation results. The drivers rarely use the possibility to accelerate with full throttle, which is not optimal in respect of the given preference. The braking behavior of the subjects is also not time-optimal, see Fig. 8.24.2 and Fig. 8.24.3. The brake points are defined as the points of the course of the vehicle velocity, when the velocity starts to decrease again, see Fig. 8.31. This definition coincides perfectly with the course of throttle position in the simulation results, see Fig. 8.24.1. But the brake points of the subjects are mostly placed before the subjects actually start braking, which means that they decelerate the vehicle by only a throttle position of 0. Therefore, distance needed for decelerating the vehicle increases. During this additional distance, is the vehicle speed lower as actually possible, which means the drivers do not behave optimally.

e Conclusion

The driver behavior of the proposed driver model is optimal in respect of the preference to drive time-optimally, but it does not reflect the human driving behavior. The human drivers to not behave optimally. In general, they do not use full throttle to accelerate the vehicle, which results in a lower vehicle speed as possible and they do not decelerate the vehicle properly. The brake points, which mark the points of a reduction of the vehicle speed, are not placed at points, where the subjects actually start to use the brake. They are placed before, which results in a longer braking distance and braking time as necessary.

System response: vehicle trajectory

- Simulation results

The driver always starts cornering at the outside shoulder and pulls toward the inside border of the road while braking. The driver accelerates again at the points of the trajectory with the highest curvature. Due to this behavior, the driver can maximize the vehicle velocity without exceeding the acceleration limits which are given in the trajectory planning layer. The driver reduces on one hand the lateral acceleration due to a trajectory with the lowest possible curvature through the HM. On the other hand the lateral acceleration due to a perfect timing of vehicle speed with respect to the vehicle trajectory. The vehicle speed is always reduced, when the trajectory curvature increases and the vehicle accelerates again; when the trajectory curvature decreases again.

o **Driving simulator results**
   The recorded vehicle trajectories are not optimal with respect to the given preference. Some of the subjects even lose control over their vehicle and drive almost of the test track, see Fig. 8.26 (first turn), Fig 8.29 (first turn), Fig. 8.30 (last turn). This is probably caused by a wrong estimation of the vehicle speed, which was actually higher than thought. The higher vehicle speed led then to a higher lateral acceleration, which exceeded the tire forces. Skidding and a loss of the vehicle control is the result. The subjects also do not choose consequently the trajectory with the least curvature, which means that the drivers do not always start cornering at the outside shoulder and pulls toward the inside border of the road while cornering and. The subjects stay very often too close to the middle line or at one side of the test track and, therefore, do not use the benefit of the entire road width in order to increase the curvature of the vehicle trajectory, see Fig. 8.27, Fig. 8.28. In addition, the acceleration points and brake points are not placed optimally. *So,* the acceleration points are not always placed at the vertex of the turn, as it would be optimal with respect to the given preference, see Fig. 8.27, Fig. 8.28. The brake points are sometimes completely misplaced, see Fig. 8.27 and often too far away from the turn, see Fig. 8.26, Fig. 8.28, which leads to a lower vehicle velocity as it is possible and to a longer time needed to cover the whole distance of the HM.

o **Conclusion**
   The vehicle trajectory of the simulation is optimal, according to the given preference. Whereas the trajectories recorded in the driving simulator experiment, are far from being optimal. In trajectories are not optimal in respect of the trajectory curvature, the initiation of turns and the position of the brake points and acceleration points with respect of the vehicle trajectory and the test track. These deviations from the optimal behavior are probably partly caused by the driving simulator. The representation of the test track in the simulator, makes it difficult for the drivers to negotiate the road curvature. The lack of flow of texture reduces the ability to estimate the vehicle speed. No acceleration feedback and no feedback of the tire noise cause difficulties to estimate the tire saturation. But regardless this constraint of the driving simulator, it is also important to see, that the subjects are not specifically trained to drive time-optimally. This preference does not occur usually in such a marked degree in an ordinary driving situation. So it is not surprising, that the subjects do not behave time-optimally and, therefore, the simulation result does not reflect the subjects behavior.

System response: velocity profile

o **Simulation results**
   The starting velocity of the vehicle is $4m/s$. The vehicle reaches its top speeds on the straight sections of the HM. The absolute top speed of $36m/s$ reaches the vehicle on the end of the 6th straight section, see Fig. 8.31. The speed maxima are always a short

distance before a curve and the speed minima at the points of the vehicle trajectory with the highest curvature, see also Fig. 8.25.

o Driving simulator results

The starting velocity is different from subject *to* subject, because of the course of the experiment, see chapter 7.2.5. They are in the range from $30 - 50m/s$. The subjects also reach their top speed in the 6th straight section of the test track. It is in the range of $25 - 38m/s$, see Fig. 8.31.2 and Fig. 8.31.3. It is not possible to assign the brake points and acceleration points to specific points of the test track as in the simulation. The distribution of these points is too wide around the curves of the test track, so that no special pattern becomes obvious, which is followed by the majority of the subjects.

o Conclusion

The sequence of brake points and acceleration points calculated by the simulation, is optimal adjusted to the test track. This is not the case in the recorded velocity profiles of the driving simulator experiment. Especially in the middle part of the test track, which is difficult to drive, is it not possible to extract a specific driver behavior for braking and accelerating. Obviously, the subjects are not able to fulfill the task optimally and, therefore, the simulation does not reflect the subjects driving behavior. The reason, why the subjects cannot fulfill the given task is probably partly caused by the constraint of the driving simulator, see chapter 7.2.3, like the lack of acceleration feedback, etc. Another reason is probably, that most of the subjects are not well trained to drive time-optimally. This preference, especially in such a marked degree does not reflect a usual driving situation on public roads. Therefore, it is not surprising, that the subject's behavior differs from the optimal behavior.
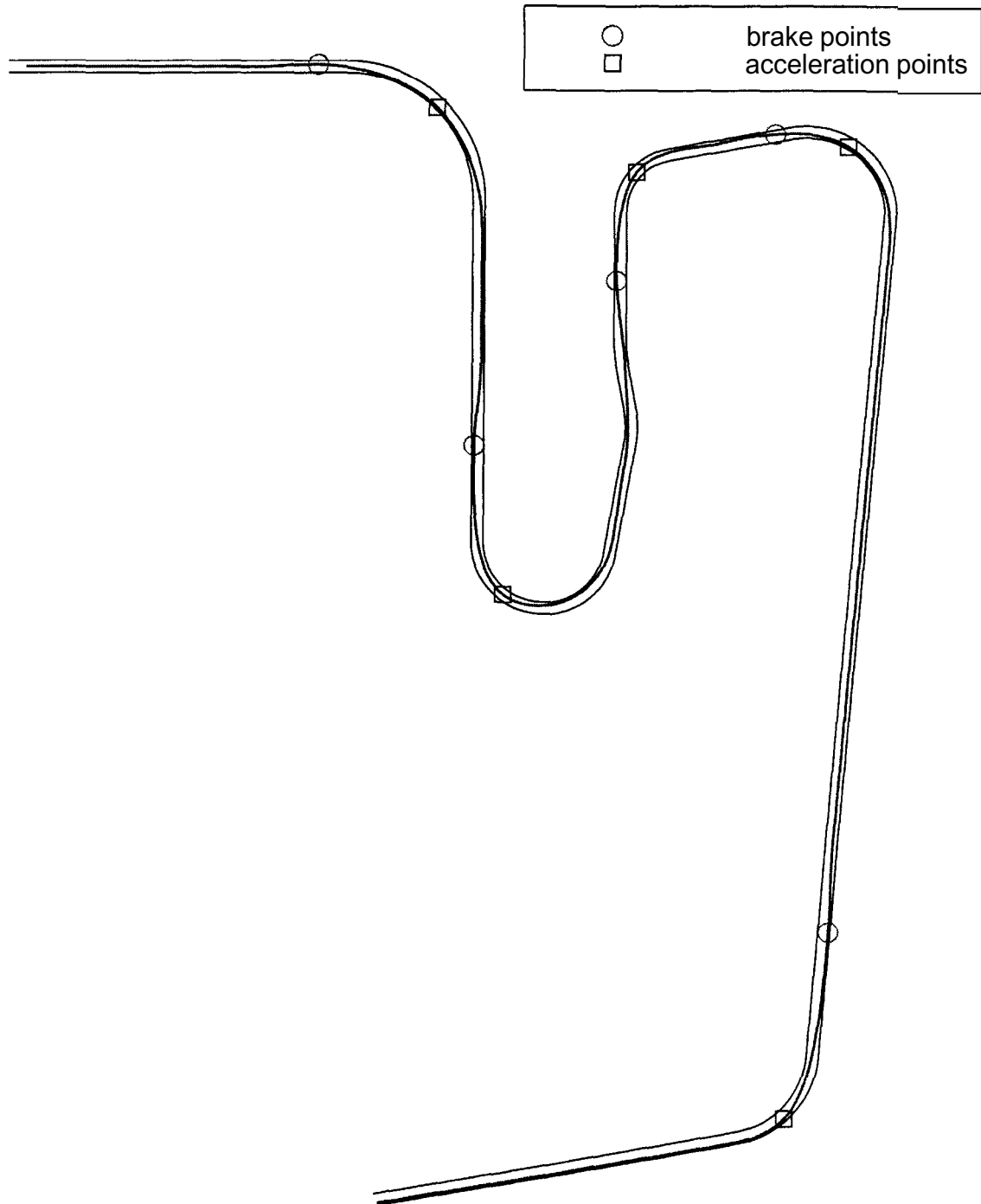
Figure *8.25:* Preference: time-optimal, Trajectory of sim-
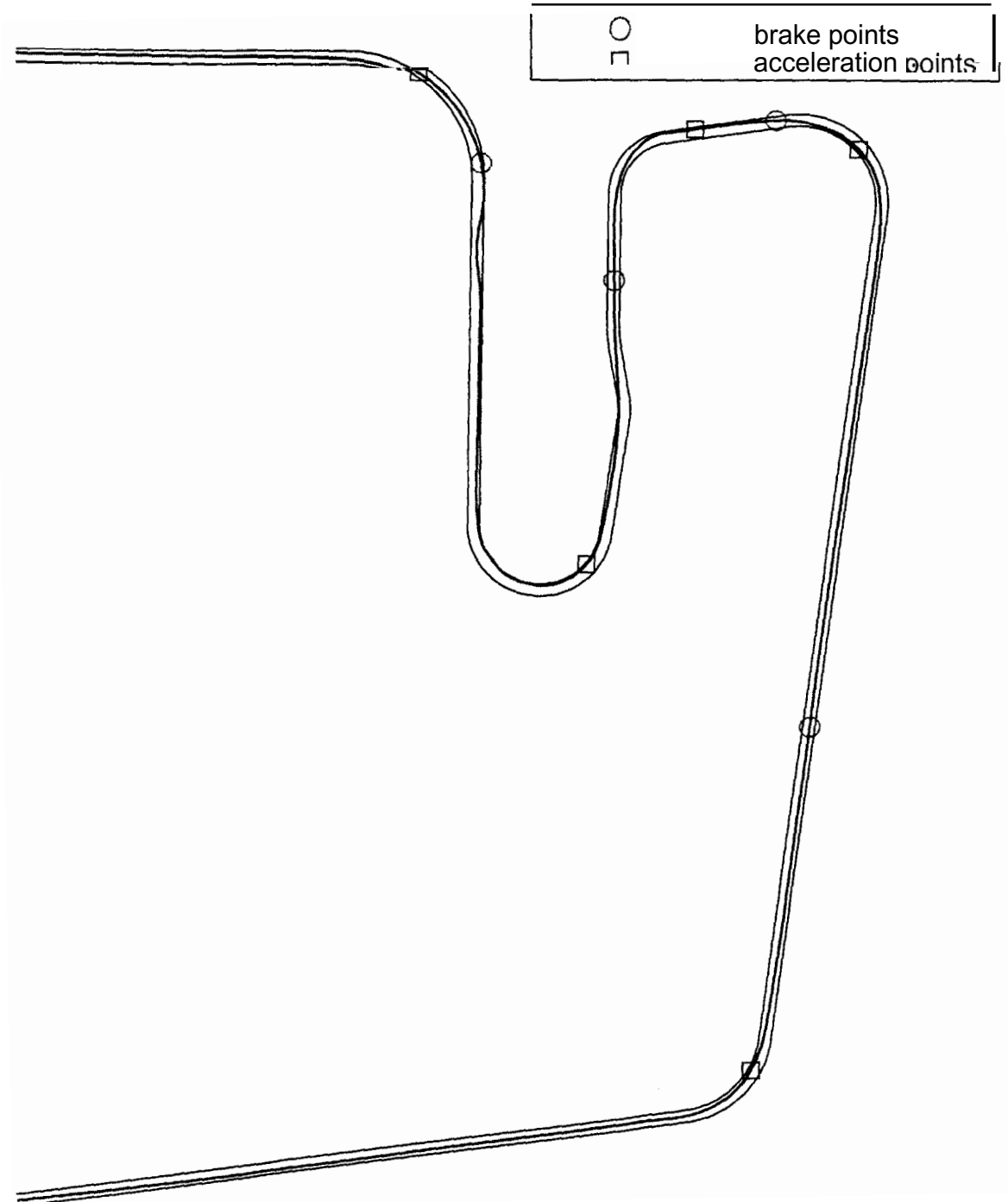ulation, with brake points and acceleration
points

Figure **8.26:** Preference: time-optimal, Trajectory recorded in driving simulator, with brake points and acceleration points
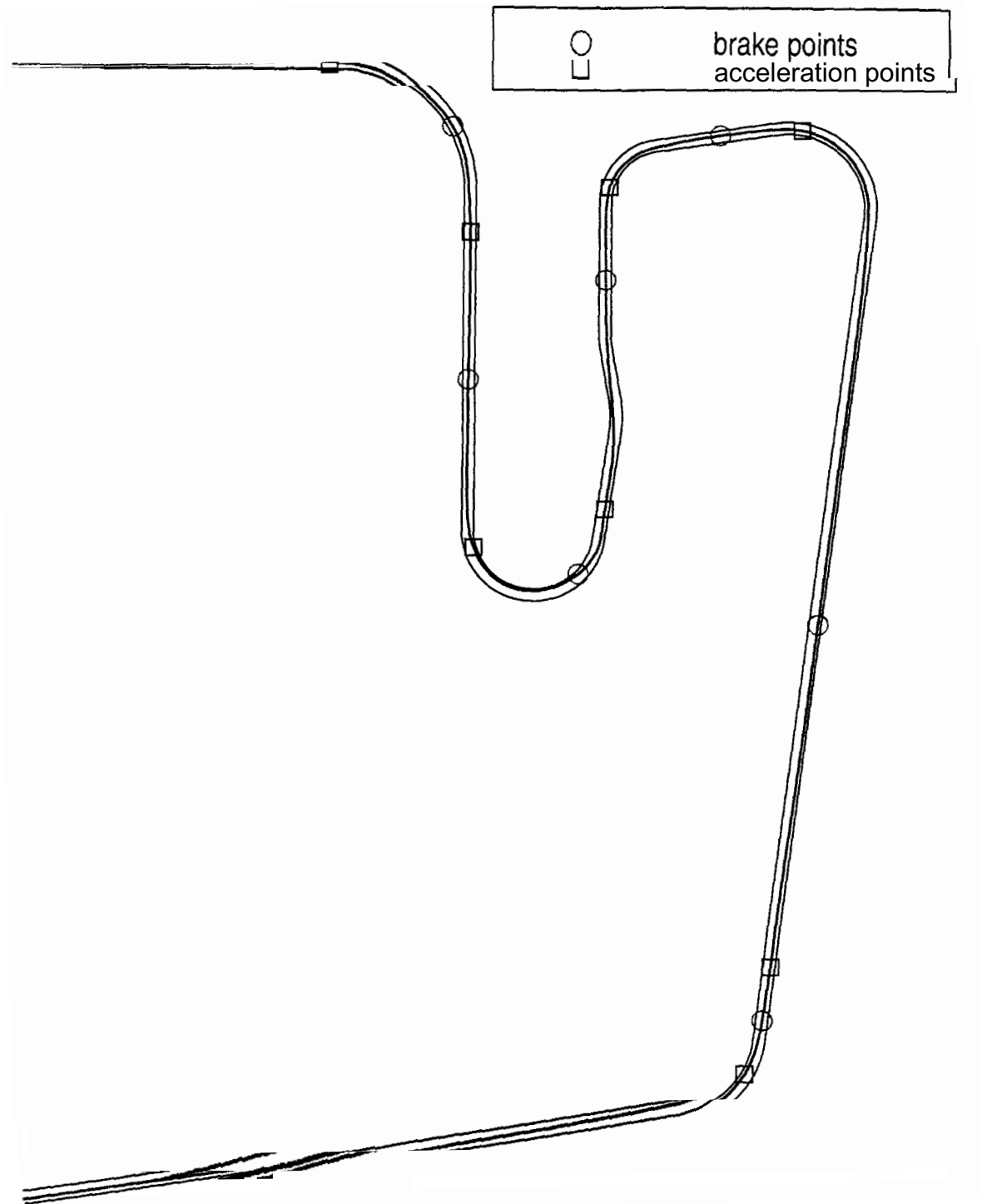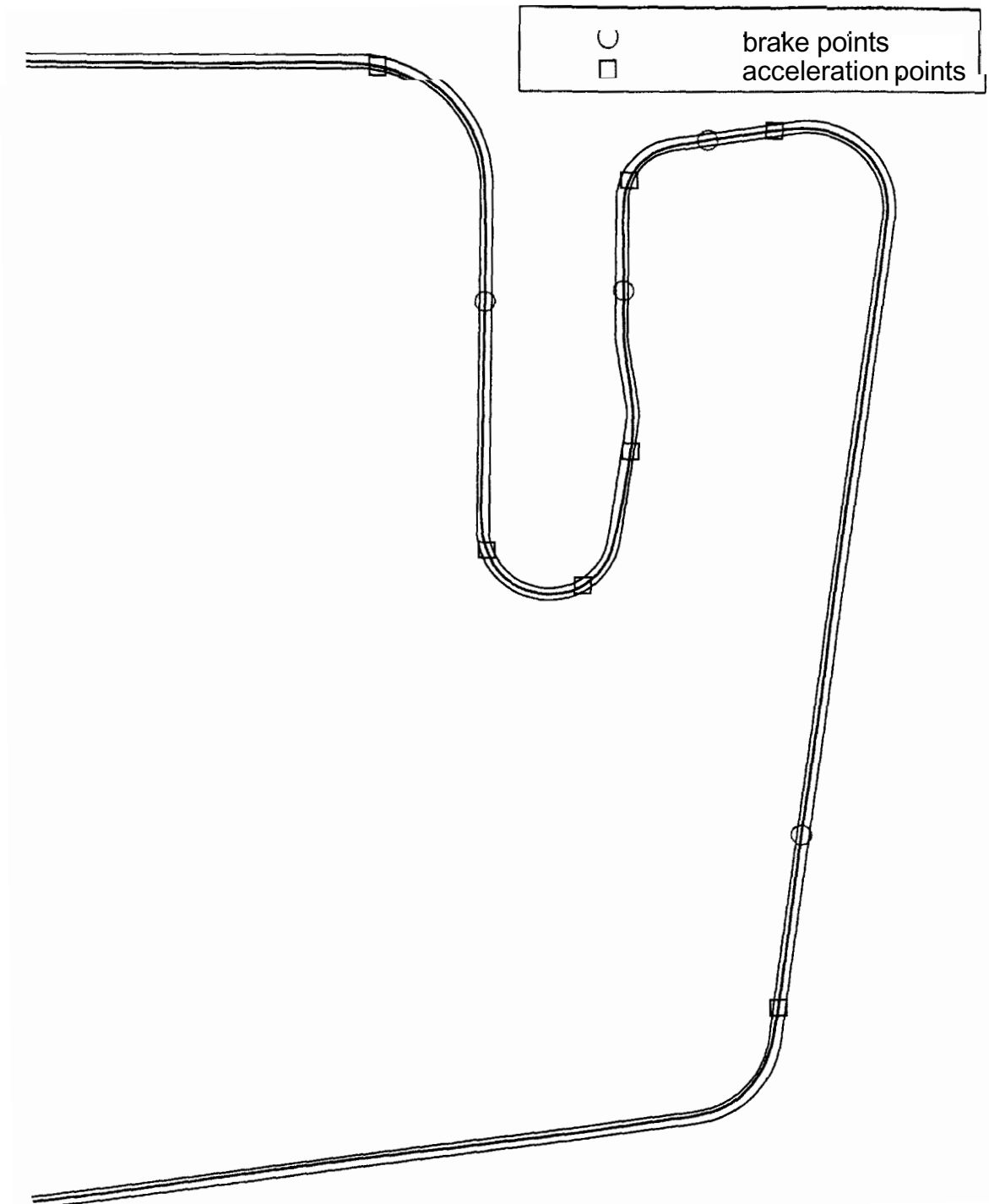
Figure **8.27:** Preference: time-optimal,   Trajectory
                 recorded in driving simulator, with brake
                 points and acceleration points

Figure 8.28: Preference: time-optimal, Trajectory recorded in driving simulator, with brake points and acceleration points

Figure **8.29:** Preference: time-optimal,   Trajectory
              recorded in driving simulator, with brake
              points and acceleration points

Figure **8.30:** Preference: time-optimal,   Trajectory
recorded in driving simulator, with brake
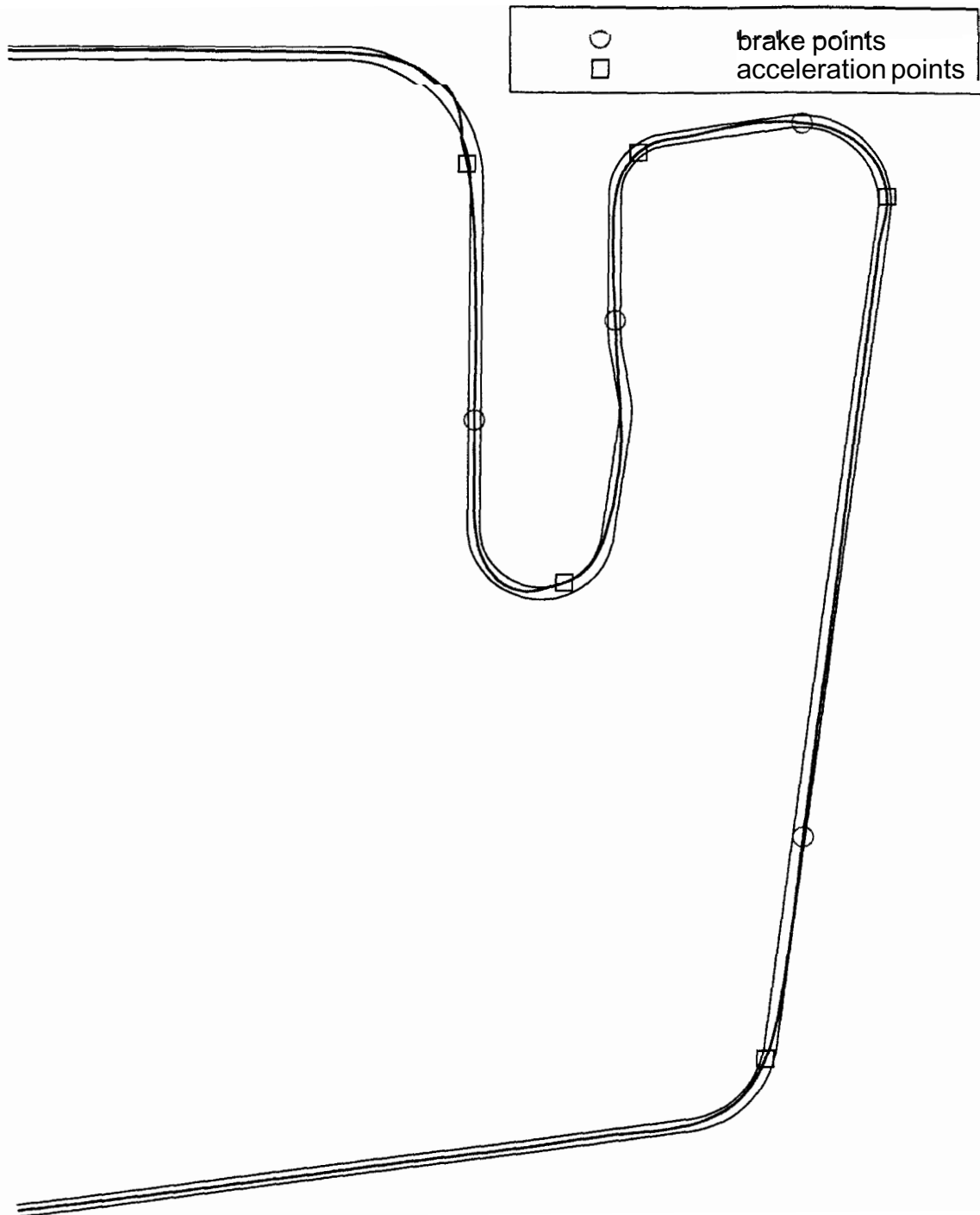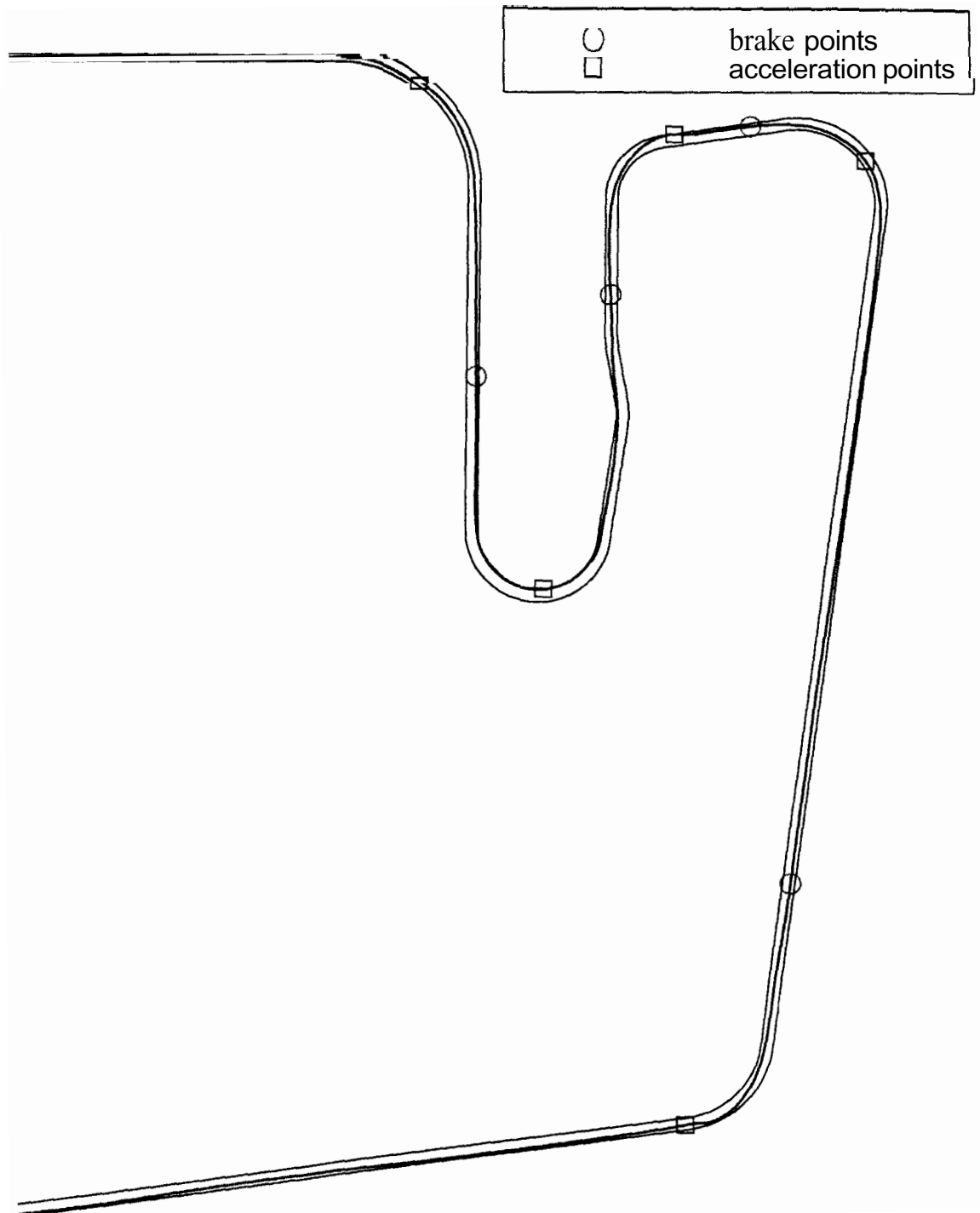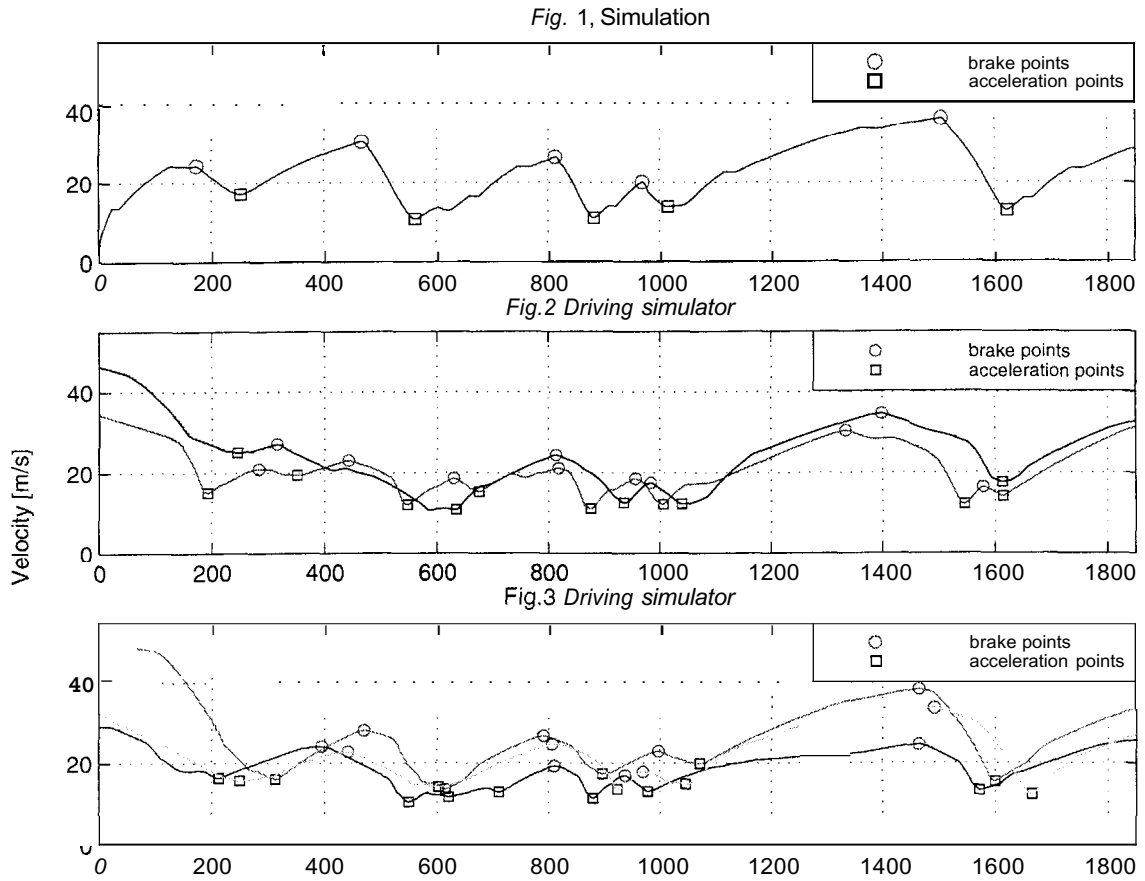points and acceleration points

Figure **8.31:** Preference: time-optimal, Velocities, with
brake points and acceleration points

Chapter 9

Conclusions

Driving can be characterized as goal directed behavior, that is propelled by aspirational factors and obstructed by constraining factors. This research project is based on the assumption, that, the aspirational factors, which are also called preferences and the constraining factors are processed by the human driver in such a way, that the result is an optimal driving maneuver. Therefore, it is also assumed, that it is possible to simulate human driving behavior using non-linear optimization. A real-world experiment and a driving simulator experiment were carried out in order to prove this assumption. The experiments included simple driving tasks like cornering a single turn and driving on a straight track as well as a more complex driving situation, which demanded to drive time-optimally through a race track (Hockenheim Motodrom).

On the simple tracks, the subjects had to perform tasks like minimizing the horizontal acceleration, maintaining a constant speed and keeping the vehicle on the right side of the road. In these experiments we were able to simulate driving behavior, which actually reflects the human driving behavior. The system input, which represents the direct driver's actions, like steering wheel angle and throttle signal is discussed as well as the system response, which is represented by the resulting trajectory, velocity, lateral acceleration and longitudinal acceleration. The system input of the driver and the system response of the vehicle match the simulation results within tenable limits. Deviations from the simulation results can be explained by the widely varying levels of perceptual abilities, physical skills and technological understanding of human drivers. Differences can also be caused by the influence of the driving simulator on human driving behavior, like no acceleration feed back, and unknown influences in the real-world experiment, like backlash in the joints of the vehicle's steering gear.

The correspondence of the simulation results and the results of the experiments enables us to predict human driving behavior to a certain extent. To foresee driving maneuvers becomes crucial, if e.g. a driver support system is supposed to share responsibilities with the human driver. With the formulation discussed in this thesis we can provide a technique, which leads to a behavior that coincides with human behavior. So it is possible to reduce the conflict, which arises between the decisions made by the human driver in contradiction to

the decisions made by the driver support system.

So far, we can draw this conclusion for simple driving maneuvers. The validity of the proposed driver model in more complex driving situations, like more difficult routes or additional traffic on the drivers lane as well as oncoming traffic has to be investigated. Therefore, we also discussed an experiment, which required to drive time-optimally through a race track (Hockenheim Motodrom). Although the simulation results are optimal with respect to the given preference, they do not reflect the behavior of the human subjects in this experiment. The influence of the driving simulator in such a extreme driving situation was to big in order to draw conclusions from this experiment. Especially, the lack of acceleration feedback and the few visual aids, which do not provide a sufficient flow of texture are the main reasons why the subjects have problems in driving optimally through the track. Another reason, that may explain the difference between the simulation results and the subject's behavior is that driving time-optimally is not a preference, which is usually applied on public roads. *So,* the subjects are not trained enough just by their general driving experience to fulfill successfully this very special task.

But in order to draw final conclusions about the driving behavior in more complex driving situations it is important to analyze and to carry out further experiments. In the course of the driving simulator experiment with the Hockenheim Motodrom as test track, experiments with additional preferences to the time-optimal behavior were carried out. The additional preferences were to minimize the horizontal acceleration, to maintain a constant speed, to keep the vehicle on the right side of the road and to use the brakes as little as possible. It is important to analyze this results and to compare them with the result of the time-optimal driver behavior. This preferences do not involve as much knowledge and information about the vehicle dynamics and the current system state as the time-optimal preference. Therefore, the constraint of the driving simulator becomes less important and the subjects behave in a more realistic way. In addition, these preferences are commonly used in public traffic. *So,* the drivers do not need special driving knowledge and can apply the driving experience, which they gained over the years.

For further experiments it is also important to simulate human driver behavior with a mix of preferences, The simulations calculated for this project are carried out with an extreme weight on special preferences. But only in rare cases human drivers have just one preference. Usually a mix of preferences is used.

It is also important to mention, that the cognitive decision layer, which gives the proposed driver model the required flexibility is not implemented yet and, therefore, the simulations in this project were calculated without the cognitive decision layer. This has just little impact on the carried out experiments and the gained results, because for one test run always just one preferences was given. But for future research, especially with increasing external disturbances, the cognitive decision layer is crucial to model human driver behavior. Environmental influences like weather, daytime or other road users have great impact on the human driving behavior and cause the human driver to change preferences. The cognitive decision layer would also enable the driver model to switch between different prediction

models according to the driving situation. Human drivers are supposed to have several different pictures of the vehicle dynamics according to their driving experience and technical knowledge. And they are also supposed to switch between the different pictures as required by the current situation.

In order to model human driving behavior in its entire variety and complexity it is important to implement the cognitive decision layer and, therefore, provide the driver model with the necessary flexibility to adjust to different external influences. In addition, further experiments have to be carried out in order to get more information about the influence of different preferences and their combination on human driving behavior as well as on the simulation results.

Bibliography

[1] Bremer H.: *Dynamik und Regelung mechanischer Systeme.* Stuttgart: Teubner Verlag, 1988.

[2] Bronstein I. N., Semendjajew K.A.: *Taschenbuch der Mathematik.* Hrsg.: *G.* Grosche, V. Ziegler, D. Ziegler; Thun, Frankfurt/Main: Harri Deutsch, 23. Auflage, 1987.

[3] Dugoff H., Fancher P. S.,Segel L.: *Tire performance characteristics affecting vehicle response to steering and braking control inputs.* Technical report, National Bureau of Standards, Contract CST-460, Highway Safety Research Institute, University of Michigan, Ann Arbor, 1969.

[4] Eschenauer H., Koski J., Osyczka A.: *Multicriteria Optimization - Fundamentals and Motivation.* - In: Multicriteria Design Optimization, Eds. H. Eschenauer, J. Koski, A. Osyczka, Springer, Berlin, 1990, pp. 1-32.

[5] Kortüm W., Lugner P.: *Systemdynamik und Regelung von Fahrzeugen - Einführung und Beispiele.* Berlin, Heidelberg, New York: Springer-Verlag, 1994.

[6] Mitschke M.: *Dynamik der Kraftfahrzeuge - Band C: Fahrverhalten.* 2nd edition, Berlin: Springer-Verlag, 1990.

[7] Pacejka H.B.: *Modeling of the pneumatic tire and its impact on vehicle dynamic behavior.* Carl-Cranz-Gesellschaft e. V., Lehrgang V2.03, Oberpfaffenhofen, Oct. 25.-27., 1989.

[8] Pfeiffer F.: *Einführung in die Roboterdynamik.* Stuttgart: Teubner-Verlag, 1989.

[9] Powell M. J. D.: *A Fast Algorithm for Nonlinearly Constrained Optimization Calculations.* Numerical Analysis, Ed. G. A. Watson, Lecture Notes in Mathematics, Springer Verlag, Vol. 630, 1978.

[10] Powell M. J. D.: *Variable Metric Methods for Constrained Optimization.* - In: Mathematical Programming: The State of the Art, Eds. A. Bachem, M. Grotschel, B. Korte, Berlin: Springer, 1983, pp. 288-311.

[11] Prokop G.: *Optimale Prozeßdynamik bei Manipulation mit Robotern.* Fortschritt-Berichte VDI, Reihe 8, No. 713, Dusseldorf VDI-Verlag, 1998.

154

[12] Roberson R.E., Schwertassek R.: *Dynamics* of *Multibody Systems.* Berlin: Springer-Verlag, 1988.

[13] Rensik R.: *Cambridge Basic Research 1998 annual Report.* Nissan Cambridge Basic Research, Boston, 1998.

[14] Schittkowski K.: *On the Convergence of a Sequential Quadratic Programming Method with an Augmented Lagrangian Line Search Function.* Mathematische Optimierungsforschung und Statistik, Section Optimization, **4** (1983), pp. 197-216.

[15] Senders J. W., Kristofferson A. B., Levison W. H., Dietrich C. W., Ward J. L.: *The attentional demand of automobile driving.* Highway Research Record 195, 1967, pp. 15-**33.**

[16] Uffelmann F.: *Berechnung des Lenk- und Bremsverhaltens von Kraftfahrzeugzügen auf rutschiger Fahrbahn.* Dissertation thesis, Technische Universitat Braunschweig, 1980.

[17] Wiegner P.: *Über den Einfluß von Blockierverhinderern auf das Fahrverhalten von Personenkraftwagen bei Panikbremsungen.* Dissertation thesis, Technische Universitat Braunschweig, 1974.